Meshfree Methods: Progress Made after 20 Years

Jiun-Shyan Chen, M.ASCE[1]; Michael Hillman[2]; and Sheng-Wei Chi[3]

Abstract: In the past two decades, meshfree methods have emerged into a new class of computational methods with considerable success. In addition, a significant amount of progress has been made in addressing the major shortcomings that were present in these methods at the early stages of their development. For instance, essential boundary conditions are almost trivial to enforce by employing the techniques now available, and the need for high order quadrature has been circumvented with the development of advanced techniques, essentially eliminating the previously existing bottleneck of computational expense in meshfree methods. Given the proper treatment, nodal integration can be made accurate and free of spatial instability, making it possible to eliminate the need for a mesh entirely. Meshfree collocation methods have also undergone significant development, which also offer a truly meshfree solution. This paper gives an overview of many classes of meshfree methods and their applications, and several advances are described in detail. **DOI: 10.1061/(ASCE)EM.1943-7889.0001176.**

Author keywords: Meshfree methods; Particle methods; Galerkin meshfree methods; Collocation meshfree methods.

Introduction

The finite-difference method (FDM) and the finite-element method (FEM) rely on a mesh (or stencil) to construct the local approximation of functions and their derivatives for solving partial differential equations (PDEs). A few drawbacks commonly encountered in these methods are:

- Time consuming in generating a quality mesh in arbitrary geometry for desired accuracy;
- Difficulty in constructing approximations with arbitrary order of continuity, making the solution of PDEs with higher order differentiation or problems with discontinuities difficult to solve;
- Tediousness in performing *h*-adaptive or *p*-adaptive refinement; and
- Ineffectiveness in dealing with mesh entanglement related difficulties (such as those in large deformation and fragment-impact problems).

Meshfree methods all share a common feature that alleviates or eliminates these issues: *the approximation of unknowns in the PDE is constructed based on scattered points without mesh connectivity.* As shown in Fig. 1, the approximation function at a point in FEM is constructed at the element-level natural coordinate and then transformed to the global Cartesian coordinate, whereas meshfree approximation functions are constructed using only nodal data in the global Cartesian coordinates directly. These compactly supported meshfree approximation functions form a partition of unity subordinate to the open cover of the domain with controllable orders of continuity and completeness, independent from one another. Using this class of approximation functions, it becomes possible to relax the strong tie between the quality of the discretization and the quality of approximation in FEM, and the procedures in *h*-adaptivity are significantly simplified. Special basis functions can be embedded in the approximation to capture essential characteristics of the PDE at hand, and arbitrary discontinuities can be introduced into the approximation as well.

Generally speaking, meshfree methods have developed under two branches of formulations:

- The Galerkin meshfree methods based on the weak form of PDEs. While no mesh is needed in the construction of the approximation, domain integration is required, and special techniques to enforce essential boundary conditions are needed. Advances in domain integration and enforcement of boundary conditions are discussed in the section "Galerkin-Based Meshfree Method"; and
- The collocation meshfree methods based on the strong form of PDEs. Because of the ease of constructing smooth meshfree approximations, PDEs can be solved directly at the collocation points without special domain integration and essential boundary condition procedures, as will be presented in the section "Strong Form Collocation-Based Meshfree Method."

A wide variety of meshfree methods have been proposed over the years. Fig. 2 summarizes the attributes of some selected methods, along with some mesh-based methods for comparison. The table is roughly ordered by the dates the methods were proposed (or when the first robust version was proposed), which also gives some historical perspective. In Fig. 3, an alternative analysis is presented and made slightly more precise, where these methods are shown at the intersection of the solution method (columns) and the approximation employed (rows). In this paper, it is the authors' intention to elucidate the relationship between the various meshfree methods, and present advancements that have been made over the years. Throughout the paper, the following abbreviations have been introduced:

- CPDI: convected particle domain interpolation (Sadeghirad et al. 2011);
- C-SPH: corrected SPH (Dilts 1999);
- DEM: diffuse element method (Nayroles et al. 1992);
- DNI: direct nodal integration;
- EFG: element free Galerkin (Belytschko et al. 1994b, 1995a; Lu et al. 1994);

[1]Prager Professor, Dept. of Structural Engineering, Univ. of California, San Diego, 9500 Gilman Dr., La Jolla, CA 92093 (corresponding author). E-mail: js-chen@ucsd.edu

[2]Kimball Assistant Professor, Dept. of Civil and Environmental Engineering, Pennsylvania State Univ., University Park, PA 16802.

[3]Assistant Professor, Dept. of Civil and Materials Engineering, Univ. of Illinois at Chicago, 842 W. Taylor St., Chicago, IL 60607.

Note. This manuscript was submitted on May 16, 2016; approved on August 9, 2016; published online on January 23, 2017. Discussion period open until June 23, 2017; separate discussions must be submitted for individual papers. This paper is part of the ***Journal of Engineering Mechanics***, © ASCE, ISSN 0733-9399.

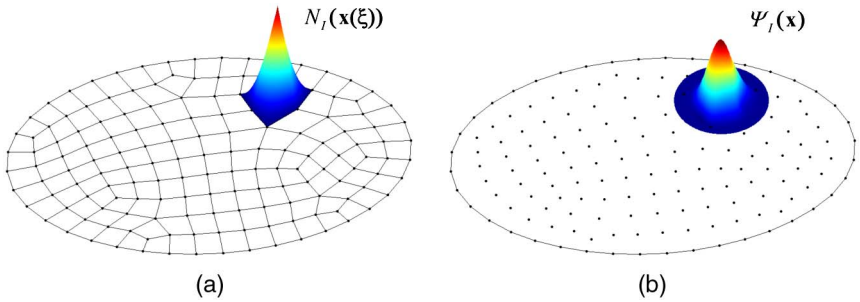

Fig. 1. (a) Patching of a finite element shape function from local element domains; (b) a meshfree approximation function constructed directly in the global Cartesian coordinates

Method	Approximation Function											Solution Scheme (Discretization)								
	Local											Weak form					Strong form			
	With Polynomial Reproduction (PR)								without PR											
	Local Polynomials	MLS/RK		WLS	Enriched		Natural neighbor	Maximum Entropy	Splines/NURBS	Smooth Kernel	Local RBF	RBF (Global)	Gauss integration	Stabilized Integration	Point Collocation	Gauss integration	Variationally Consistent	Point Collocation	Subdomain Collocation	Weighted Collocation	Lagrangian-Eulerian form
		Direct	Diffuse		Polynomials	MLS/RK (PU)															
FEM[a], SFEM[a]	•												•	•							
SPH[b,c]										•					•						
GFD			•															•			
RBCM											•	•						•	•	•	
DEM			•										•								
EFG, XEFG		•				•							•	•							
MPM, GIMP, CPDI, PFEM-2	•																				•
RKPM, SLRKPM[c]		•											•	•							
GFEM, XFEM					•								•								
MPS[d]				•														•			
PUM	•				•	•							•								
hp clouds						•							•								
FPM				•														•			
FMM[c]	•												•								
C-SPH/MLSPH[b,c]		•													•						
MLPG		•								•						•					
NEM							•						•								
PPU						•							•								
MFS						•							•								
RKCM, GRKCM		•	•															•		•	
Meshfree SCNI		•												•							
LRPIM	•									•	•					•					
RPIM	•										•		•								
MFEM[a], PFEM[c]							•						•								
MaxEnt								•					•								
IGA[a]									•				•				•				
Peridynamics (PD)[e]			•															•			
OTM[c]								•					•								
Meshfree VCI[f]		•											•	•	•		•				

[a] Mesh-based
[b] Considered weak form here due to weakened approximation requirements
[c] Continually reconstructed
[d] WLS-type approximation of pair-wise gradients
[e] Employs diffuse derivatives (Bessa et al. 2014)
[f] Can construct for any integration.

Fig. 2. Attributes of selected mesh-based and meshfree methods

J. Eng. Mech., 2017, 143(4): 04017001

Approximation				Solution Scheme (Discretization)	
				Weak form	Strong form
Local Polynomial	Lagrangian mesh	No enrichment	Direct derivatives	FEM	
			Smoothed derivatives	SFEM	
		Enriched		GFEM, XFEM	
	Continuously reconstructed			FMM	
	Eulerian mesh, Lagrangian points	Points carry history and mass		MPM, GIMP, CPDI	
		Points carry history		PFEM-2	
Spline / NURBS	No enrichment			IGA	IGC
	Enriched			XIGA	
MLS	No enrichment	Direct derivatives		EFG, MLPG, MLSPH[c]/C-SPH[c]	
		Diffuse derivatives[a]		DEM	Peridynamics (PD)[b], GFD
		VCI derivatives		Meshfree VCI, Meshfree SCNI	
	Enriched			XEFG	
RK	Lagrangian	Smoothed derivatives		Meshfree SCNI	
		Direct derivatives		RKPM	RKCM
		Diffuse derivatives[a]			GRKCM
	Continuously reconstructed			SLRKPM	
PU	Polynomial enriched			*hp* clouds (HPC), MFS	
	Polynomial and/or other enriched			PUM, PPU	
MaxEnt	Lagrangian			MaxEnt method	
	Continuously reconstructed			OTM	
Natural neighbor	Lagrangian			NEM	
	Continuously reconstructed			MFEM, PFEM	
Radial basis functions				RPIM, LRPIM	RBCM
Weighted least squares					FPM
Kernel approximation				SPH[3]	
WLS of pair-wise gradients					MPS

[a]Implicit, diffuse and synchronized derivatives, and generalized finite differences are equivalent, see the section "Derivative Approximations in Meshfree Methods"
[b]Employs diffuse derivatives (Bessa et al. 2014)
[c]Considered weak form here due to weakened approximation requirements.

Fig. 3. Methods shown at the intersection of approximation function and solution method

- FEM: finite element method (Zienkiewicz and Taylor 1977);
- FMM: free mesh method (Yagawa and Yamada 1996);
- FPM: finite point method (Oñate et al. 1996a);
- GFD: generalized finite difference (Liszka and Orkisz 1980; Liszka 1984);
- GFEM: generalized finite element method (Melenk 1995; Strouboulis et al. 2001);
- GI: gauss integration;
- GIMP: generalized interpolation material point (Bardenhagen and Kober 2004);
- GRKCM: gradient RKCM (Chi et al. 2013);
- HPC: *hp* clouds (Duarte and Oden 1996b, a);
- IGC: isogeometric collocation (Auricchio et al. 2010);
- IGA: isogeometric analysis (Cottrell et al. 2009; Hughes et al. 2005);
- KC: kernel contact (Chi et al. 2015; Guan et al. 2011);
- L-RBCM: localized RBCM (Chen et al. 2008);
- LRPIM: local radial point interpolation method (Liu and Gu 2001);
- LS: least squares;
- MaxEnt: maximum entropy (Arroyo and Ortiz 2006; Sukumar 2004);
- MFEM: meshless finite element method (Idelsohn et al. 2003f);
- MFS: method of finite spheres (De and Bathe 2000);
- MLPG: meshless local Petrov-Galerkin (Atluri and Zhu 1998);
- MLS: moving least squares (Lancaster and Salkauskas 1981; Liszka 1984);
- MLSPH: moving least squares particle hydrodynamics (Dilts 1999);
- MPM: material point method (Sulsky et al. 1994, 1995);
- MPS: moving particle semi-implicit (Koshizuka and Oka 1996);
- MQ: multiquadrics;
- M-SCNI: modified SCNI (Puso et al. 2008);
- M-SNNI: modified SNNI (Chen et al. 2007b);
- NEM: natural element method (Braun and Sambridge 1995; Sukumar and Belytschko 1998);
- NSNI: naturally stabilized nodal integration (Hillman and Chen 2016);
- NURBS: non-uniform rational B-splines;
- OTM: optimal transportation meshfree (Li et al. 2010);
- PD: peridynamics (Silling and Askari 2005; Silling et al. 2007);
- PFEM: particle finite element method (Idelsohn et al. 2003b, 2004);
- PFEM-2: second generation PFEM (Idelsohn et al. 2012, 2014);
- PPU: particle partition of unity method (Griebel and Schweitzer 2000);
- PU: partition of unity;
- PUM: partition of unity method (Babuška and Melenk 1997; Melenk and Babuška 1996);
- RBCM: radial basis collocation method (Hu et al. 2007; Kansa 1990a; b; Wong et al. 1999);
- RBF: radial basis function (Hardy 1971, 1990);
- RK: reproducing kernel (Liu et al. 1995b);

- RKCM: reproducing kernel collocation method (Aluru 2000; Hu et al. 2011);
- RKPM: reproducing kernel particle method (Chen et al. 1996; Liu et al. 1995b);
- RPIM: radial point interpolation method (Wang and Liu 2002);
- SCNI: stabilized conforming nodal integration (Chen et al. 2001, 2002);
- SFEM: smoothed finite element method (Liu et al. 2007a);
- SGFEM: stable GFEM (Gupta et al. 2013, 2015);
- SLRKPM: semi-Lagrangian RKPM (Guan et al. 2009);
- SNNI: stabilized nonconforming nodal integration (Chen et al. 2007b);
- SPH: smoothed particle hydrodynamics (Gingold and Monaghan 1977; Lucy 1977);
- VCI: variationally consistent integration (Chen et al. 2013);
- VC-MSNNI: variationally consistent MSNNI (Hillman et al. 2014);
- VC-NSNI: variationally consistent NSNI (Hillman and Chen 2016);
- WLS: weighted least squares;
- XEFG: extended EFG (Rabczuk and Areias 2006; Rabczuk et al. 2007i);
- XFEM: extended finite element method (Belytschko and Black 1999; Moës et al. 1999); and
- XIGA: extended IGA (Benson et al. 2010; Ghorashi et al. 2012).

Early Development

The early development of meshfree methods can be traced back to smoothed particle hydrodynamics (SPH) by Lucy (1977) and Gingold and Monaghan (1977) for astrophysics modeling. SPH was formulated by kernel estimation (Monaghan 1982, 1988) of conservation equations. The method later gained traction in solid mechanics as a way to solve problems difficult for mesh-based methods such as fragment-impact problems (Benz and Asphaug 1995; Johnson et al. 1996; Libersky and Petschek 1991; Randles and Libersky 1996). The accuracy, tensile instability, and spatial instability of SPH have been examined (Belytschko et al. 2000; Liu et al. 1995b; Swegle et al. 1994, 1995), and formulations have been proposed to correct the deficiencies in SPH (Bonet and Kulasegaram 2000; Dilts 1999; Monaghan 2000; Randles and Libersky 1996, 2000). These later enhancements of SPH have motivated the development of many more modern meshfree methods. A prime example is the introduction of RKPM (Liu et al. 1995b) as a correction of SPH for enhanced consistency and stability.

Another branch of numerical methods for solving PDEs that do not rely on a grid structure is the class of generalized finite difference (GFD) methods. One of the earliest finite difference methods using scattered points is attributable to Jensen (1972). However, a difficulty associated with this method was the selection of an appropriate star (collection of neighbors) such that the resulting matrix for determining weights at a point is not singular, analogous to the moving least-squares (MLS) requirements (this is in fact not a coincidence, see the section "Meshfree Approximation Functions"). An algorithm was introduced to avoid this difficulty, and also improve the accuracy of mixed derivatives (Perrones and Kao 1974). A robust GFD method by Liszka and Orkisz (Liszka and Orkisz 1980; Liszka 1984) considered an arbitrary number of neighbors for higher accuracy and matrix stability, resulting in an overdetermined system solved by weighted least-squares. In meshfree terminology, this method employs second order basis with diffuse derivatives for the solution of the strong form of the problem (see the section "Derivative Approximations in Meshfree Methods"). Liszka later formalized the inclusion of the approximation of the primary variable (Liszka 1984) and independently arrived at the moving least-squares (MLS) approximation (Lancaster and Salkauskas 1981) by Lancaster and Salkauskas. Many modern meshfree methods originate from the employment of this approximation for solving PDEs.

Galerkin Meshfree Methods

The first general meshfree approach for solving boundary value problems under the Galerkin framework was the diffuse-element method (DEM) introduced by Nayroles, Touzot, and Villon, which employed an MLS approximation for test and trial functions (Nayroles et al. 1992). They also independently derived the MLS approximation (Lancaster and Salkauskas 1981). In this method, derivatives in the weak form are approximated by the differentiation of a certain portion of the basis functions, which are considered diffuse derivatives. The section "Meshfree Approximation Functions" gives an in depth discussion on the relationship between diffuse derivatives and several other meshfree approximations. Belytschko et al. (1994b, 1995a) and Lu et al. (1994) introduced the element-free Galerkin (EFG) method as an improvement of DEM. They introduced Lagrange multipliers to enforce boundary conditions, and used the full derivative of the MLS approximation functions in the Galerkin solutions of PDEs. Further, they introduced higher order quadrature based on a background mesh to achieve enhanced accuracy in the Galerkin solution. Taking advantage of the ability to embed discontinuities into the approximation without remeshing, as well as straightforward h-refinement, EFG was effectively applied to fracture mechanics problems (Belytschko and Tabbara 1996; Belytschko et al. 1994a, 1995a).

Motivated by wavelet analysis, Liu, Jun, and Zhang (Liu et al. 1995b) introduced the reproducing kernel particle method (RKPM) based on the reproducing kernel (RK) approximation around the same time as the EFG method was proposed (Fig. 2). They demonstrated that the discrete version of the RK kernel estimate offered favorable properties over DEM and SPH, and could serve as a correction to SPH, which is particularly inaccurate near boundaries. It was shown by Chen et al. (1996) that the discretizations of the continuous form of the RK approximation and the moment matrix needs to be done in a consistent manner in order to preserve polynomial reproducibility. A direct discrete reproducing kernel approximation was then introduced (Chen et al. 1997) to avoid the trouble of determining the integration weights based on the continuous RK approximation. Error and convergence estimates for RKPM with monomial bases have since been well established (Chen et al. 2003; Han and Meng 2001; Liu et al. 1996a, 1997c). Based on the RKPM method, a multiresolution extension has been proposed (Liu and Chen 1995; Liu et al. 1996a, c, 1997a), as well as a related framework that can yield synchronized convergence and a hierarchical partition of unity (Li and Liu 1998, 1999b, a). RKPM has been shown to be particularly effective for large deformation problems (Chen and Wu 1997; Chen et al. 1996, 1998a, 2000a, e; Yoon and Chen 2002; Yoon et al. 2001), smooth contact (Chen and Wang 2000a; Wang 2000; Wang et al. 2014), multibody contact, and fragment-impact problems (Chen et al. 2011; Chi et al. 2015; Sherburn et al. 2015), among others (see "Applications of Meshfree Methods"). Adaptive refinement can also be implemented with relative ease compared to the conventional mesh-based methods (Liu and Chen 1995; Liu et al. 1997a; Rabczuk and Belytschko 2005; Rabczuk and Samaniego 2008; You et al. 2003).

One major difference between meshfree and finite-element approximations is that the meshfree approximations such as MLS and RK are constructed without the need of mesh topology and they are typically rational functions. Domain integration of the weak form

poses considerable complexity in the Galerkin meshfree method. Employment of Gauss quadrature rules yields integration errors when background calls do not coincide with the shape function supports (Dolbow and Belytschko 1999). Conversely, direct nodal integration results in rank deficiency and loss of accuracy. The previously mentioned EFG and RKPM methods with Gauss quadrature or nodal integration do not pass the linear patch test for nonuniform point distributions. A stabilized conforming nodal integration (SCNI) has been introduced by Chen et al. (2001) to ensure passing the linear patch test in arbitrary discretizations and to remedy rank deficiency of direct nodal integration. More recently, an extension of SCNI for quadratic basis functions has been proposed (Duan et al. 2012). A generalization of conditions for passing the linear patch test (for Galerkin exactness) to arbitrary order has also been recently introduced by Chen, Hillman, and Rüter under the framework of variational consistency (Chen et al. 2013). A variationally consistent integration (VCI) approach has been proposed that can be used as a correction of any quadrature rules such as nodal integration to achieve optimal rates of convergence. Stabilization of nodal integration has also been proposed, including adding a residual of the equilibrium equation to the nodally-integrated potential energy functional (Beissel and Belytschko 1996), the stress point method by taking derivatives away from the nodal points (Randles and Libersky 2000), and an approach based on an iterative correction of nodal integration for passing the patch test in conjunction with a least-squares type stabilization (Bonet and Kulasegaram 2000). Methods based on implicit gradients embedded in the RK approximation as a stabilization of SCNI, called gradient SCNI (G-SCNI) (Chen et al. 2007b) and implicit gradient expansion of nodal integration, named naturally stabilized nodal integration (NSNI) (Hillman and Chen 2015) have also been proposed. An in depth discussion of progress made on quadrature will be presented in the section "Domain Integration in Galerkin Meshfree Methods."

A series of meshfree methods have emerged based on the partition of unity (PU) framework by Melenk and Babuška (Babuška and Melenk 1997; Melenk and Babuška 1996). A general survey of mathematical results concerning PU methods has been provided (Babuška et al. 2003). Duarte and Oden introduced a meshfree method called hp clouds based on PU, where the MLS approximations were enriched *extrinsically* (adding additional degrees of freedom in the PU approximation) with higher order complete polynomials (Duarte and Oden 1996a). This gave the ability to perform p-adaptivity since bases could vary in space, in contrast to the MLS-based methods where this would introduce a discontinuity. The completeness of the approximation depends on the order of the complete monomials in the higher order enrichment. They also proposed p-refinement in the enrichment of MLS with constant bases [using the Shepard function (Shepard 1968)]. This concept was extended to FEM for an h-p finite-element method (Oden et al. 1998). An important offshoot of the PU method is the celebrated XFEM (Belytschko and Black 1999; Moës et al. 1999), which is an active area of research in finite elements.

The partition of unity finite-element method was later redesigned in a more general fashion and was labeled the generalized finite-element method (GFEM) (Strouboulis et al. 2000a, b, 2001). Efforts have been devoted to algorithms that ease the linear dependency that can occur in PU methods, and adaptive integration techniques have been proposed to enhance integration of enrichment functions (Strouboulis et al. 2000a). A GFEM implementation has been proposed where meshes that are completely independent of geometry can be employed by using automatic generation of domain-conforming integration cells, with handbook enrichments for features like corners, which greatly alleviates difficulty in meshing for solving PDEs on complex domains (Strouboulis et al. 2000b, 2001). In this approach, opposite to many meshfree Galerkin methods, the approximation is mesh-based but the integration scheme is meshfree. More recently, stable GFEM (SGFEM) has been proposed that gives better conditioning of the stiffness matrix over GFEM (Gupta et al. 2013, 2015). An approach where a local solution can be embedded in the global solution under the framework of partition of unity to achieve computational efficiency and accuracy has also been recently introduced (Duarte and Kim 2008; Gupta et al. 2012). In this global-local approach, the local solution is patched together by the global partition of unity functions. This method has been applied to fracture modeling (Kim et al. 2010; Kim and Duarte 2015; Pereira et al. 2012).

Based on the partition of unity methods, Griebel and Schweitzer (2000) introduced the particle-partition of unity method, which considered the aspects of constructing a meshfree partition of unity method under an arbitrary distribution of points. They systematically examined issues such as quadrature and constructing a PU subordinate to open cover (Griebel and Schweitzer 2002a), solvers and parallelization (Griebel and Schweitzer 2002b, 2003a), and boundary conditions in this noninterpolatory method (Griebel and Schweitzer 2003b).

In Galerkin meshfree methods, integration of the weak form often performed by a background mesh [cf. (Belytschko et al. 1994b)]. The *meshless local Petrov-Galerkin* (MLPG) method (Atluri and Shen 2002; Atluri and Zhu 1998) introduced by Atluri and Zhu (1998) employed a *local weak form* for an MLS-based meshfree method, where the weak form is formulated in local domains and avoids background cell integration. The local domain was selected to coincide with supports of test functions, resulting in each row of the stiffness matrix being integrated over the local support of the test functions. They have also extended this method to a boundary integral technique (Zhu et al. 1998). De and Bathe introduced the method of finite spheres (De and Bathe 2000, 2001) as a special case of MLPG, with additional modifications to improve boundary condition enforcement and quadrature.

A number of other Galerkin meshfree methods have been introduced, a selection of methods is discussed here for the sake of brevity. The natural-element methods (NEMs) (Braun and Sambridge 1995; Sukumar and Belytschko 1998) employ natural neighbor interpolation, based on Voronoi diagrams of a set of arbitrarily distributed points. This includes the Sibson interpolants (Sibson 1980) and Laplace interpolants (non-Sibsonian interpolants) (Belikov et al. 1997), which are positive functions with partition of unity and first order completeness. The radial point interpolation method (RPIM) (Wang and Liu 2002) uses a combination of radial and polynomial basis functions, which gives completeness, the interpolation property, and offers efficient derivative computation. The local RPIM (LRPIM) (Liu and Gu 2001) employs the same approximation, but with a local weak form for a method without background cells. Convex approximations for meshfree computation based on the principle of maximum entropy (MaxEnt) (Jaynes 1957) to achieve unbiased statistical influence of nodal data have been proposed for the Galerkin solution of PDEs (Arroyo and Ortiz 2006; Sukumar 2004). The approximation functions constructed by maximum entropy (a measure of uncertainty) subjected to monomial reproducibility constraints are positive, can interpolate affine functions exactly, and have a weak Kronecker-delta property at the boundary. Based on the framework of optimal transport theory (Benamou and Brenier 1999), the optimal transportation meshfree (OTM) method (Li et al. 2010) has been introduced, which uses maximum entropy approximations. In order to discretize the equations, material points are employed for mass transport, and MaxEnt is employed for mapping of configurations. The MaxEnt

approximation is continually reconstructed and has been applied to fragment-impact problems (Li et al. 2012, 2013). Recently, higher order versions of maximum entropy approximations have been developed (Cyron et al. 2009; González et al. 2010; Rosolen et al. 2013; Sukumar 2013). This approximation, as well as the RK and MLS approximations, were recently generalized under a unified framework (Wu et al. 2011), and have been employed for convex approximations and the weak Kronecker-delta property in the meshfree method (Wang and Chen 2014; Wu et al. 2015; Zhuang et al. 2014).

Several other methods employ a mesh in an unconventional sense to alleviate mesh distortion difficulties in the mesh-based methods. Based on the particle-in-cell methods by Harlow, Brackbill and coauthors (Brackbill and Ruppel 1986; Brackbill et al. 1988; Harlow 1964), Sulsky et al. introduced the material point method (Sulsky and Schreyer 1996; Sulsky et al. 1994, 1995), which employs an Eulerian background mesh for discretization of PDEs while the masses, stresses, and state variables live and are updated at Lagrangian points. The generalization of MPM (Bardenhagen and Kober 2004) to the generalized interpolation material point (GIMP) method avoids the cell-crossing instability due to rough interpolation functions in MPM by employing particle functions that smooth the grid approximation. The convected particle domain interpolation (CPDI) method has been developed to improve GIMP by allowing the particle domains to distort for more accuracy under shear deformation and large rotations (Sadeghirad et al. 2011). CPDI also incorporates a modification to the background discretization to avoid the expensive integration that would be necessary for integrating over the distorted particle domains. The free mesh method (Yagawa and Yamada 1996) reconstructs nodal connectivity of a point cloud for FEM computation on the fly. Similarly, the meshless finite-element method (Idelsohn et al. 2003f) and the particle finite-element method (PFEM) (Idelsohn et al. 2003b, 2004) reconstruct Delaunay tessellations (Idelsohn et al. 2003a) that give bounded $O(n)$ time for efficiency, and use non-Sibsonian interpolation (Belikov et al. 1997). In more recent developments, a second generation of PFEM (PFEM-2) has been proposed that uses a fixed mesh that allows much larger time steps and avoids mesh reconstruction (Idelsohn et al. 2012, 2014).

Collocation Meshfree Methods

An alternative approach to address domain integration issues in the Galerkin meshfree method is by collocation of strong forms. In fact, collocation methods have been around eight decades (Barta 1937; Frazer et al. 1937; Lanczos 1938; Slater 1934). Although methods for interpolation of scattered data have existed for at least five decades (cf. Franke 1982 and references therein), it appears that employing them for strong form collocation methods for solving PDEs did not emerge until Kansa's seminal work (Kansa 1990a, b). The radial basis collocation method (RCBM) (Kansa 1990a, b) employs radial basis functions in the numerical solution of PDEs using strong form collocation. The originator of the radial basis function (RBF) is Hardy (Hardy 1971, 1990) who introduced them for interpolation problems. Hardy showed that multiquadric RBFs are related to a consistent solution of the biharmonic potential problem and thus have a physical foundation (Hardy 1990). It has been shown that RBFs are related to prewavelets (Buhmann and Micchelli 1992; Chui et al. 1996) and multiquadric RBFs and their partial derivatives have exponential convergence (Madych and Nelson 1990). The theoretical foundation of the RBF method for solving PDEs has been established (Franke and Schaback 1998), and error estimates for the solution of smooth problems have been derived (Wendland 1999). A radial basis collocation method has been applied to singularity problems (Hu et al. 2005), Hamilton-Jacobi equations (Cecil et al. 2004), and fourth-order elliptic and parabolic problems (Li 2005). The weights for the weighted radial basis collocation equations for optimal convergence have been derived (Hu et al. 2007). Methods for incorporating weak and strong discontinuities have also been proposed (Chen et al. 2009; Wang et al. 2010), and mixed formulations have been developed for constraint problems (Chi et al. 2014).

Most RBFs with collocation lead to very ill-conditioned discrete systems. Remedies have been suggested by the use of multizone decomposition of the domain (Wong et al. 1999). It has been observed that the condition numbers of the discrete system of direct collocation methods can be greatly reduced by domain decomposition (Kansa and Hon 2000). The shape parameter of an RBF determines the locality of the RBF function and thus greatly influences the linear dependency and in turn the condition number of the discrete system (Hon and Schaback 2001). Localized RBFs have been introduced (Wendland 1995) and truncated multiquadric RBFs have been proposed by Kansa and Hon (2000) to reduce the bandwidth of the discrete system. Global and local RBFs have been investigated (Fasshauer 1999) and smoothing methods and multilevel algorithms have been suggested. More recently, introducing compactly supported partition of unity functions in conjunction with RBFs has been proposed to alleviate ill-conditioning while maintaining exponential convergence (Chen et al. 2008).

Alternatively, approximations such as MLS or RK can be employed for the collocation solution of PDEs, which naturally introduces compactly supported approximations. The finite-point method (Oñate and Idelsohn 1998; Oñate et al. 1996a, b) employs weighted least-squares approximations at each node. Collocation methods based on the RK approximation have also been introduced (Aluru 2000; Hu et al. 2011). It has been shown that strong form collocation methods based on approximations with monomial reproducing conditions exhibit algebraic convergence rates (Hu et al. 2011). Implicit gradients (Li and Liu 1999b, a) have been introduced to ease the burden of computing second order derivatives of RK shape functions in the collocation of second order PDEs (Chi et al. 2013).

The moving particle semi-implicit method (Koshizuka and Oka 1996) has been proposed as an improvement of SPH in the simulation of incompressible fluids. A Lagrangian description is utilized such that the tracking of free surfaces is handled naturally. Derivative approximations based on a weighted average of gradients calculated for each particle pair are employed to solve the Navier-Stokes equation explicitly, and the Poisson problem for pressure is solved implicitly. This method has been applied to the analysis of dam breaking (Koshizuka and Oka 1996), breaking waves (Koshizuka et al. 1998), and vapor explosions (Koshizuka et al. 1999), among others. More recently, several stability enhancements have been proposed for this method (Ataie-Ashtiani and Farhadi 2006; Khayyer and Gotoh 2010, 2011; Kondo and Koshizuka 2011).

A strong form-based meshfree method peridynamics (Silling and Askari 2005) has been proposed based on the reformulation of governing solid mechanics equations into nonlocal integral equations (Silling 2000). Because the governing equations do not contain derivatives, the formulation accommodates the presence of discontinuities without modification. This method has been shown to be a simple and effective approach in modeling fracture and fragmentation as it does not employ explicit tracking of cracks or enrichment functions. A state-based peridynamics (a generalization of the original bond-based method) has been proposed (Silling et al. 2007) to allow standard constitutive models to be employed with the method. Recently, plasticity, viscoplasticity, and continuum damage mechanics have been incorporated in this context

(Foster et al. 2010; Tupek et al. 2013; Warren et al. 2009). Peridynamics has been shown to converge to the local model when the length-scale goes to zero (Silling and Lehoucq 2008). Very recently, this method has been shown to be related to classical meshfree methods (Bessa et al. 2014), where it was demonstrated that for uniform discretizations, the deformation gradient in peridynamics is equivalent to one constructed by implicit gradients with quadratic basis, or Savitzky-Golay filters (Savitzky and Golay 1964).

This paper is organized as follows. MLS and RK type approximations are first introduced in the section "Meshfree Approximation Functions," to demonstrate the unique properties of this class of approximations that rely only on a point discretization, and elucidate the relationship between several meshfree approximations commonly employed. For consistency in presenting the procedures of formulating discrete meshfree equations, and to introduce the recent advances in meshfree solution procedures and their applications, the RK approximation is generally employed throughout the paper although other types of meshfree approximations are available as described previously. In the section "Galerkin-Based Meshfree Method," the Galerkin meshfree method is presented, and the associated approaches for imposing the essential boundary conditions are discussed. Recent advances in domain integration and the associated convergence, stability, and efficiency issues are also addressed. An alternative approach for solving PDEs by strong form collocation with meshfree approximations is presented in the section "Strong Form Collocation-Based Meshfree Method." The well-established radial basis collocation method and the most recent reproducing kernel collocation methods are discussed, and their convergence and stability properties are outlined. Various meshfree formulations for large deformation problems are introduced in the section "Meshfree Method for Large Deformation Problems," and the recent developments of meshfree-based kernel contact formulations and numerical algorithms are also presented. Several application problems in hyperelasticity, plasticity, damage, contact, and fragment-impact are given in the section "Applications of Meshfree Methods" to demonstrate the effectiveness of meshfree methods compared to the conventional finite-element methods. The paper concludes with closing remarks in the section "Conclusions and Outlook."

Meshfree Approximation Functions

In this section, several approximation functions employed in meshfree methods are reviewed. Although there are many, for brevity, a few representative meshfree approximations have been chosen as they form the basis for many Galerkin-based and collocation-based meshfree methods.

Approximations Based on Least-Squares Methods

Let the domain of interest $\bar{\Omega} = \Omega \cup \partial\Omega$ be discretized by a set of Np points $S = \{\mathbf{x}_1, \ldots, \mathbf{x}_{Np} | \mathbf{x}_I \in \bar{\Omega}\}$ with corresponding point numbers that form a set $Z = \{I | \mathbf{x}_I \in S\}$. The weighted least-squares approximation of a set of sample data $\{(\mathbf{x}_I, u_I)\}_{I \in Z}$ near $\bar{\mathbf{x}}$, denoted by $u^h_{\bar{\mathbf{x}}}(\mathbf{x})$, can be expressed as

$$u^h_{\bar{\mathbf{x}}}(\mathbf{x}) = \sum_{i=1}^{n} p_i(\mathbf{x}) b_i(\bar{\mathbf{x}}) = \mathbf{p}(\mathbf{x})^T \mathbf{b}(\bar{\mathbf{x}}) \tag{1}$$

where $\{p_i(\mathbf{x})\}_{i=1}^n$ is the set of basis functions; and $\{b_i(\bar{\mathbf{x}})\}_{i=1}^n$ are the corresponding coefficients that are functions of the local position $\bar{\mathbf{x}}$. The coefficients $\{b_i(\bar{\mathbf{x}})\}_{i=1}^n$ are obtained by the minimization of a weighted least-squares measure, sampled at the discrete points in S

$$J_{\bar{\mathbf{x}}} = \sum_{I \in Z} w_a(\bar{\mathbf{x}} - \mathbf{x}_I)[\mathbf{p}^T(\mathbf{x}_I)\mathbf{b}(\bar{\mathbf{x}}) - u_I]^2 \tag{2}$$

where $w_a(\bar{\mathbf{x}} - \mathbf{x}_I)$ is a weight function with compact support $\omega_I = \{\mathbf{x} | w_a(\mathbf{x} - \mathbf{x}_I) \neq 0\}$; and the support size is denoted as a. The cardinality of the set of point numbers of neighbors of $\mathbf{x}$, $G_{\mathbf{x}} = \{I | w_a(\mathbf{x} - \mathbf{x}_I) \neq 0\}$ defines m neighbors of $\mathbf{x}$ whose weight functions $w_a(\mathbf{x} - \mathbf{x}_I)$ are nonzero at $\mathbf{x}$.

Minimization of $J_{\bar{\mathbf{x}}}$ with respect to $\mathbf{b}(\bar{\mathbf{x}})$ leads to

$$\mathbf{b}(\bar{\mathbf{x}}) = \mathbf{A}(\bar{\mathbf{x}})^{-1} \sum_{I \in G_{\bar{\mathbf{x}}}} w_a(\bar{\mathbf{x}} - \mathbf{x}_I)\mathbf{p}(\mathbf{x}_I)u_I,$$
$$\mathbf{A}(\bar{\mathbf{x}}) = \sum_{I \in G_{\bar{\mathbf{x}}}} \mathbf{p}(\mathbf{x}_I)\mathbf{p}^T(\mathbf{x}_I) w_a(\bar{\mathbf{x}} - \mathbf{x}_I) \tag{3}$$

Substituting Eq. (3) into the local approximation in Eq. (1) the weighted least squares (WLS) approximation can be expressed as

$$u^h_{\bar{\mathbf{x}}}(\mathbf{x}) = \sum_{I \in G_{\bar{\mathbf{x}}}} \Psi_I(\bar{\mathbf{x}}, \mathbf{x}) u_I,$$
$$\Psi_I(\bar{\mathbf{x}}, \mathbf{x}) = \mathbf{p}(\mathbf{x})^T \mathbf{A}(\bar{\mathbf{x}})^{-1} \mathbf{p}(\mathbf{x}_I) w_a(\bar{\mathbf{x}} - \mathbf{x}_I) \tag{4}$$

The WLS approximation constructs a polynomial function (as a function of $\mathbf{x}$), which is a least-squares fit of the local data near $\bar{\mathbf{x}}$, with each data point weighted with $w_a(\bar{\mathbf{x}} - \mathbf{x}_I)$. In the finite-point method (Oñate et al. 1996a), the WLS approximation is employed at each nodal point (setting $\bar{\mathbf{x}} = \mathbf{x}_I$ for each node I).

An interesting case is obtained if $\bar{\mathbf{x}} \to \mathbf{x}$ in Eqs. (1)–(3). The approximation is then no longer defined with respect to some point in the domain $\bar{\mathbf{x}}$, but is only a function of $\mathbf{x}$, and thus a global approximation is obtained in contrast to WLS. Essentially, for any given point $\mathbf{x}$, one finds a weighted least squares fit of the local data, but it is never evaluated anywhere else like in WLS. This approximation is termed the moving-least squares (MLS) approximation (Lancaster and Salkauskas 1981), which is obtained by letting $\bar{\mathbf{x}} \to \mathbf{x}$ in Eqs. (1)–(3):

$$u^h(\mathbf{x}) = \sum_{I \in G_{\mathbf{x}}} \Psi_I(\mathbf{x}) u_I,$$
$$\Psi_I(\mathbf{x}) = \mathbf{p}(\mathbf{x})^T \mathbf{A}(\mathbf{x})^{-1} \mathbf{p}(\mathbf{x}_I) w_a(\mathbf{x} - \mathbf{x}_I),$$
$$\mathbf{A}(\mathbf{x}) = \sum_{I \in G_{\mathbf{x}}} \mathbf{p}(\mathbf{x}_I)\mathbf{p}^T(\mathbf{x}_I) w_a(\mathbf{x} - \mathbf{x}_I) \tag{5}$$

The authors would like to provide remarks as follows:

- By setting $w_a(\bar{\mathbf{x}} - \mathbf{x}_I) = 1$, one obtains the least-squares (LS) approximation

$$u^h(\mathbf{x}) = \sum_{I \in Z} \Psi_I(\mathbf{x}) u_I,$$
$$\Psi_I(\mathbf{x}) = \mathbf{p}(\mathbf{x})^T \mathbf{A}^{-1} \mathbf{p}(\mathbf{x}_I),$$
$$\mathbf{A} = \sum_{I \in G_{\mathbf{x}}} \mathbf{p}(\mathbf{x}_I)\mathbf{p}^T(\mathbf{x}_I) \tag{6}$$

- The relationship between the least squares (LS), weighted least squares (WLS), and moving least squares (MLS) approximations is summarized in Table 1 (Chen and Belytschko 2011);
- In the case that $m = n$ minimization of Eq. (2) leads to the solution $\mathbf{p}^T(\mathbf{x}_I)\mathbf{b}(\mathbf{x}_I) = u_I$, equivalent to enforcing interpolation of the data. In this context, it has been shown that the finite-element approximation can be interpreted as a least-squares fit of the nodal values in each element with $m = n$ (Nayroles et al. 1992);
- In the case $m > n$ a weighted least-squares fit of the data is obtained. This means that the MLS functions $\{\Psi_I(\mathbf{x})\}_{I \in Z}$ are

J. Eng. Mech., 2017, 143(4): 04017001

Table 1. Comparison of LS, WLS, and MLS Approximations

Method	Approximation	Least-squares measure	Least-squares approximation
LS	$u^h(\mathbf{x}) = \mathbf{p}(\mathbf{x})^T\mathbf{b}$	$J = \sum_{I\in Z}[\mathbf{p}^T(\mathbf{x}_I)\mathbf{b} - u_I]^2$	$u^h(\mathbf{x}) = \mathbf{p}(\mathbf{x})^T\mathbf{A}^{-1}\sum_{I\in Z}\mathbf{p}(\mathbf{x}_I)u_I$ $\mathbf{A} = \sum_{I\in Z}\mathbf{p}(\mathbf{x}_I)\mathbf{p}^T(\mathbf{x}_I)$
WLS	$u^h_{\bar{\mathbf{x}}}(\mathbf{x}) = \mathbf{p}(\mathbf{x})^T\mathbf{b}(\bar{\mathbf{x}})$	$J_{\bar{\mathbf{x}}} = \sum_{I\in G_{\bar{\mathbf{x}}}} w_a(\bar{\mathbf{x}} - \mathbf{x}_I)[\mathbf{p}^T(\mathbf{x}_I)\mathbf{b}(\bar{\mathbf{x}}) - u_I]^2$	$u^h_{\bar{\mathbf{x}}} = \mathbf{p}(\mathbf{x})^T\mathbf{A}^{-1}(\bar{\mathbf{x}})\sum_{I\in G_{\bar{\mathbf{x}}}}\mathbf{p}(\mathbf{x}_I)w_a(\bar{\mathbf{x}} - \mathbf{x}_I)u_I$ $\mathbf{A}(\bar{\mathbf{x}}) = \sum_{I\in G_{\bar{\mathbf{x}}}}\mathbf{p}(\mathbf{x}_I)\mathbf{p}^T(\mathbf{x}_I)w_a(\bar{\mathbf{x}} - \mathbf{x}_I)$
MLS	$u^h(\mathbf{x}) = \mathbf{p}(\mathbf{x})^T\mathbf{b}(\mathbf{x})$	$J_{\mathbf{x}} = \sum_{I\in G_{\mathbf{x}}} w_a(\mathbf{x} - \mathbf{x}_I)[\mathbf{p}^T(\mathbf{x}_I)\mathbf{b}(\mathbf{x}) - u_I]^2$	$u^h(\mathbf{x}) = \mathbf{p}(\mathbf{x})^T\mathbf{A}(\mathbf{x})^{-1}\sum_{I\in G_{\mathbf{x}}}\mathbf{p}(\mathbf{x}_I)w_a(\mathbf{x} - \mathbf{x}_I)u_I$ $\mathbf{A}(\mathbf{x}) = \sum_{I\in G_{\mathbf{x}}}\mathbf{p}(\mathbf{x}_I)\mathbf{p}^T(\mathbf{x}_I)w_a(\mathbf{x} - \mathbf{x}_I)$

not interpolants, and u_I is not the nodal value of $u^h(\mathbf{x})$, i.e., $u^h(\mathbf{x}_I) \neq u_I$. The imposition of Dirichlet boundary conditions in the Galerkin approximation requires a different approach than in FEM, and will be discussed in the section "Enforcement of Essential Boundary Conditions";

- Choosing constant basis $\mathbf{p}(\mathbf{x}) = \{1\}$ in MLS results in a Shepard function (Shepard 1968);
- The order of continuity in the weight function determines the order of continuity in the MLS approximation. The weight function is directly analogous to the kernel function in the RK approximation, so the discussion of constructing weights is deferred to section "Construction of Weight Functions and Kernel Functions for MLS and RK";
- If the basis function vector consists of complete monomials, that is, $\mathbf{p}^T(\mathbf{x}) = \{\mathbf{x}^\alpha\}^n_{|\alpha|=0}$, $\mathbf{x}^\alpha \equiv x_1^{\alpha_1}\cdot x_2^{\alpha_2},\ldots,x_d^{\alpha_d}$, $|\alpha| = \sum_{i=1}^d \alpha_i$, then the approximation in Eq. (5) is nth order complete

$$\sum_{I\in G_{\mathbf{x}}}\Psi_I(\mathbf{x})\mathbf{p}(\mathbf{x}_I) = \mathbf{p}(\mathbf{x}) \tag{7}$$

- At any given point $\mathbf{x}$, a sufficient number of points' weight functions need to cover $\mathbf{x}$ for $\mathbf{A}(\mathbf{x})$ to be invertible. In addition, the points' position cannot be collinear (or coplanar in three dimensions) so that a linearly dependent system is avoided, see Liu et al. (1997c) for details; and
- For better conditioning of $\mathbf{A}(\mathbf{x})$, MLS with shifted and normalized bases can be considered

$$\Psi_I(\mathbf{x}) = \mathbf{p}(\mathbf{0})^T\mathbf{A}(\mathbf{x})^{-1}\mathbf{p}\left(\frac{\mathbf{x}-\mathbf{x}_I}{a}\right)w_a(\mathbf{x}-\mathbf{x}_I),$$
$$\mathbf{A}(\mathbf{x}) = \sum_{I\in G_{\mathbf{x}}}\mathbf{p}\left(\frac{\mathbf{x}-\mathbf{x}_I}{a}\right)\mathbf{p}^T\left(\frac{\mathbf{x}-\mathbf{x}_I}{a}\right)w_a(\mathbf{x}-\mathbf{x}_I) \tag{8}$$

The MLS approximation in Eq. (5) was introduced for surface fitting through a given data set $\{(\mathbf{x}_I, u_I)\}_{I\in Z}$ (Lancaster and Salkauskas 1981; Liszka 1984). This approach was later rediscovered in the diffuse-element method (Nayroles et al. 1992) for solving PDEs, where $\Psi_I(\mathbf{x})$ is used as an approximation function, and u_I in Eq. (5) became the unknown coefficients to be solved by the Galerkin procedure. In the diffuse-element method, derivatives in the weak form are approximated by the differentiation of the basis functions in Eq. (1), which are considered diffuse derivatives, which will be discussed further in the section "Derivative Approximations in Meshfree Methods."

The celebrated element free Galerkin method by Belytschko (Belytschko 1994b, 1995a; Lu et al. 1994), which is regarded as the pioneering work that popularized meshfree methods, is an improvement of DEM where the full derivatives of the MLS approximation are used in the Galerkin method. The MLS approximation is also employed in MLPG (Atluri and Zhu 1998), moving least squares particle hydrodynamics (MLSPH) (Dilts 1999), moving least squares RKPM (Li and Liu 1996; Liu et al. 1997c), hp clouds (Duarte and Oden 1996b, a), and the finite-point method (Oñate et al. 1996a) among others (Fig. 2).

Kernel Estimate

The concept of a kernel estimate (KE) was first introduced by Lucy (1977) and Gingold and Monaghan (1977) as a starting point of formulating SPH. Although in SPH the kernel estimate is applied directly to a PDE, the smoothing function used in this process plays the same role as the test function in the Galerkin approximation. To examine the completeness in the KE, consider the kernel estimate of a function $u(\mathbf{x})$, denoted by $u^h(\mathbf{x})$, as

$$u^h(\mathbf{x}) = \int_{\mathbb{R}^d} u(\mathbf{s})\varphi_a(\mathbf{x}-\mathbf{s})d\mathbf{s} \tag{9}$$

where $\varphi_a(\mathbf{x})$ is a kernel function (called a smoothing function in SPH) with support measure a. If the compactly supported kernel $\varphi_a(\mathbf{x})$ mimics a delta function

1. $\varphi_a(\mathbf{x}) \to \delta(\mathbf{x})$ as $a \to 0$; and
2. $\int\varphi_a(\mathbf{x})d\Omega = 1$.

then the kernel estimate of a function when $a \to 0$ can be obtained by replacing $\varphi_a(\mathbf{x}-\mathbf{s})$ by $\delta(\mathbf{x}-\mathbf{s})$ in Eq. (9), and thus $u^h(\mathbf{x}) \to u(\mathbf{x})$ as $a \to 0$.

Considering a finite domain, the integration in Eq. (9) can then be carried out numerically at the set of points S, as before, as

$$u^h(\mathbf{x}) = \int_\Omega \phi_a(\mathbf{x}-\mathbf{s})u(\mathbf{s})\mathbf{ds} \simeq \sum_{I\in G_{\mathbf{x}}}\phi_a(\mathbf{x}-\mathbf{x}_I)\Delta V_I u_I \tag{10}$$

The approximation in Eq. (10) can be written in terms of KE shape functions $\Psi_I(\mathbf{x})$

$$u^h(\mathbf{x}) = \sum_{I\in G_{\mathbf{x}}}\Psi_I(\mathbf{x})u_I,$$
$$\Psi_I(\mathbf{x}) = \phi_a(\mathbf{x}-\mathbf{x}_I)\Delta V_I \tag{11}$$

For kernels with properties such as normalization and symmetry, the KE approximation can satisfy partition of unity or even first order completeness under certain conditions such as in uniform node distributions of the interior of the domain. However, near the boundary and in irregular node distributions, partition of unity is not satisfied in general, as illustrated in Fig. 4. This has motivated the development of several corrections to SPH [there are numerous reviews, refer to Li and Liu (2007) for more details] and alternative meshfree methods such as RKPM (Chen et al. 1996; Liu et al. 1995a, b).

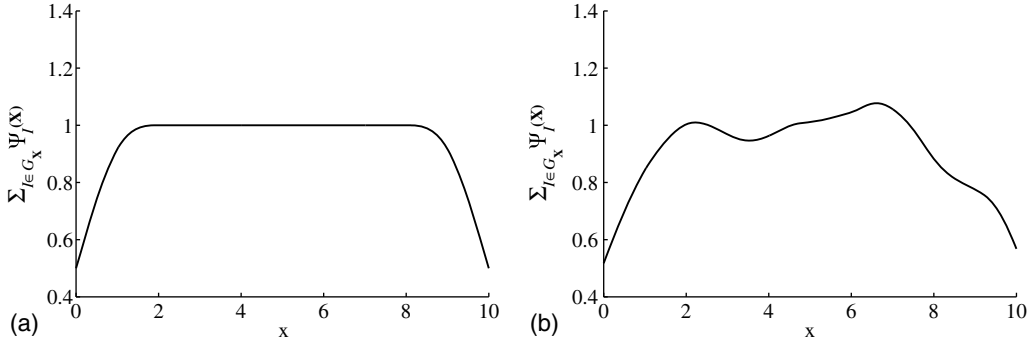

Fig. 4. Partition of unity check of KE approximation in (a) uniform discretization; (b) nonuniform discretization

Reproducing Kernel Approximation

The reproducing kernel particle method (Chen et al. 1996; Liu et al. 1995a, b) was formulated based on the reproducing kernel (RK) approximation under the Galerkin framework. The RK approximation (Liu et al. 1995a, b) was proposed for solving PDEs to improve the accuracy of the SPH method for finite domain problems. In this method, the kernel function in the kernel estimate was modified by introducing a correction function to allow reproduction of various functions

$$u^h(\mathbf{x}) = \int_\Omega \Phi(\mathbf{x}, \mathbf{x}-\mathbf{s})u(\mathbf{s})\mathrm{d}\mathbf{s},$$
$$\Phi(\mathbf{x}, \mathbf{x}-\mathbf{s}) = \phi_a(\mathbf{x}-\mathbf{s})C(\mathbf{x}, \mathbf{x}-\mathbf{s}),$$
$$C(\mathbf{x}, \mathbf{x}-\mathbf{s}) = \mathbf{P}^T(\mathbf{x}-\mathbf{s})\mathbf{c}(\mathbf{x}) \tag{12}$$

where $C(\mathbf{x}, \mathbf{x}-\mathbf{s})$ is the correction function. The vector $\mathbf{P}(\mathbf{x}-\mathbf{s})$ forms a basis, while the coefficients $\mathbf{c}(\mathbf{x})$ are solved for by considering the Taylor expansion of $u(\mathbf{s})$

$$u(\mathbf{s}) = \sum_{|\alpha|=0}^{\infty} \frac{(-1)^\alpha}{\alpha!}(\mathbf{x}-\mathbf{s})^\alpha \partial^\alpha u(\mathbf{x}) \tag{13}$$

where α is a multi-index with the notation $\alpha=(\alpha_1,\alpha_2,\ldots,\alpha_d)$, $|\alpha|=\alpha_1+\alpha_2+\cdots+\alpha_d$; $\mathbf{x}^\alpha=x_1^{\alpha_1}\cdot x_2^{\alpha_2},\ldots,x_d^{\alpha_d}$; $\alpha!=\alpha_1!\alpha_2!,\ldots,\alpha_d!$; and $\partial^\alpha=\partial^{\alpha_1}\partial^{\alpha_2},\ldots,\partial^{\alpha_d}/\partial x_1^{\alpha_1}\partial x_2^{\alpha_2},\ldots,\partial x_d^{\alpha_d}$. Substituting Eq. (13) into the kernel estimation in Eq. (12) leads to

$$u^h(\mathbf{x}) = \tilde{m}_0(\mathbf{x})u(\mathbf{x}) + \sum_{|\alpha|=1}^{\infty} \frac{(-1)^\alpha}{\alpha!}\tilde{m}_\alpha(\mathbf{x})\partial^\alpha u(\mathbf{x}),$$
$$\tilde{m}_0(\mathbf{x}) = \int_\Omega \Phi(\mathbf{x}, \mathbf{x}-\mathbf{s})\mathrm{d}\mathbf{s},$$
$$\tilde{m}_\alpha(\mathbf{x}) = \int_\Omega (\mathbf{x}-\mathbf{s})^\alpha \Phi(\mathbf{x}, \mathbf{x}-\mathbf{s})\mathrm{d}\mathbf{s} \tag{14}$$

For nth order completeness, the following conditions for the *moments* $\tilde{m}_\alpha(\mathbf{x})$ should be satisfied

$$\tilde{m}_0(\mathbf{x}) = 1,$$
$$\tilde{m}_\alpha(\mathbf{x}) = 0, \quad |\alpha| = 1, \ldots, n \tag{15}$$

These conditions can be expressed as

$$\left\{\int_\Omega \mathbf{P}(\mathbf{x}-\mathbf{s})\mathbf{P}^T(\mathbf{x}-\mathbf{s})\mathrm{d}\mathbf{s}\right\}\mathbf{c}(\mathbf{x}) = \mathbf{P}(\mathbf{0}) \tag{16}$$

Solving for $\mathbf{c}(\mathbf{x})$, one obtains the continuous reproducing kernel approximation

$$u^h(\mathbf{x}) = \int_\Omega \Phi(\mathbf{x}, \mathbf{x}-\mathbf{s})u(\mathbf{s})d\mathbf{s},$$
$$\Phi(\mathbf{x}, \mathbf{x}-\mathbf{s}) = \phi_a(\mathbf{x}-\mathbf{s})\mathbf{P}^T(\mathbf{0})\mathbf{M}^{-1}(\mathbf{x})\mathbf{P}(\mathbf{x}-\mathbf{s}),$$
$$\mathbf{M}(\mathbf{x}) = \int_\Omega \mathbf{P}(\mathbf{x}-\mathbf{s})\mathbf{P}^T(\mathbf{x}-\mathbf{s})\mathrm{d}\mathbf{s} \tag{17}$$

where $\mathbf{M}(\mathbf{x})$ is the moment matrix; the term comes from the vanishing moments of the Taylor expansion of $u(\mathbf{s})$.

In practice, numerical integration must be employed in order to form an approximation, which can be carried out as

$$u^h(\mathbf{x}) = \sum_{I\in G_\mathbf{x}} \Phi(\mathbf{x}, \mathbf{x}-\mathbf{x}_I)u_I\Delta V_I \equiv \sum_{I\in G_\mathbf{x}} \Psi_I(\mathbf{x})u_I,$$
$$\Phi(\mathbf{x}, \mathbf{x}-\mathbf{x}_I) = \phi_a(\mathbf{x}-\mathbf{x}_I)\mathbf{P}^T(\mathbf{0})\mathbf{M}^{-1}(\mathbf{x})\mathbf{P}(\mathbf{x}-\mathbf{x}_I),$$
$$\mathbf{M}(\mathbf{x}) = \sum_{I\in G_\mathbf{x}} \mathbf{P}(\mathbf{x}-\mathbf{x}_I)\mathbf{P}^T(\mathbf{x}-\mathbf{x}_I)\Delta V_I \tag{18}$$

The shape functions in Eq. (18) and their summation are shown in Fig. 5 for $n = 1$ for illustration, where the same kernel as the KE is employed, demonstrating that the correction corrects incompleteness in the KE approximation near boundaries in uniform discretizations. The KE and corresponding RK shape functions and their summation is shown in Fig. 6 for a nonuniform discretization, which demonstrates that the RK approximation also corrects for incompleteness in the KE in nonuniform node distributions as well. The RK approximation can also provide arbitrarily higher order completeness if desired.

Chen et al. (1996) showed that the numerical integration of the moment matrix and the RK approximation in Eq. (17) must be evaluated in a consistent manner [i.e., using the same quadrature weights ΔV_I in Eq. (18)] in order to preserve the consistency of the approximation. A discrete reproducing kernel approximation was then introduced that satisfies the reproducing conditions while omitting the quadrature weights (Chen et al. 1997)

$$u^h(\mathbf{x}) = \sum_{I\in G_\mathbf{x}} \Phi_I(\mathbf{x})u_I,$$
$$\Psi_I(\mathbf{x}) = \mathbf{p}^T(\mathbf{x}-\mathbf{x}_I)\mathbf{c}(\mathbf{x})\phi_a(\mathbf{x}-\mathbf{x}_I) \tag{19}$$

Under the discrete framework, $\phi_a(\mathbf{x}-\mathbf{x}_I)$ plays the same role as the weight function $w_a(\mathbf{x}-\mathbf{x}_I)$ in MLS. The coefficient vector $\mathbf{c}(\mathbf{x})$ is obtained by enforcing the exact reproduction of the bases, that is, if $u_I = p_i(\mathbf{x}_I)$, then $u^h(\mathbf{x}) = p_i(\mathbf{x})$

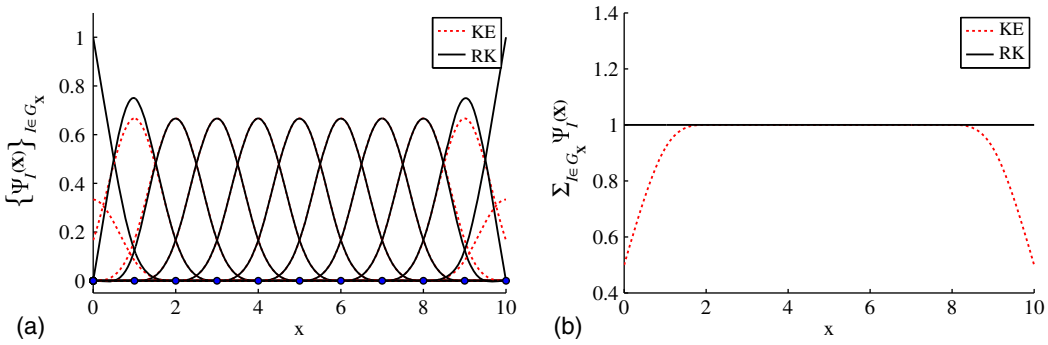

Fig. 5. KE and RK approximations in a uniform discretization: (a) shape functions; (b) partition of unity check

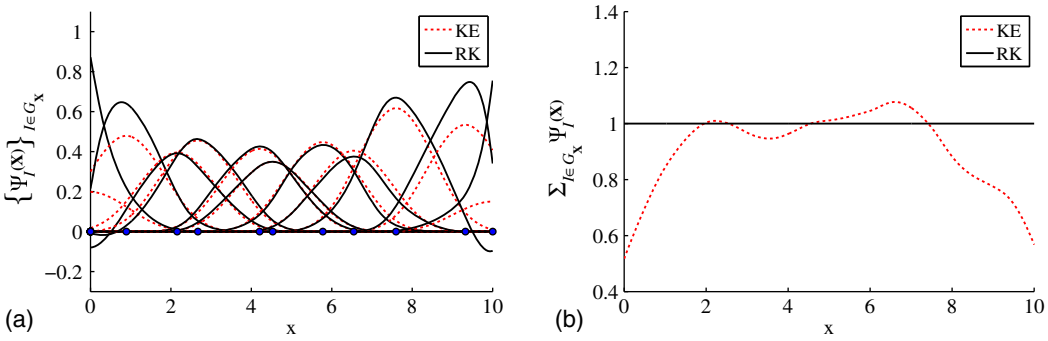

Fig. 6. KE and RK approximations in a nonuniform discretization: (a) shape functions; (b) partition of unity check

$$\sum_{I\in G_x}\Phi_I(\mathbf{x})\mathbf{p}(\mathbf{x}_I)=\mathbf{p}(\mathbf{x}) \tag{20}$$

When $\{p_i(\mathbf{x})\}_{i=1}^n$ is a set of complete monomials, obtaining $\mathbf{c}(\mathbf{x})$ from Eq. (20) yields the same approximation as MLS in Eq. (5), and the remarks in the section "Approximations Based on Least-Squares Methods" apply. Conversely, if nonmonomial bases are used as $\{p_i(\mathbf{x})\}_{i=1}^n$, solving $\mathbf{c}(\mathbf{x})$ from Eq. (20) yields a different approximation than MLS. Further, the RK approximation can be extended to achieve synchronized convergence (Li and Liu 1998, 1999b, a) and implicit gradient approximations (Chen et al. 2004), which deviate from the MLS approximation as will be discussed in the section "Derivative Approximations in Meshfree Methods." Detailed discussions of RK approximation properties can be found in the literature [cf. (Han et al. 2002; Liu et al. 1996b, 1997c)]. The RK approximation is the basis of the reproducing kernel particle method (RKPM) (Chen et al. 1996; Liu et al. 1995b), the reproducing kernel collocation method (RKCM) (Hu et al. 2011), among others (Figs. 2 and 3).

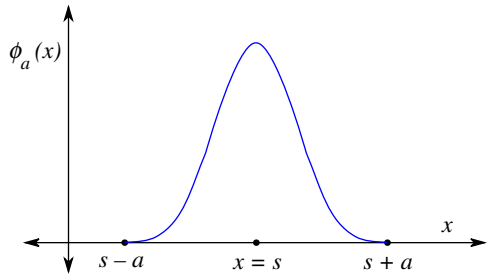

Fig. 7. Kernel function

Construction of Weight Functions and Kernel Functions for MLS and RK

Hereafter the terms kernel and weights are used interchangeably, as they play the exact same role in the least squares of Eqs. (1) and (2) and discrete RK of Eqs. (19) and (20) approximations. Typically kernel functions are chosen as smooth, compactly supported functions. For example, the cubic B-spline kernel function shown in Fig. 7 is

$$\phi_a(x-s)\equiv\phi_a(z)=\begin{cases}\frac{2}{3}-4z^2+4z^3 & \text{for } 0\le z\le\frac{1}{2}\\ \frac{4}{3}-4z+4z^2-\frac{4}{3}z^3 & \text{for } \frac{1}{2}\le z\le 1\\ 0 & \text{for } z>1\end{cases},\quad z=\frac{|x-s|}{a} \tag{21}$$

A multidimensional kernel function $\phi_a(\mathbf{x}-\mathbf{x}_I)$ can be constructed by using the kernel function in one-dimension with box support as

$$\phi_a(\mathbf{x}-\mathbf{x}_I)=\prod_{i=1}^{d}\phi_{a_i}(x_i-x_{iI}) \tag{22}$$

Alternatively, one can construct a multidimensional kernel with spherical support from the one-dimensional kernel as

$$\phi_a(\mathbf{x}-\boldsymbol{s})=\phi_a(z),\quad z=\frac{\|\mathbf{x}-\mathbf{s}\|}{a} \tag{23}$$

The box support in Eq. (22) and spherical support in Eq. (23) are illustrated in Fig. 8.

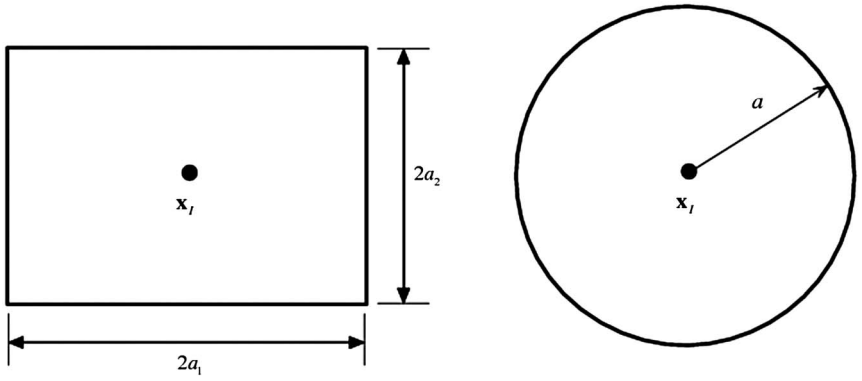

Fig. 8. Supports of the two-dimensional kernel function: (a) rectangular; (b) circular

Partition of Unity Methods

The hp clouds (HPC) (Duarte and Oden 1996b, a) and the generalized finite-element method (GFEM) (Duarte et al. 2000; Strouboulis et al. 2001) were developed based on the general framework of the partition of unity (Babuška and Melenk 1997; Melenk and Babuška 1996). The partition of unity property is essential for convergence in Galerkin approximation of PDEs (Babuška and Melenk 1997). Let a domain be covered by overlapping patches ω_I, $\bar{\Omega} \subset \cup_{I \in Z} \omega_I$, each of which is associated with a function that is nonzero only in ω_I, and has the following property:

$$\sum_{I \in G_{\mathbf{x}}} \Psi_I^0(\mathbf{x}) = 1 \tag{24}$$

An example of a partition of unity function is the Shepard function. The partition of unity can be used as a paradigm for construction of approximation functions with desired order of completeness or with enrichment of special bases representing characteristics of the PDEs. An example of PU is the following approximation (Babuška and Melenk 1997):

$$u^h(\mathbf{x}) = \sum_{I \in G_{\mathbf{x}}} \Psi_I^0(\mathbf{x}) \left[\sum_{i=1}^{k} a_{iI} P_i(\mathbf{x}) + \sum_{i=1}^{l} q_{iI} g_i(\mathbf{x}) \right] \tag{25}$$

where $\{P_i(\mathbf{x})\}_{i=1}^k$ are monomial bases used to impose completeness; and $\{q_{iI}(\mathbf{x})\}_{i=1}^l$ are other enhancement functions. Eq. (25) is called an *extrinsic* adaptivity.

MLS and RK with constant basis yields a PU function $\Psi_I^0(\mathbf{x})$, and MLS and RK with complete monomials of degree k, denoted as $\Psi_I^k(\mathbf{x})$, can be viewed as PU with *intrinsic* enrichment (adding functions to the bases) (Belytschko et al. 1996b). Duarte and Oden (1996a) extended PU with extrinsic refinement as follows:

$$u^h(\mathbf{x}) = \sum_{I \in G_{\mathbf{x}}} \Phi_I^k(\mathbf{x}) \left[u_I + \sum_{i=1}^{l} b_{iI} q_i(\mathbf{x}) \right] \tag{26}$$

where $q_i(\mathbf{x})$ is an extrinsic basis which can be a monomial basis of any order greater than k or a special enhancement function. The extrinsic adaptivity allows the basis to vary from node to node, whereas intrinsic basis in MLS and RK cannot be changed without introducing a discontinuity. A good overview and comparison of the meshfree approximations discussed can be found in the literature [cf. (Belytschko et al. 1996b; Li and Liu 2007; Liu 2009)]. A reproducing kernel element method (RKEM) that uses finite element shape functions as the PU function with enriched bases has been proposed to achieve combined advantages of FEM (Kronecker-delta property) and polynomial reproducibility (Liu et al. 2004).

Derivative Approximations in Meshfree Methods

Several techniques have been employed for approximating derivatives in meshfree methods. Remarkably, though several researchers independently arrived at various approximations that seem unique, all of the approximations discussed in this paper are very closely related, and in most cases equivalent. The derivations of these methods can be unified and made clear under the discrete RK/MLS approximation with nonshifted monomial basis.

Direct Derivatives

The simplest way to obtain an approximation of derivatives is to directly differentiate an approximation of the primary variable. In this way, the derivatives in the solution of PDEs are consistent with the approximation. This was first introduced in the EFG method (Belytschko et al. 1994b) for solving the PDEs with MLS. If the MLS approximation in Eq. (5) is considered, an approximation for the derivative can be obtained by differentiating the approximation of the primary variable

$$\begin{aligned} \partial^\alpha u(\mathbf{x}) \simeq \partial^\alpha u^h(\mathbf{x}) &= \sum_{I \in G_{\mathbf{x}}} \partial^\alpha \Psi_I(\mathbf{x}) u_I, \\ \partial^\alpha \Psi_I(\mathbf{x}) &= \partial^\alpha \mathbf{p}(\mathbf{x})^T \mathbf{A}(\mathbf{x})^{-1} \mathbf{p}(\mathbf{x}_I) w_a(\mathbf{x} - \mathbf{x}_I) \\ &\quad + \mathbf{p}(\mathbf{x})^T \partial^\alpha \mathbf{A}(\mathbf{x})^{-1} \mathbf{p}(\mathbf{x}_I) w_a(\mathbf{x} - \mathbf{x}_I) \\ &\quad + \mathbf{p}(\mathbf{x})^T \mathbf{A}(\mathbf{x})^{-1} \mathbf{p}(\mathbf{x}_I) \partial^\alpha w_a(\mathbf{x} - \mathbf{x}_I) \end{aligned} \tag{27}$$

where α is a multi-index. The cost of computing the previous equation is generally high because the cost in computing MLS/RK shape functions is mostly comprised of matrix operations (Hu et al. 2009). Thus, differentiation of $\mathbf{A}(\mathbf{x})^{-1}$, and the many matrix operations involved makes this type of derivative computationally expensive. Conversely, using these definitions, one is able to obtain higher accuracy in the solution of PDEs than diffuse derivatives used in DEM (Belytschko et al. 1994b). The direct derivative is employed in most Galerkin and collocation methods.

Diffuse Derivatives

In the diffuse-element method (Nayroles et al. 1992), derivatives in the Galerkin equation are approximated by diffuse derivatives of $u^h(\mathbf{x})$. In this method, when differentiating the MLS approximation, the derivatives of the coefficients of the bases in Eq. (1) are neglected, which actually vary due to the moving nature of the

approximation ($\bar{\mathbf{x}} \to \mathbf{x}$). To make this clear, examining Eqs. (1) and (5) one can observe that for the MLS approximation

$$u^h(\mathbf{x}) = \underbrace{\mathbf{p}(\mathbf{x})^T \mathbf{A}(\mathbf{x})^{-1} \sum_{I \in G_{\mathbf{x}}} \mathbf{p}(\mathbf{x}_I) w_a(\mathbf{x} - \mathbf{x}_I) u_I}_{\mathbf{b}(\mathbf{x})} \tag{28}$$

In the diffuse derivatives, the derivatives of $u(\mathbf{x})$ are approximated as

$$\begin{aligned} \partial^\alpha u(\mathbf{x}) &\simeq \partial^\alpha \mathbf{p}(\mathbf{x})^T \mathbf{b}(\mathbf{x}) \\ &= \partial^\alpha \mathbf{p}(\mathbf{x})^T \mathbf{A}(\mathbf{x})^{-1} \sum_{I \in G_{\mathbf{x}}} \mathbf{p}(\mathbf{x}_I) w_a(\mathbf{x} - \mathbf{x}_I) u_I \\ &\equiv \sum_{I \in G_{\mathbf{x}}} \Psi_I^\alpha(\mathbf{x}) u_I \end{aligned} \tag{29}$$

By employing Eq. (29) the approximation to $\partial^\alpha u(\mathbf{x})$ is just as smooth as the approximation to $u(\mathbf{x})$, and it retains the completeness properties of the true derivative $\partial^\alpha u^h(\mathbf{x})$ (Nayroles et al. 1992). One other advantage of this method is that taking derivatives of $\mathbf{A}(\mathbf{x})^{-1}$ is circumvented, although at the cost of accuracy in the solution of PDEs as mentioned earlier.

The diffuse derivative can be derived as follows. Rather than differentiating the approximation of the primary variable to obtain an approximation of derivatives, one can consider constructing an approximation to the derivative directly. First, at a given fixed point $\bar{\mathbf{x}}$, one can construct a weighted least-squares approximation as in Eq. (4). Then, an approximation to $\partial^\alpha u(\mathbf{x})$ at $\bar{\mathbf{x}}$, can be obtained by differentiation of that approximation with respect to the moving variable $\mathbf{x}$

$$\begin{aligned} \partial^\alpha u(\mathbf{x}) \simeq \partial^\alpha u^h_{\bar{\mathbf{x}}}(\mathbf{x}) &= \sum_{I \in G_{\bar{\mathbf{x}}}} \partial^\alpha \Psi_I(\mathbf{x}, \bar{\mathbf{x}}) u_I, \\ \partial^\alpha \Psi_I(\mathbf{x}, \bar{\mathbf{x}}) &= \partial^\alpha \mathbf{p}(\mathbf{x})^T \mathbf{A}(\bar{\mathbf{x}})^{-1} \mathbf{p}(\mathbf{x}_I) w_a(\bar{\mathbf{x}} - \mathbf{x}_I), \\ \mathbf{A}(\bar{\mathbf{x}}) &= \sum_{I \in G_{\bar{\mathbf{x}}}} \mathbf{p}(\mathbf{x}_I) \mathbf{p}^T(\mathbf{x}_I) w_a(\bar{\mathbf{x}} - \mathbf{x}_I) \end{aligned} \tag{30}$$

Finally, the approximation is made global by taking $\bar{\mathbf{x}} \to \mathbf{x}$ as in the MLS approximation

$$\partial^\alpha u(\mathbf{x}) \simeq [\partial^\alpha u^h_{\bar{\mathbf{x}}}(\mathbf{x})]_{\bar{\mathbf{x}} \to \mathbf{x}} = \sum_{I \in G_{\mathbf{x}}} \Psi_I^\alpha(\mathbf{x}) u_I \tag{31}$$

where Ψ_I^α is the diffuse derivative shape function in Eq. (29).

Implicit Gradients and Synchronized Derivatives

The implicit gradient was introduced as a regularization in strain localization problems without taking direct derivatives (Chen et al. 2004), where the idea came directly from the synchronized RK approximation (Li and Liu 1998, 1999b, a) as a way to approximate derivatives. In the implicit gradient method, derivative approximations are constructed directly by employing the same form as the RK shape function in Eq. (19)

$$\Psi_I^\alpha(\mathbf{x}) = \mathbf{c}^\alpha(\mathbf{x}) \mathbf{p}(\mathbf{x} - \mathbf{x}_I) \phi_a(\mathbf{x} - \mathbf{x}_I) \tag{32}$$

The coefficients $\mathbf{c}^\alpha(\mathbf{x})$ are obtained from the following gradient reproducing conditions, analogous to Eq. (20)

$$\sum_{I \in G_{\mathbf{x}}} \Psi_I^\alpha(\mathbf{x}) \mathbf{p}(\mathbf{x}) = \partial^\alpha \mathbf{p}(\mathbf{x}) \tag{33}$$

Following the usual procedures in RK approximations, the implicit gradient RK approximation can be obtained as

$$\begin{aligned} \partial^\alpha u(\mathbf{x}) &\simeq \sum_{I \in G_{\mathbf{x}}} \Psi_I^\alpha(\mathbf{x}) u_I, \\ \Psi_I^\alpha(\mathbf{x}) &= \partial^\alpha \mathbf{p}(\mathbf{x})^T \mathbf{M}(\mathbf{x})^{-1} \mathbf{p}(\mathbf{x}_I) w_a(\mathbf{x} - \mathbf{x}_I), \\ \mathbf{M}(\mathbf{x}) &= \sum_{I \in G_{\mathbf{x}}} \mathbf{p}(\mathbf{x}_I) \mathbf{p}^T(\mathbf{x}_I) w_a(\mathbf{x} - \mathbf{x}_I) \end{aligned} \tag{34}$$

Comparing Eq. (34) to Eq. (29), one can see that implicit gradient are indeed diffuse derivatives. Implicit gradients have been employed for regularization in strain localization problems (Chen et al. 2004) to avoid the need of ambiguous boundary conditions associated with the standard gradient-type regularization methods, and easing the computational cost of meshfree collocation methods (Chi et al. 2013). The idea has also been introduced as a stabilization of meshfree solutions of convection dominated problems without the need for high order differentiation of the test function (Hillman and Chen 2016).

It has been shown that Eq. (34) is equivalent to (Chen et al. 2004)

$$\begin{aligned} \Psi_I^\alpha(\mathbf{x}) &= \mathbf{p}^\alpha \mathbf{M}(\mathbf{x})^{-1} \mathbf{p}(\mathbf{x} - \mathbf{x}_I) w_a(\mathbf{x} - \mathbf{x}_I), \\ \mathbf{M}(\mathbf{x}) &= \sum_{I \in G_{\mathbf{x}}} \mathbf{p}(\mathbf{x} - \mathbf{x}_I) \mathbf{p}^T(\mathbf{x} - \mathbf{x}_I) w_a(\mathbf{x} - \mathbf{x}_I), \\ \mathbf{p}^\alpha &= [0, \quad \ldots, \quad 0, \quad \underset{\uparrow \alpha \text{ entry}}{\alpha!(-1)^{|\alpha|}}, \quad 0, \quad \ldots, \quad 0]^T, \end{aligned} \tag{35}$$

which is the same expression as the synchronized derivatives (Li and Liu 1998, 1999b, a), scaled by $\alpha!$, with the difference in sign emanating from the convention in shifting the bases. In this form the reproduction of derivative terms can be seen by examining alternative vanishing moment conditions in Eqs. (14) and (15). Using this idea, it was shown that by employing certain linear combinations of synchronized derivatives and the RK approximation, synchronized convergence can be obtained in the L_2 norm and H^k norms up to some order k with the proper selection of coefficients C^α in the following (Li and Liu 1998):

$$\tilde{\Psi}_I(\mathbf{x}) = \Psi_I(\mathbf{x}) + \sum_{|\alpha|=1}^{n} C^\alpha \Psi_I^\alpha(\mathbf{x}) \tag{36}$$

Because the additional terms in the previous equation satisfy partition of nullity, they termed the resulting approximation in Eq. (36) a hierarchical partition of unity (Li and Liu 1999b, a). Synchronized derivatives have been developed for improving accuracy in the Helmholtz equation, obtaining high resolution in localization problems, and stabilization in computational fluid dynamics (Li and Liu 1999a).

Generalized Finite Difference Methods

The finite difference work by Liszka and Orkisz (1980) and Liszka (1984) generalized previous works in finite differences to arbitrary point distributions. Derivative approximations were constructed directly by satisfaction of truncated Taylor expansions. The generalized finite difference method starts with the Taylor expansion of function $u(\mathbf{x})$ about at point $u(\mathbf{x}_I)$ truncated to a given order n (Liszka 1984)

$$u(\mathbf{x}_I) = \sum_{|\alpha|=0}^{n} \frac{(-1)^\alpha}{\alpha!} (\mathbf{x} - \mathbf{x}_I)^\alpha \partial^\alpha u(\mathbf{x}) \tag{37}$$

In order to solve for approximations of the derivatives, and the approximation of $u(\mathbf{x})$, the previous equation can be evaluated at m points in a stencil (or star in GFD terminology) surrounding $\mathbf{x}$, and one obtains the system

$$\mathbf{u} = \mathbf{R}(\mathbf{x})\mathbf{J}\mathbf{u}^h(\mathbf{x}) \equiv \mathbf{R}(\mathbf{x})\mathbf{u}^h_{\mathbf{J}}(\mathbf{x}) \tag{38}$$

where $\mathbf{u}^h(\mathbf{x}) \simeq \{u(\mathbf{x}), \ldots, \partial^\alpha u(\mathbf{x}), \ldots, \partial^{|\alpha|=n} u(\mathbf{x})\}^T$ is the vector of unknowns; $\mathbf{J}$ is a diagonal matrix of $\{(-1)^\alpha/\alpha!\}^n_{|\alpha|=0}$; and

$$\mathbf{u} = \{u(\mathbf{x}_1), \ldots, u(\mathbf{x}_I), \ldots, u(\mathbf{x}_m)\}^T \tag{39}$$

$$\mathbf{R}(\mathbf{x}) = \begin{Bmatrix} 1 & x - x_1 & \ldots & (\mathbf{x} - \mathbf{x}_1)^\alpha \\ \vdots & \vdots & & \vdots \\ 1 & x - x_I & \ldots & (\mathbf{x} - \mathbf{x}_I)^\alpha \\ \vdots & \vdots & & \vdots \\ 1 & x - x_m & \ldots & (\mathbf{x} - \mathbf{x}_m)^\alpha \end{Bmatrix} = \begin{Bmatrix} \mathbf{p}^T(\mathbf{x} - \mathbf{x}_1) \\ \vdots \\ \mathbf{p}^T(\mathbf{x} - \mathbf{x}_I) \\ \vdots \\ \mathbf{p}^T(\mathbf{x} - \mathbf{x}_m) \end{Bmatrix} \tag{40}$$

where $I = 1, \ldots, m$ is a local node numbering. If the number of points in the star (stencil) is equal to the number of unknowns, then a solution to the system can be obtained by solving Eq. (38) directly, which is the method proposed by Jensen (1972). Selecting a suitable star such that the resulting system is not linearly dependent was one of the essential troubles of the early GFD methods, as the number of points in the star was fixed, and each point in the star had to be of sufficient quality to avoid linear dependence, leading to a difficult situation. While effort was made at the time for better star selection (Liszka and Orkisz 1980; Liszka 1984) greatly improved upon the method by considering that a larger number of points in the star could be used, and the resulting overdetermined system could be solved by least squares, or weighted least squares

$$\mathbf{T}(\mathbf{x})\mathbf{u}^h_{\mathbf{J}}(\mathbf{x}) = \mathbf{R}^T(\mathbf{x})\mathbf{W}(\mathbf{x})\mathbf{u} \tag{41}$$

where $\mathbf{W}(\mathbf{x})$ is a matrix of weights; and with the proper selection of $\mathbf{W}(\mathbf{x})$

$$\mathbf{W}(\mathbf{x}) = \begin{bmatrix} w_a(\mathbf{x} - \mathbf{x}_1) & \cdots & 0 & \cdots & 0 \\ \vdots & \ddots & & & \vdots \\ 0 & & w_a(\mathbf{x} - \mathbf{x}_I) & & 0 \\ \vdots & & & \ddots & \vdots \\ 0 & \cdots & 0 & \cdots & w_a(\mathbf{x} - \mathbf{x}_m) \end{bmatrix} \tag{42}$$

$\mathbf{T}(\mathbf{x}) = \mathbf{R}^T(\mathbf{x})\mathbf{W}(\mathbf{x})\mathbf{R}(\mathbf{x})$ is exactly the matrix $\mathbf{A}(\mathbf{x})$ for MLS, and the moment matrix $\mathbf{M}(\mathbf{x})$ in the discrete RK approximation with monomials.

Solving the system in Eq. (41) results in

$$\mathbf{u}^h(\mathbf{x}) = \sum_{I \in G_{\mathbf{x}}} \mathbf{J}^{-1}\mathbf{M}^{-1}(\mathbf{x})\mathbf{P}(\mathbf{x} - \mathbf{x}_I) w_a(\mathbf{x} - \mathbf{x}_I) u_I \tag{43}$$

Then, to obtain the approximation for $u(\mathbf{x})$, one can premultiply the right hand side of Eq. (43) by $\mathbf{P}(\mathbf{0})$ to obtain the first row of the vector $\mathbf{u}^h$ on the left hand side of Eq. (43), and as the first entry of $\mathbf{J}^{-1}$ is unity, immediately the MLS approximation is obtained. One can also identify a row in the left hand side of Eq. (43) corresponding to the approximation of $\partial^\alpha u(\mathbf{x})$, as the premultiplication of the right hand side of Eq. (43) by $\mathbf{p}^\alpha$ in Eq. (35), and one can see immediately that the generalized finite differences are also indeed the diffuse derivative approximations.

Comparing the GFD and synchronized derivatives to the RK approximation, one can observe that the moment matrix contains information on how to approximate the primary variable as well as derivatives.

Savitzky–Golay Filters and Peridynamics

Very recently, Bessa et al. (2014) made the connection between synchronized derivatives, Savitzky-Golay filters (Savitzky and Golay 1964), and peridynamics. They showed that under uniform discretizations, the deformation gradient in nodally collocated state-based peridynamics (Silling et al. 2007) is equivalent to employing Savitzky-Golay filters for constructing the deformation gradient. In addition, they showed that this approximation was a special case of diffuse derivatives with the quadratic basis and flat kernels. They suggested that this was likely also true in the nonuniform case, as the procedures described in this paper to generate diffuse derivatives could be considered as a generalization of Savitzky-Golay filters. The precise connection between meshfree approximations and peridynamics under general nonuniform discretizations will be discussed in a forthcoming paper by the authors.

Galerkin-Based Meshfree Method

The meshfree approximation functions discussed in the previous sections can be used to form finite dimensional spaces for the numerical solution of PDEs under either the Galerkin framework (this section) or the strong form collocation framework (see "Strong Form Collocation-Based Meshfree Method"). For demonstration purposes, consider the following elasticity problem:

$$\nabla \cdot \boldsymbol{\sigma} + \mathbf{b} = \mathbf{0} \quad \text{in } \Omega \tag{44}$$

$$\mathbf{n} \cdot \boldsymbol{\sigma} = \mathbf{h} \quad \text{on } \partial\Omega_h \tag{45}$$

$$\mathbf{u} = \mathbf{g}, \quad \text{on } \partial\Omega_g \tag{46}$$

where $\mathbf{u}$ is the displacement vector; $\boldsymbol{\sigma} = \mathbf{C}{:}\boldsymbol{\varepsilon}(\mathbf{u})$ is the Cauchy stress tensor; $\mathbf{C}$ is the elasticity tensor; $\boldsymbol{\varepsilon}(\mathbf{u}) = \nabla^s\mathbf{u} \equiv 1/2(\nabla \otimes \mathbf{u} + \mathbf{u} \otimes \nabla)$ is the strain tensor; $\mathbf{n}$ is the surface normal on $\partial\Omega$; $\mathbf{b}$ is the body force; $\mathbf{h}$ is the prescribed traction on $\partial\Omega_h$; $\mathbf{g}$ is the prescribed displacement on $\partial\Omega_g$; $\partial\Omega_g \cup \partial\Omega_h = \partial\Omega$; and $\partial\Omega_g \cap \partial\Omega_h = \emptyset$.

In the Galerkin statement of the problem, the solution and its variation are approximated by $\mathbf{u}^h$ and $\mathbf{v}^h$, respectively, as

$$\mathbf{u}^h(\mathbf{x}) = \sum_{I \in G_{\mathbf{x}}} \Psi_I(\mathbf{x})\mathbf{u}_I,$$
$$\mathbf{v}^h(\mathbf{x}) = \sum_{I \in G_{\mathbf{x}}} \hat{\Psi}_I(\mathbf{x})\mathbf{v}_I \tag{47}$$

where Ψ_I and $\hat{\Psi}_I$ are meshfree shape functions, possibly different from each other; and $\{\mathbf{u}_I\}^{Np}_{I=1}$ is the set of unknowns. In the Bubnov-Galerkin case $\hat{\Psi}_I(\mathbf{x}) = \Psi_I(\mathbf{x})$.

Enforcement of Essential Boundary Conditions

Essential boundary condition enforcement in the traditional finite-element method is generally straightforward because of the property that nodal coefficients in the approximation coincide with the values at the nodes, and therefore, kinematic constraints can be imposed directly on the nodal coefficients. Conversely, most meshfree methods do not enjoy this property, and special attention must be paid to enforcing essential (Dirichlet) boundary conditions. The enforcement of essential boundary conditions in meshfree methods can generally be classified into two types of enforcement: (1) strong

enforcement at nodes, i.e., collocation of the essential boundary condition at nodes on the essential boundary; and (2) weak enforcement of conditions along the essential boundary. A few exceptions to these cases are noted later in the text. The Galerkin approximation of Eqs. (44)–(46) has been formulated with the methods to be discussed as follows.

Strong Enforcement of Essential Boundary Conditions

One way to strongly enforce essential boundary conditions at nodes is to utilize the relationship between nodal coefficients and field values at the nodes (Atluri et al. 1999; Chen and Wang 2000b; Chen et al. 1996; Günther and Liu 1998; Wagner and Liu 2000; Zhu and Atluri 1998), called the *transformation method* or *collocation method*. It appears that several researchers had arrived at this formulation independently around the same time. These relationships yield matrix equations that operate on nodal values, and thus kinematic constraints can be imposed directly with static condensation. This transformation can be constructed such that inverting a transformation matrix only related to the constrained degrees of freedom is necessary (Chen and Wang 2000b; Wagner and Liu 2000; Zhu and Atluri 1998). In essence, this method is a special case of the Lagrange multiplier method where the approximation of the multiplier is a delta function (Chen and Wang 2000b).

Modification to the standard meshfree approximation functions has been proposed so that nodal degrees of freedom coincide with field variables (Chen and Wang 2000b; Chen et al. 2003; Gosz and Liu 1996; Kaljevic and Saigal 1997). Some of these special constructions of shape functions are introduced at constrained nodes only, such as the use of a singular weight function (Chen and Wang 2000b; Kaljevic and Saigal 1997), as first suggested by Shepard, as well as Lancaster and Salkauskas (Lancaster and Salkauskas 1981; Shepard 1968). MLS and RK methods that have interpolation property can also be constructed (Chen et al. 2003). Coupling with FEM shape functions in the discretization on the boundary has also been proposed, to take advantage of the finite-element method's ability to easily impose boundary conditions [see, e.g., (Fernández-Méndez and Huerta 2004; Krongauz and Belytschko 1996)].

Methods that impose boundary conditions strongly offer very simple implementation of enforcement of essential boundary conditions. In addition, compared to other methods mentioned later in the text, no additional degrees of freedom, special matrix terms with boundary integration, or parameters to choose are present. With these approaches, a kinematically admissible finite dimensional space can be constructed, and the Galerkin approximation of Eqs.(44)–(46) can be formulated as seeking $\mathbf{u}^h \in U^h \subset [H_g^1]^d$ such that $\forall \mathbf{v}^h \in V^h \subset [H_0^1]^d$

$$\int_\Omega \boldsymbol{\varepsilon}(\mathbf{v}^h):\mathbf{C}:\boldsymbol{\varepsilon}(\mathbf{u}^h)\mathrm{d}\Omega = \int_\Omega \mathbf{v}^h \cdot \mathbf{b}\mathrm{d}\Omega + \int_{\partial\Omega_h} \mathbf{v}^h \cdot \mathbf{h}\mathrm{d}\Gamma \tag{48}$$

Weak Enforcement of Essential Boundary Conditions

In the seminal work on EFG by Belytschko et al. (1994b), Lagrange multipliers were employed to weakly enforce boundary conditions. In this approach, the Galerkin approximation seeks $(\mathbf{u}^h, \boldsymbol{\lambda}^h) \in U^h \times \Lambda^h$ such that $\forall (\mathbf{v}^h, \boldsymbol{\gamma}^h) \in V^h \times \Gamma^h$, with $U^h \subset U$, $V^h \subset V$, $\Gamma \subset \Gamma^h$, and $\Lambda \subset \Lambda^h$, the following equation holds:

$$\begin{aligned}&\int_\Omega \boldsymbol{\varepsilon}(\mathbf{v}^h):\mathbf{C}:\boldsymbol{\varepsilon}(\mathbf{u}^h)\mathrm{d}\Omega + \int_{\partial\Omega_g} \boldsymbol{\gamma}^h \cdot \mathbf{u}^h \mathrm{d}\Gamma \\ &= \int_\Omega \mathbf{v}^h \cdot \mathbf{b}\mathrm{d}\Omega + \int_{\partial\Omega_h} \mathbf{v}^h \cdot \mathbf{h}\mathrm{d}\Gamma + \int_{\partial\Omega_g} \mathbf{v}^h \cdot \boldsymbol{\lambda}^h \mathrm{d}\Gamma - \int_{\partial\Omega_g} \boldsymbol{\gamma}^h \cdot \mathbf{g}\mathrm{d}\Gamma\end{aligned} \tag{49}$$

where $U = V = [H^1(\Omega)]^d$; $\Lambda = \Gamma = [L^2(\partial\Omega_g)]^d$; and $\boldsymbol{\lambda}^h$ and $\boldsymbol{\gamma}^h$ are approximations of the Lagrange multiplier $\boldsymbol{\lambda}$ and its variation $\boldsymbol{\gamma}$, respectively

$$\begin{aligned}\boldsymbol{\lambda}^h(\mathbf{x}) &= \sum_{I \in G_\mathbf{x}} \varphi_I(\mathbf{x})\boldsymbol{\lambda}_I, \\ \boldsymbol{\gamma}^h(\mathbf{x}) &= \sum_{I \in G_\mathbf{x}^B} \hat{\varphi}_I(\mathbf{x})\boldsymbol{\gamma}_I\end{aligned} \tag{50}$$

where φ_I and $\hat{\varphi}_I$ are shape functions; $G_\mathbf{x}^B$ is the set of nodes associated with the enforcing the essential boundary conditions which cover $\mathbf{x}$; and $\{\boldsymbol{\lambda}_I\}_{I=1}^{Np}$ is a set of additional unknowns, representing tractions on the essential boundary.

While straightforward, this method results in a positive semidefinite matrix and also adds degrees of freedom to the system. In addition, to ensure numerical stability, the choice of the finite dimensional spaces is subject to the *Babuška-Brezzi stability condition.* Alternatively, the Lagrange multiplier can be replaced by its physical counterpart (e.g., the traction in elasticity) as constructed by the primary approximation space, and the resulting method does not suffer from these issues (Lu et al. 1994). This approach is a special case of Nitche's method (Nitsche 1971) with penalty parameter of zero, which in this case the bilinear form is not guaranteed to be coercive (Griebel and Schweitzer 2003b).

Imposing essential boundary conditions weakly using the penalty method has been employed in meshfree formulations (cf. Atluri and Zhu 1998; Zhu and Atluri 1998), and is an attractive choice due to its simplicity. It does not add degrees of freedom, and it is simple to implement. However, using this approach, the solution may not converge optimally (Fernández-Méndez and Huerta 2004). In addition, the solution error is sensitive to the choice of penalty parameter employed, as large parameters can cause ill-conditioning of the system, while smaller parameters do not enforce boundary conditions well (Fernández-Méndez and Huerta 2004). Also, with the penalty method the weak form does not attest to the strong form.

Nitche's method (Nitsche 1971) can also be employed, which is essentially a combination of the penalty method and the modified variational principle. This method attests to the strong form, and also relaxes the strong dependence of the solution accuracy on the choice of the penalty parameter, thus addressing the issues with the penalty method. Using this technique, the solution is stable and convergent with the proper selection of the penalty parameter (Fernández-Méndez and Huerta 2004; Griebel and Schweitzer 2003a; Nitsche 1971). It has been shown that for two-dimensional problems, if the penalty parameter is of order h^{-2} optimal convergence can be achieved (Fernández-Méndez and Huerta 2004). Alternatively, one can estimate a parameter that gives optimal

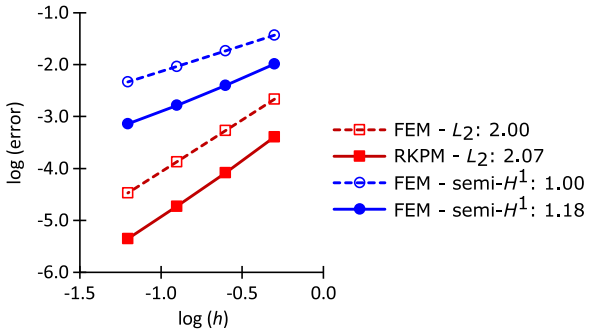

Fig. 9. Convergence of linear FEM and linear RKPM in a second order PDE with a smooth solution

convergence by using an eigenvalue problem (Griebel and Schweitzer 2003a). Using this approach, the Galerkin problem is to find $\mathbf{u}^h \in U^h$ such that $\forall\, \mathbf{v}^h \in U^h$ the following equation holds:

$$\int_\Omega \boldsymbol{\varepsilon}(\mathbf{v}^h):\mathbf{C}:\boldsymbol{\varepsilon}(\mathbf{u}^h)\mathrm{d}\Omega - \int_{\partial\Omega_g} \mathbf{n}\cdot[\mathbf{C}:\boldsymbol{\varepsilon}(\mathbf{v}^h)]\cdot\mathbf{u}^h\mathrm{d}\Gamma - \int_{\partial\Omega_g} \mathbf{v}^h\cdot\mathbf{n}\cdot[\mathbf{C}:\boldsymbol{\varepsilon}(\mathbf{u}^h)]\mathrm{d}\Gamma + \beta\int_{\partial\Omega_g}\mathbf{v}^h\cdot\mathbf{u}^h\mathrm{d}\Gamma = \int_\Omega \mathbf{v}^h\cdot\mathbf{b}\mathrm{d}\Omega + \int_{\partial\Omega_h}\mathbf{v}^h\cdot\mathbf{h}\mathrm{d}\Gamma + \int_{\partial\Omega_g}\mathbf{n}\cdot[\mathbf{C}:\boldsymbol{\varepsilon}(\mathbf{v}^h)]\cdot\mathbf{g}\mathrm{d}\Gamma + \beta\int_{\partial\Omega_g}\mathbf{v}^h\cdot\mathbf{g}\mathrm{d}\Gamma \tag{51}$$

where β is a penalty parameter; and $U^h \subset [H^1]^d$. It is useful to mention a few other approaches that do not strictly fall into any one of the two categories. D'Alembert's principle can also be used to enforce constraints (Günther and Liu 1998). Boundary conditions can also be imposed strongly by employing one layer of finite elements in a novel way (Zhang et al. 2002).

To summarize, due to the lack of Kronecker delta property, imposing boundary conditions in meshfree methods is not as straightforward as in finite elements. However, substantial efforts have been made to address this issue, and many methods offer ease of implementation as well as other attractive features. In particular, Nitche's method is straightforward to implement, efficient, and optimally convergent and stable given the proper selection of the penalty parameter (Griebel and Schweitzer 2003a). Another attractive option is modifying the approximation space near the boundary (Chen and Wang 2000b; Chen et al. 2003; Kaljevic and Saigal 1997), where no matrix construction and operations are involved as in transformation methods (Atluri et al. 1999; Chen and Wang 2000b; Chen et al. 1996; Günther and Liu 1998; Wagner and Liu 2000; Zhu and Atluri 1998). In this approach, there is also no stability condition, nor selection of any parameters. The method is simple to implement, efficient, and it can be easily introduced into existing finite-element codes that implicitly operate on generalized displacements.

Lastly, several meshfree methods do not require special treatment of boundary conditions such as the maximum entropy method (Arroyo and Ortiz 2006; Sukumar 2004), which enjoys the weak Kronecker delta property. An interesting recent development is the introduction of a generalization of MLS, RK, and ME approximations, where consistency, convexity, and the weak Kronecker delta property can be obtained in various combinations such as MLS with weak Kronecker delta at the boundary, and higher order convex approximations (Wu et al. 2011, 2015).

Convergence of the Galerkin Meshfree Method in PDEs

The convergence of the Galerkin meshfree method using MLS/RK/PU approximation with pth order completeness has been shown to be (Chen et al. 2003; Han and Meng 2001; Liu et al. 1996a, 1997c)

$$\|u - u^h\|_{\ell,\Omega} \le Ca^{p+1-\ell}|u|_{p+1,\Omega}, \quad \ell \ge 0 \tag{52}$$

where a is the maximum support dimension of the approximation functions; and C is independent of a and p. While the convergence rate in meshfree approximations with pth order completeness yields the same rate of convergence compared to that of p-order finite elements, the constant C can be made smaller in meshfree methods with proper selection of smoothness in the meshfree approximation. Consider a Poisson problem on $\Omega{:}(0,1)\times(0,1)$ with a high order solution

$$\begin{aligned} &\nabla^2 u = (x^2+y^2)e^{xy} && \text{in } \Omega \\ &u = e^{xy} && \text{on } \partial\Omega \end{aligned} \tag{53}$$

The problem is solved with linear finite elements ($p=1$, C^0 continuity) and linear RKPM with quintic B-spline kernels with normalized support of 2.5 ($p=1$, C^4 continuity), both with uniform discretizations of 81; 289; 1,089; and 4,225 nodes. As shown in Fig. 9, both methods yield similar rates of convergence, yet the error is much lower for RKPM. The final ratio between the errors in this case is roughly $1/8$ for the L_2 norm and $1/6$ for the H^1 seminorm.

Domain Integration in Galerkin Meshfree Methods

A key issue in weak form-based Galerkin methods is the choice of a quadrature scheme to perform domain integration. The problems at hand can be generally categorized as follows: (1) influence of domain integration error on solution error and convergence rates; and (2) rank instability in the solution with the choice of particular quadrature schemes such as nodal integration.

Quadrature Schemes for Efficient and Convergent Meshfree Solutions

In the early development of meshfree methods, Gauss integration using background cells, as shown in Fig. 10, was commonly employed (Belytschko et al. 1994b, 1996b; Chen et al. 1996; Liu et al. 1995a). However, difficulty in obtaining accuracy in domain integration can be encountered when shape functions are rational, as they often are in meshfree methods (Fig. 2), and Gauss integration cannot always accurately evaluate integrals in the Galerkin equation. Another major source of quadrature error is the

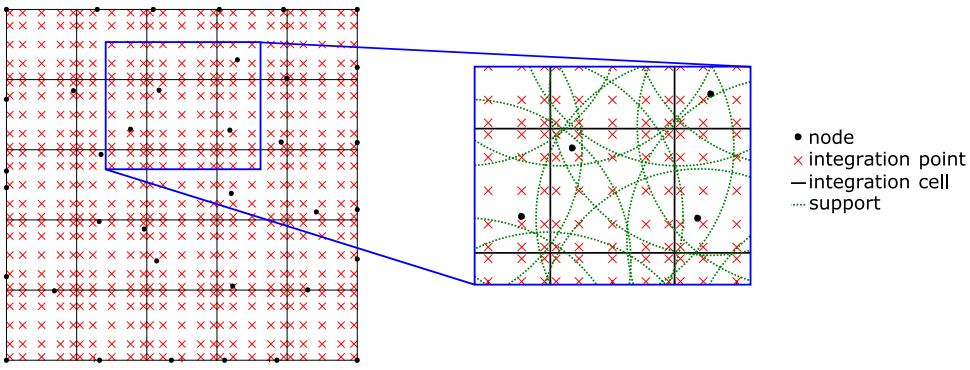

Fig. 10. Gauss integration with a zoom-in showing nodal supports

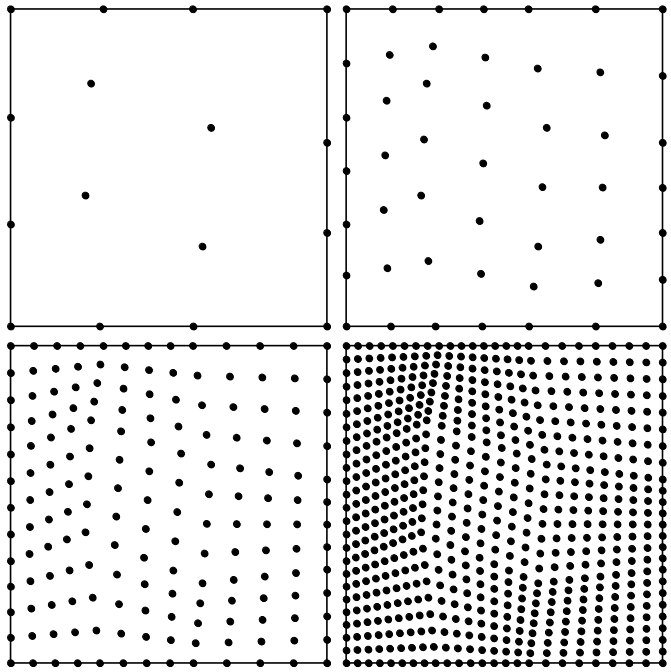

Fig. 11. Nonuniform discretizations used in the convergence study

misalignment of integration cells and shape function supports (Dolbow and Belytschko 1999), which is typically the case in a general setting, as shown in Fig. 10. As a result of these difficulties, large errors can be introduced into the solution if careful attention is not paid to domain integration, and optimal convergence rates can be lost. In particular, the solutions under uniform discretizations generally do not suffer from integration issues, while the solutions under nonuniform discretizations are sensitive to the choice of domain integration (Chen et al. 2013).

For illustration, various orders of quadrature are employed in background Gauss cells for RKPM with linear basis, for solving Eq. (53) with the nonuniform discretizations shown in Fig. 11. As shown in Fig. 12, 5×5 Gauss integration is needed to attain optimal convergence rates (at least a rate of two and one in the L_2 norm H^1 seminorm, respectively).

It has been recognized by many researchers that high order quadrature is necessary in order to ensure acceptable convergence rates and accuracy in the solution (Babuška et al. 2008; Chen et al. 2001, 2013; Dolbow and Belytschko 1999); this is prohibitively expensive in any practical problem. Because of this difficulty, many approaches have been developed to circumvent this issue.

The solution error due to misalignment of meshfree supports and integration cells has motivated several algorithms. Constructing cells that align with the supports can significantly reduce the solution error due to numerical integration (Dolbow and Belytschko 1999). Procedures have been proposed to construct integration cells based on the structure of approximations as well as the overlapping compact supports (Griebel and Schweitzer 2002a). In a similar spirit, other support integration schemes have also been developed (Liu and Belytschko 2010).

One condition leveraged in meshfree literature is the divergence constraint (often termed the *integration constraint*) on the test function space and numerical integration, necessary for satisfying the linear patch test (Bonet and Kulasegaram 2000; Chen et al. 2001; Krongauz and Belytschko 1997):

$$\int_{\Omega}^{\wedge} \nabla \hat{\Psi}_I \mathrm{d}\Omega = \int_{\partial\Omega}^{\wedge} \hat{\Psi}_I \mathbf{n} \mathrm{d}\Gamma \tag{54}$$

where $\wedge$ over the integral symbol denotes numerical integration. An iterative technique to satisfy this condition via modification of approximation functions has been proposed (Bonet and Kulasegaram 2000).

One particularly effective approach to achieve Eq. (54) is the stabilized conforming nodal integration (SCNI) by Chen et al. (2001), which employs nodal integration with gradients smoothed over conforming representative nodal domains, as shown in Fig. 13(c), converted to boundary integration using the divergence theorem

$$\tilde{\nabla} \Psi_I(\mathbf{x}_L) = \frac{1}{W_L} \int_{\Omega_L} \nabla \Psi_I \mathrm{d}\Omega = \frac{1}{W_L} \int_{\partial\Omega_L} \Psi_I \mathbf{n} \mathrm{d}\Gamma \tag{55}$$

where W_L is the integration weight associated with node L; and $\tilde{\nabla}$ denotes the smoothed gradient operator. In this method, smoothed gradients are employed for both test and trial functions, as the approximation in Eq. (55) enjoys first order completeness (Chen et al. 2013). If the smoothing domains $\{\Omega_L\}_{L=1}^{NP}$ are conforming, nodal integration with smoothed gradients $\tilde{\nabla}$ meets the condition of Eq. (54) (Chen et al. 2001). The smoothed gradient at the nodal point in Eq. (55) is then introduced in the weak form and integrated with nodal integration to form the stiffness matrix [see Chen et al. (2001) for details]. This approach has also been applied to large deformation problems with strain smoothing applied to the nodal evaluation of the deformation gradient (Chen et al. 2002).

This method yields optimal convergence for linear approximation spaces, as shown in Fig. 14, and provides a far more effective approach than Gauss integration. In addition, the method can serve as a correction to direct nodal integration (DNI), as shown in Fig. 13(a), which suffers from significant convergence problems, as shown in Fig. 12. For fragment-impact problems where maintaining conforming cells is cumbersome, a nonconforming version of SCNI has been proposed (Guan et al. 2009, 2011), termed

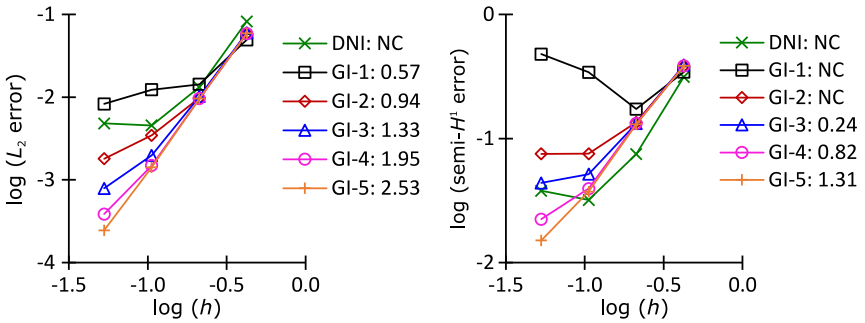

Fig. 12. Convergence of RKPM with linear basis with various integration methods Gauss integration with qth order quadrature is denoted GI-q

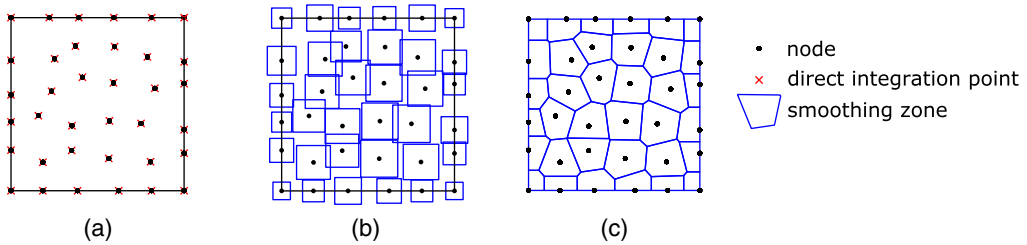

Fig. 13. Nodal integration schemes in meshfree methods: (a) direct nodal integration; (b) stabilized nonconforming nodal integration; (c) stabilized conforming nodal integration

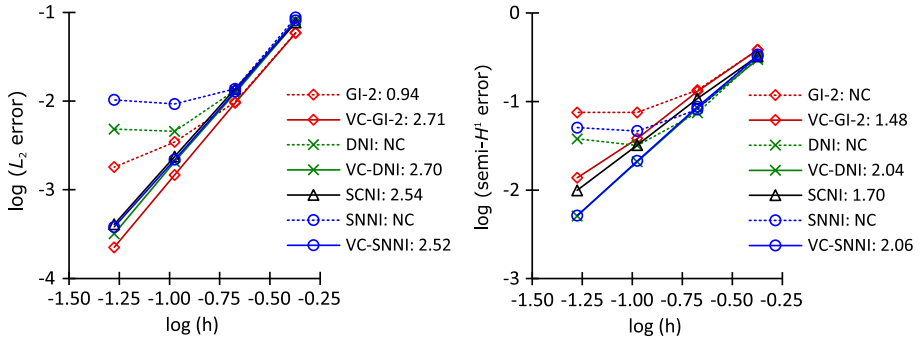

Fig. 14. Convergence of RKPM with linear basis with various integration methods with and without variational consistency

stabilized nonconforming nodal integration (SNNI); this scheme is depicted in Fig. 13(b). The relaxation of the conforming condition sacrifices optimal convergence, as shown in Fig. 14, but is still efficient, and maintains superior stability over DNI. The reduced accuracy in SNNI compared to SCNI can be corrected to recover optimal convergence by variationally consistent integration (Chen et al. 2013), and will be discussed later in the text.

The SCNI method has been extended to many methods and problems: nonlinear solid mechanics problems (Chen et al. 2002), the natural element method (Yoo et al. 2004), the Schrödinger equation (Chen et al. 2007a), plate and shell problems (Chen and Wang 2006; Wang and Chen 2004, 2008), and more recently, convection dominated problems (Hillman and Chen 2016) and coupled analysis of fluid-saturated porous media (Wei et al. 2016).

The concept of strain smoothing in SCNI has also been applied to the finite-element methods. The doctoral thesis of Guan (2009) first introduced the strain smoothing in SCNI to finite elements as the basis for coupling FEM and RKPM with unified discretization and domain integration. Various nodal and element strain smoothing techniques have been proposed by Liu et al. for finite elements, and are termed the smoothed finite-element methods (Liu and Nguyen-Thoi 2010; Liu 2008; Liu et al. 2007a). The SCNI method has been shown to be grounded in variational principles (Sze et al. 2004).

In a recent development, a framework of variationally consistent integration (VCI) has been proposed by Chen et al. (2013), where a generalization of the integration constraints in SCNI to arbitrary order revealed that the divergence condition in Eq. (54) is a special case of an integration by parts constraint necessary in order to obtain nth order Galerkin exactness in the solution

$$\int_\Omega \nabla\hat{\Psi}_I \cdot \boldsymbol{\varepsilon}(\mathbf{u}^\alpha)\mathrm{d}\Omega = -\int_\Omega \hat{\Psi}_I \nabla\cdot\boldsymbol{\varepsilon}(\mathbf{u}^\alpha)\mathrm{d}\Omega + \int_\Gamma \hat{\Psi}_I \mathbf{n}\cdot\boldsymbol{\varepsilon}(\mathbf{u}^\alpha)\mathrm{d}\Gamma \quad \forall\, I, \quad |\alpha| = 0,1,\ldots,n \tag{56}$$

where $\mathbf{u}^\alpha = \mathbf{c}_\alpha \mathbf{x}^\alpha$, and here the possibility of different test and trial functions is considered. One significant result is that with the satisfaction of these constraints, Galerkin orthogonality is restored up to order n (Rüter et al. 2013). Approximation spaces compatible with numerical integration in the form of the previous equation have been termed VCI methods. Using this technique, optimal convergence can be attained using far lower-order quadrature than would otherwise be required (Chen et al. 2013). For VC conditions for other mechanics problems, consult reference Chen et al. (2013).

A Petrov-Galerkin method with enriched test functions has been proposed to satisfy the constraints, by leveraging the fact that Eq. (56) involves the test functions, while the trial functions are constructed to be nth order complete (Chen et al. 2013). This method can be employed to correct any integration method at hand (as well as any approximation space cf. Hillman et al. 2015), such as nodal integration. As shown in Fig. 14, optimal convergence rates can be attained using various low order quadrature schemes (including DNI and SNNI) using the variationally consistent methods (denoted with prefix "VC"). A conforming method QC3 has been proposed that satisfies the second order constraints, which was shown to be a generalization of the SCNI technique to second order (Duan et al. 2012). Recently, a second-order exact two-level smoothing technique has been proposed that can provide further efficiency over QC3 (Wang and Wu 2016). Mathematical analysis of the effect of the accuracy of domain integration has been provided, where a zero-row sum condition and corrected quadrature scheme to achieve VC conditions was proposed (Babuška et al. 2008, 2009).

Stabilization of Nodal Integration

Several of the methods discussed previously offer viable quadrature techniques to yield efficient and convergent solutions in the Galerkin meshfree method. However, nodal integration such as the direct nodal integration scheme shown in Fig. 13(a), is often desired so that stress and state variables live at the nodes, and also because it offers a technique devoid of meshes. Another reason this method is

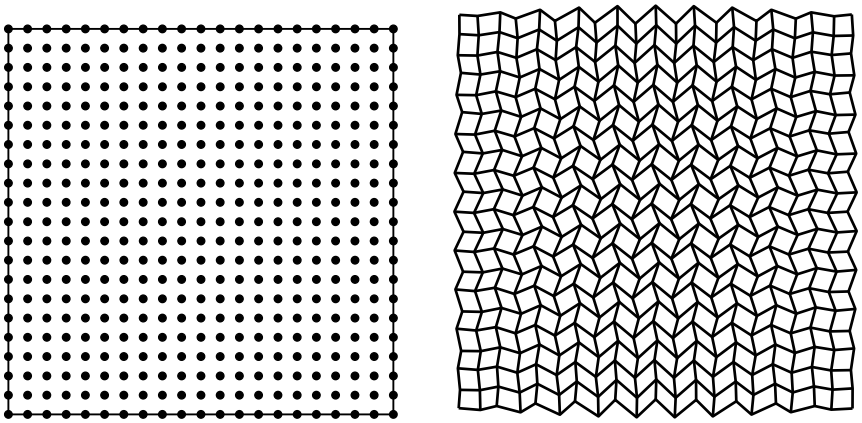

Fig. 15. (a) Discretization; (b) lowest energy mode of SNNI

often pursued is its simplicity and efficiency. While the inaccuracy and nonconvergent properties of nodal integration (see Beissel and Belytschko 1996; Chen et al. 2001, 2013 for additional examples) can be addressed by methods mentioned earlier, as shown in Fig. 14, the instability in the solution due to nodal integration type methods is widely recognized (Beissel and Belytschko 1996; Belytschko et al. 2000; Chen et al. 2001).

The instability resulting from nodal integration can be attributed to vanishing derivatives of short-wavelength (two times the nodal spacing) modes, and thus have little or no energy, and can grow unbounded in the solution (Beissel and Belytschko 1996; Belytschko et al. 2000; Chen et al. 2001). In essence, the strain energy density is severely underestimated for this mode.

One way to circumvent this instability is to employ methods that minimize the least-squares residual (Beissel and Belytschko 1996; Bonet and Kulasegaram 2000; Duan and Belytschko 2009; Fries and Belytschko 2008). However, these methods involve second-order derivatives of approximation functions, and typically a stabilization parameter. Another way to circumvent this difficulty is to calculate gradients in locations other than the nodes, often called the stress point method (Dyka and Ingel 1995; Dyka et al. 1997; Randles and Libersky 2000), which gives more reasonable strain energy at the stress points. However, this method does require additional techniques such as residual-based stabilization in order to ensure convergent and stable solutions in all situations (Fries and Belytschko 2008).

Utilizing Taylor expansions also allows one to obtain extra information around the integration points, and thus stabilize modes that have zero or near-zero energy associated with them. The origin of these methods is the unification of stabilization in finite elements (Liu et al. 1985). The technique has been used to stabilize nodal integration (Liu et al. 2007b; Nagashima 1999), and also other types of low order quadrature (Chen et al. 2000e; Liu et al. 1996b). While stable, the drawback of this technique is that it requires the calculation of high order derivatives.

Part of the dual motivation for the SCNI technique was that it also stabilizes zero energy modes in direct nodal integration by avoiding evaluating derivatives directly at nodal points (Chen et al. 2001, 2002). In this method, the order of differentiation for constructing a stable method is actually reduced, also leading to enhanced efficiency. However, the smoothed integrations SCNI and SNNI are subject to spurious, oscillatory low-energy modes that can show up when the surface to volume ratio is sufficiently small, or in sufficiently fine discretizations (Puso et al. 2008). An example of this mode for the SNNI method, obtained by eigenvalue analysis, is shown in Fig. 15.

Stabilization of these modes for SCNI and SNNI has been proposed (Puso et al. 2008), where these modes are penalized throughout the smoothing domain, resulting in modified SCNI (MSCNI) and modified SNNI (MSNNI) in the strain energy

$$a_{MS}\langle \mathbf{v}^h, \mathbf{u}^h \rangle = a_S\langle \mathbf{v}^h, \mathbf{u}^h \rangle + a_M\langle \mathbf{v}^h, \mathbf{u}^h \rangle \tag{57}$$

where $a_S\langle \cdot, \cdot \rangle$ is the strain energy with strain smoothing

$$a_S\langle \mathbf{v}^h, \mathbf{u}^h \rangle = \sum_{L=1}^{NP} \tilde{\boldsymbol{\varepsilon}}_L(\mathbf{v}^h) : \mathbf{C} : \tilde{\boldsymbol{\varepsilon}}_L(\mathbf{u}^h) W_L \tag{58}$$

Here $\tilde{\boldsymbol{\varepsilon}}_L(\mathbf{u}^h) = 1/2[\tilde{\nabla} \otimes \mathbf{u}(\mathbf{x}_L) + \mathbf{u}(\mathbf{x}_L) \otimes \tilde{\nabla}]$ is the smoothed strain, and

$$a_M\langle \mathbf{v}^h, \mathbf{u}^h \rangle = \sum_{L=1}^{NP} \sum_{K=1}^{NS} \beta \{ [\tilde{\boldsymbol{\varepsilon}}_L(\mathbf{v}^h) - \boldsymbol{\varepsilon}_L^K(\mathbf{v}^h)] : \mathbf{C} : [\tilde{\boldsymbol{\varepsilon}}_L(\mathbf{u}^h) - \boldsymbol{\varepsilon}_L^K(\mathbf{u}^h)] W_L^K \} \tag{59}$$

is the additional stabilization where $0.0 \le \beta \le 1.0$, $\boldsymbol{\varepsilon}_L^K(\mathbf{u}^h) = \boldsymbol{\varepsilon}[\mathbf{u}^h(\mathbf{x}_L^K)]$ is the strain evaluated at the centroid of subcells $\mathbf{x}_L^K$, and W_L^K is the weight of the subcell calculated from the weight W_L. It is clear from Eq. (59) that for $\beta > 0.0$ additional coercivity is added to the solution. The key to the success of this method in SCNI is that the additional stabilization maintains linear exactness of SCNI. The stabilized mode corresponding to the previous example is shown for SNNI in Fig. 16(a).

An implicit gradient expansion has been proposed (Hillman and Chen 2015) that employs implicit gradients (Chen et al. 2004; Chi et al. 2013) (see section "Derivative Approximations in Meshfree Methods") in a Taylor expansion to yield stabilization without explicit computation of higher order derivatives. In this approach, the implicit gradient expansion of the strain around a node $\mathbf{x}_L$ is defined as, in two dimensions

$$\boldsymbol{\varepsilon}[\mathbf{u}^h(\mathbf{x})] \approx \boldsymbol{\varepsilon}_L(\mathbf{u}^h) + (x - x_L)\boldsymbol{\varepsilon}_L(\hat{\mathbf{u}}_x^h) + (y - y_L)\boldsymbol{\varepsilon}_L(\hat{\mathbf{u}}_y^h) \tag{60}$$

where $\boldsymbol{\varepsilon}_L(\hat{\mathbf{u}}_x^h) \equiv \boldsymbol{\varepsilon}[\hat{\mathbf{u}}_x^h(\mathbf{x}_L)]$; $\boldsymbol{\varepsilon}_L(\hat{\mathbf{u}}_y^h) \equiv \boldsymbol{\varepsilon}[\hat{\mathbf{u}}_y^h(\mathbf{x}_L)]$; and first order implicit gradients $\{\Psi_I^\alpha(\mathbf{x})\}_{|\alpha|=1}$ are used to approximate the terms in the expansion

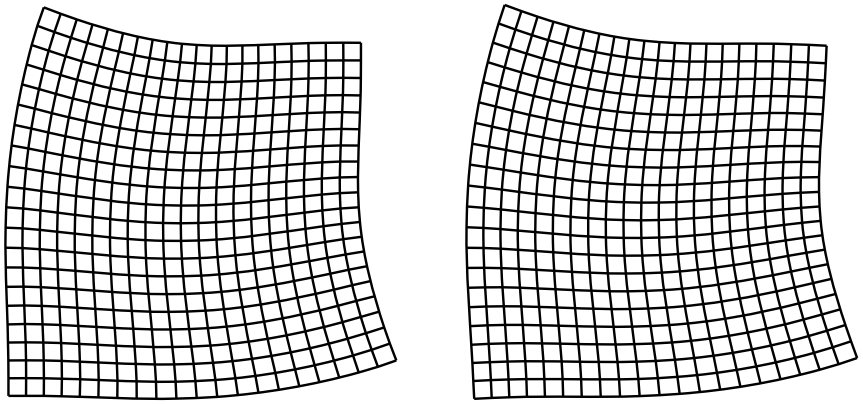

Fig. 16. Lowest energy modes of (a) modified SNNI; (b) NSNI

$$\hat{\mathbf{u}}_x^h(\mathbf{x}_L) = \sum_{I\in G_{\mathbf{x}_L}} \Psi_I^{(1,0)}(\mathbf{x}_L)\mathbf{u}_I,$$
$$\hat{\mathbf{u}}_y^h(\mathbf{x}_L) = \sum_{I\in G_{\mathbf{x}_L}} \Psi_I^{(0,1)}(\mathbf{x}_L)\mathbf{u}_I \tag{61}$$

where $\Psi_I^{\alpha}(\mathbf{x})$ is the implicit gradient shape function in Eq. (35). Substituting Eq. (60) for the strains near each node, following Hillman and Chen (2015), one obtains a stabilized strain energy $a_{ND}\langle\cdot,\cdot\rangle$

$$a_{ND}\langle\mathbf{v}^h,\mathbf{u}^h\rangle = a_D\langle\mathbf{v}^h,\mathbf{u}^h\rangle + a_N\langle\mathbf{v}^h,\mathbf{u}^h\rangle \tag{62}$$

where $a_D\langle\cdot,\cdot\rangle$ is the quadrature version of the nodally integrated strain energy

$$a_D\langle\mathbf{v}^h,\mathbf{u}^h\rangle = \sum_{L=1}^{NP} \boldsymbol{\varepsilon}_L(\mathbf{v}^h):\mathbf{C}:\boldsymbol{\varepsilon}_L(\mathbf{u}^h)W_L \tag{63}$$

where $\boldsymbol{\varepsilon}_L(\mathbf{u}^h) = \boldsymbol{\varepsilon}[\mathbf{u}^h(\mathbf{x}_L)]$ is the nodal strain; and

$$a_N\langle\mathbf{v}^h,\mathbf{u}^h\rangle = \sum_{L=1}^{NP}[\boldsymbol{\varepsilon}_L(\hat{\mathbf{v}}_x^h):\mathbf{C}:\boldsymbol{\varepsilon}_L(\hat{\mathbf{u}}_x^h)M_{Lx} + \boldsymbol{\varepsilon}_L(\hat{\mathbf{v}}_y^h):\mathbf{C}:\boldsymbol{\varepsilon}_L(\hat{\mathbf{u}}_y^h)M_{Ly}] \tag{64}$$

is the additional stabilization, where M_{Lx} and M_{Ly} are the second moments of inertia of the nodal domains about node L. Clearly, for coercive forms of $a(\cdot\,,\cdot)$, Eq. (64) adds additional stabilization for the strain energy. The stabilized nodal integration in Eqs. (62)–(64) has been termed naturally stabilized nodal integration (NSNI) because the constants in the stabilization come naturally from the discretization. Performing an eigenvalue analysis of the associated stiffness matrix, the first non-zero energy mode is stable, as shown in Fig. 16(b). It has been demonstrated through complexity analysis that speed-up factors of up to 20 times could be achieved over methods that involve additional sampling points (Hillman and Chen 2015).

Another form of stabilization considers a displacement smoothing and Taylor expansion Wu et al. (2016, 2015). This method has been shown to be a very effective approach to give a stable solution by nodal integration, without the use of numerical parameters or background cells. Integration techniques based on the partition of unity have been developed that do not require a mesh, and have been applied as a nodal subdomain integration technique (Duflot and Nguyen-Dang 2002; Romero and Armero 2002). Nodal integrations with corrective VCI procedures and stabilization can be formulated such that they do not detract from the meshfree character of the method (Chen et al. 2013; Hillman et al. 2014; Puso et al. 2008; Rüter et al. 2013; Wu et al. 2016, 2015).

To summarize, careful attention must be paid to domain integration in meshfree methods. If one does nothing and employs Gauss integration, prohibitively expensive high order quadrature is required to ensure accuracy and optimal convergence in all discretizations. Conversely, without special treatment, nodal integration yeilds both inaccurate and unstable solutions. Despite this fact, several effective methods have been developed over the past two decades to address these issues of accuracy, efficiency, and stability. The SCNI method (Chen et al. 2001) has proven to be a robust method in a variety of settings (Chen and Wang 2006; Chen et al. 2001, 2002; Hillman and Chen 2016; Wang and Chen 2004, 2008; Wei et al. 2016), and is effective in terms of high accuracy and low CPU time (Chen et al. 2001). While this method necessitates the additional stabilization of Eqs. (57)–(59), this can be accomplished straightforwardly [see Chen et al. (2007b), Hillman and Chen (2016), and Puso et al. (2007, 2008) for more details and variations on implementation]. A few new promising recent developments are: (1) corrections to achieve arbitrary order Galerkin exactness in any given integration method, which can achieve optimal convergence with low order quadrature (Chen et al. 2013), and can correct nodal integration methods for optimal convergence; (2) extensions of SCNI to achieve higher order Galerkin exactness (Duan et al. 2012; Wang and Wu 2016); and (3) the accelerated stabilization of Eqs. (60)–(64) [see Hillman and Chen (2015) for details], which can avoid many issues associated with stabilized nodal integration proposed in the past. Although quadrature for meshfree methods is still an active research topic, it appears that many of the problems with domain integration are being resolved.

Strong Form Collocation-Based Meshfree Method

Meshfree Collocation Method

An alternative approach to address domain integration issues in meshfree methods is to employ strong form collocation methods, such as the finite-point method (Oñate et al. 1996a), the radial basis collocation methods (Kansa 1990a, b), and the reproducing kernel collocation method (Aluru 2000; Hu et al. 2011). For demonstration, consider the application of strong form collocation to the boundary value problem for elasticity in Eqs. (44)–(46).

Introducing the approximation $\mathbf{u}^h(\mathbf{x})$ into Eqs. (44)–(46) and enforcing the residuals to be zero at N_C collocation points $\{\boldsymbol{\xi}_J\}_{J=1}^{N_C} \in \bar{\Omega} \equiv \Omega \cup \partial\Omega$, one has

$$\begin{aligned} &\nabla \cdot \boldsymbol{\sigma}[\mathbf{u}^h(\boldsymbol{\xi}_J)] = -\mathbf{b}(\boldsymbol{\xi}_J) && \forall\ \boldsymbol{\xi}_J \in \Omega, \\ &\mathbf{n} \cdot \boldsymbol{\sigma}[\mathbf{u}^h(\boldsymbol{\xi}_J)] = \mathbf{h}(\boldsymbol{\xi}_J) && \forall\ \boldsymbol{\xi}_J \in \partial\Omega_h, \\ &\mathbf{u}^h(\boldsymbol{\xi}_J) = \mathbf{g}(\boldsymbol{\xi}_J) && \forall\ \boldsymbol{\xi}_J \in \partial\Omega_g \end{aligned} \tag{65}$$

The collocation in Eq. (65) is equivalent to the weighted residual of Eqs. (44)–(46) as seeking $\mathbf{u}^h \in [H^2]^d$ such that $\forall\ \mathbf{w}, \mathbf{w}_h, \mathbf{w}_g \in [L^2]^d$

$$\begin{aligned} &\int_\Omega \mathbf{w}(\mathbf{x}) \cdot \{\nabla \cdot \boldsymbol{\sigma}[\mathbf{u}^h(\mathbf{x})] + \mathbf{b}(\mathbf{x})\} d\Omega, \\ &+ \int_{\partial\Omega_h} \mathbf{w}_h(\mathbf{x}) \cdot \{\mathbf{n} \cdot \boldsymbol{\sigma}[\mathbf{u}^h(\mathbf{x})] - \mathbf{h}(\mathbf{x})\} d\Gamma \\ &+ \int_{\partial\Omega_g} \mathbf{w}_g(\mathbf{x}) \cdot [\mathbf{u}^h(\mathbf{x}) - \mathbf{g}(\mathbf{x})] d\Gamma = 0 \end{aligned} \tag{66}$$

The weighted residual in Eq. (66) leads to Eq. (65) when $\mathbf{w} = \mathbf{w}_h = \mathbf{w}_g = \sum_{J=1}^{N_C} \delta(\mathbf{x} - \boldsymbol{\xi}_J)\bar{\mathbf{w}}_J$, where $\delta(\cdot)$ is the Dirac delta function in d-dimensional space, and $\bar{\mathbf{w}}_J$ is the associated arbitrary coefficient. In this approach the admissible approximation $\mathbf{u}^h$ is required to be in $[H^2]^d$, which is difficult for the conventional FEM approximation to achieve. However, for the general meshfree approximations discussed in the section "Meshfree Approximation Functions," the regularity requirement can be readily met.

Let the approximation of $\mathbf{u}$ be

$$\mathbf{u}^h(\mathbf{x}) = \sum_{I \in G_{\mathbf{x}}} g_I(\mathbf{x})\mathbf{u}_I \tag{67}$$

where g_I is the meshfree shape function associated with $\mathbf{x}_I$; and $\mathbf{u}_I$ is the corresponding coefficient. To use the terminology of collocation methods, in this paper when discussing collocation, the nodes in the set Z are called *source points*, and the number of source points in the set is denoted by Ns. In matrix form, Eq. (65) can be rewritten as

$$\begin{aligned} &\sum_{I \in G_{\boldsymbol{\xi}_J}} \mathbf{L} g_I(\boldsymbol{\xi}_J)\mathbf{u}_I = -\mathbf{b}(\boldsymbol{\xi}_J) && \forall\ \boldsymbol{\xi}_J \in \Omega, \\ &\sum_{I \in G_{\boldsymbol{\xi}_J}} \mathbf{B}_h g_I(\boldsymbol{\xi}_J)\mathbf{u}_I = \mathbf{h}(\boldsymbol{\xi}_J) && \forall\ \boldsymbol{\xi}_J \in \partial\Omega_h, \\ &\sum_{I \in G_{\boldsymbol{\xi}_J}} \mathbf{B}_g g_I(\boldsymbol{\xi}_J)\mathbf{u}_I = \mathbf{g}(\boldsymbol{\xi}_J) && \forall\ \boldsymbol{\xi}_J \in \partial\Omega_g \end{aligned} \tag{68}$$

where for two dimensions

$$\begin{aligned} \mathbf{L} &= \begin{bmatrix} (\lambda+2\mu)\dfrac{\partial^2}{\partial x^2} + \mu\dfrac{\partial^2}{\partial y^2} & (\lambda+\mu)\dfrac{\partial}{\partial x \partial y} \\ (\lambda+\mu)\dfrac{\partial}{\partial x \partial y} & \mu\dfrac{\partial^2}{\partial x^2} + (\lambda+2\mu)\dfrac{\partial^2}{\partial y^2} \end{bmatrix}, \\ \mathbf{B}_h &= \begin{bmatrix} (\lambda+2\mu)n_x\dfrac{\partial}{\partial x} + \mu n_y\dfrac{\partial}{\partial y} & \mu n_y\dfrac{\partial}{\partial x} + \lambda n_x\dfrac{\partial}{\partial y} \\ \lambda n_y\dfrac{\partial}{\partial x} + \mu n_x\dfrac{\partial}{\partial y} & \mu n_x\dfrac{\partial}{\partial x} + (\lambda+2\mu)n_y\dfrac{\partial}{\partial y} \end{bmatrix}, \\ \mathbf{B}_g &= \begin{bmatrix} 1 & 0 \\ 0 & 1 \end{bmatrix} \end{aligned} \tag{69}$$

If $N_c = N_s$, the approach is termed as the direct collocation method (Hu et al. 2007). When $N_c > N_s$, Eq. (68) leads to an overdetermined system and its solution can be obtained using a least-squares method. The solution from an overdetermined system usually offers better accuracy and is less sensitive to the nodal distribution; however, to achieve optimal accuracy, the least-squares system needs to be properly weighted, which is referred to as the weighted collocation method. The details will be discussed in the section "Weighted Collocation Methods and Optimal Weights."

Approximation Functions and Convergence for Strong Form Collocation

Radial Basis Functions

Although any approximation in the C^2 space can be used in the collocation methods, the radial basis functions (RBFs) are popular for collocation solutions of PDEs, tracing back to the seminal work of Kansa (1990a, b). RBFs have been used in many applications, such as surface fitting, turbulence analysis, neural networks, meteorology, and so forth. Hardy (1971) first investigated multiquadric RBFs for interpolation problems, and good performance in scattered data interpolation using multiquadric and thin-plate spline radial basis functions has been observed (Franke and Schaback 1998). Since then, the advances in applying RBFs to various problems has progressed constantly. A few commonly used radial basis functions are given as follows:

$$\text{Multiquadrics(MQ)}: g_I(\mathbf{x}) = (r_I^2 + c^2)^{n-3/2} \tag{70}$$

$$\text{Gaussian}: g_I(\mathbf{x}) = \begin{cases} \exp\left(-\dfrac{r_I^2}{c^2}\right) \\ (r_I^2 + c^2)^{n-3/2} \exp\left(-\dfrac{r_I^2}{a^2}\right) \end{cases} \tag{71}$$

$$\text{Thin plate splines}: g_I(\mathbf{x}) = \begin{cases} r_I^{2n} \ln r_I \\ r_I^{2n-1} \end{cases} \tag{72}$$

$$\text{Logarithmic}: g_I(\mathbf{x}) = r_I^n \ln r_I \tag{73}$$

where $r_I = \|\mathbf{x} - \mathbf{x}_I\|$ with $\|\cdot\|$ the Euclidean norm; and $\mathbf{x}_I$ is the source point of the RBF. The constant c involved in Eq. (70) and Eq. (71) is called the *shape parameter* of RBF. The MQ RBF in Eq. (70) is the most popular function used in the solution of PDEs; the function is called reciprocal MQ RBF if $n = 1$, linear MQ RBF if $n = 2$, cubic MQ RBF if $n = 3$, and so on. Several types of error bounds for MQ have been established (Madych 1992), local errors of scattered data interpolation by RBFs in suitable variational formulations have been investigated (Wu and Schaback 1993), and the convergence of RBFs in Sobolev spaces has been demonstrated (Yoon 2001). All of these studies show that there exists an exponential convergence rate in RBFs. It has also been shown that the convergence rate is accelerated for monotonically ordered c (Buhmann and Micchelli 1992).

For a smooth function $u(\mathbf{x})$, the approximation, denoted by $u^h(\mathbf{x})$, is expressed by Eq. (67). There exists an exponential convergence rate of RBFs given by Madych (1992)

$$\|u - u^h\|_{\ell} \le C_\nu \eta^{c/H} \|u\|_t \tag{74}$$

where $0 < \eta < 1$ is a real number; C_ν is a generic constant with the subscript ν denoting that it is dependent on the Poisson's ratio ν; $\|\cdot\|_{\ell}$ is the Sobolev ℓ-norm; $\|\cdot\|_t$ is induced from the regularity requirements of the approximated function u and the RBFs (Madych and Nelson 1990; Madych 1992), H is the radial distance defined as $H \equiv H(\Omega, \mathbf{S}) = \sup_{\mathbf{x}\in\Omega} \min_{\mathbf{x}_I \in Z} \|\mathbf{x} - \mathbf{x}_I\|$; and

$\eta = \exp(-\theta)$ with $\theta > 0$. The accuracy and rate of convergence of MQ-RBF approximations are determined by the number of basis functions (the number of source points) N_S and the shape parameter c. The application of RBFs to partial differential equations is natural as the RBFs are infinitely differentiable [$g_I(\mathbf{x}) \in C^\infty$].

Moving Least Squares and Reproducing Kernel

The MLS/RK approximations described in the section "Meshfree Approximation Functions" can be adopted in the collocation methods, e.g., the reproducing kernel collocation method (RKCM) (Aluru 2000; Hu et al. 2009, 2011), and the gradient reproducing kernel collocation method (G-RKCM) (Chi et al. 2013). In addition to first derivatives, higher order derivatives of MLS/RK approximations are mandatory when using strong form collocation. They can be obtained by direct differentiation of the MLS/RK approximations or by implicit gradients (Chen et al. 2004; Li and Liu 1999b, a), as discussed in the section "Derivative Approximations in Meshfree Methods."

Although the employment of the C^2 continuous kernel in Eq. (21) in MLS/RK would satisfy the regularity requirements of strong form collocation, higher-order continuous kernels offers better numerical stability, especially when the point density is high. Therefore, a quintic B-spline is often adopted in RKCM

$$\phi_a(z) = \begin{cases} \frac{11}{20} - \frac{9}{2}z^2 + \frac{81}{4}z^4 - \frac{81}{4}z^5 & \text{for } 0 \le z \le \frac{1}{3} \\ \frac{17}{40} + \frac{15}{8}z - \frac{63}{4}z^2 + \frac{135}{4}z^3 - \frac{243}{8}z^4 + \frac{81}{8}z^5 & \text{for } \frac{1}{3} \le z \le \frac{2}{3} \\ \frac{81}{40} - \frac{81}{8}z + \frac{81}{4}z^2 - \frac{81}{4}z^3 + \frac{81}{8}z^4 - \frac{81}{40}z^5 & \text{for } \frac{2}{3} \le z \le 1 \\ 0 & \text{for } z > 1 \end{cases} \tag{75}$$

For a smooth function $u(\mathbf{x})$, the approximation, denoted by $u^h(\mathbf{x})$, can be expressed by the linear combination of MLS/RK shape functions. Solving the PDE by collocation Eq. (65) with the MLS/RK approximation, there exists an algebraic convergence rate as shown by Hu et al. (2009)

$$\|u - u^h\|_E \le C\chi a^{p-1}|u|_{p+1,\Omega} \tag{76}$$

where C is the generic constant; χ is the overlapping parameter; a is the support measure; p is the order of complete monomials in the MLS/RK shape functions; and

$$\|v\|_E \equiv (\|v\|^2_{1,\Omega} + \|\mathcal{L}v\|^2_{0,\Omega} + \|\mathcal{B}_h v\|^2_{0,\partial\Omega_h} + \|\mathcal{B}_g v\|^2_{0,\partial\Omega_g})^{1/2} \tag{77}$$

where $\mathcal{L}$, $\mathcal{B}_h$, and $\mathcal{B}_g$ denote the differential operators associated with the domain, Neumann boundary, and Dirichlet boundary, respectively. From Eq. (76), it is important to note that the solution does not converge when $p = 1$. An order p of at least 2 is mandatory for convergence.

Reproducing Kernel Enhanced Local Radial Basis

The commonly used RBF approximation function in the strong form collocation method offers exponential convergence; however, the method suffers from large condition numbers because of its nonlocal approximation. Conversely, the MLS/RK functions provide polynomial reproducibility in a local approximation, and the corresponding discrete systems are relatively well conditioned. Nonetheless, RKCM produces only algebraic convergence (Hu et al. 2011). An approach has been proposed to combine the advantages of RBF and RK functions to yield a local approximation that is better conditioned than that of the RBF, while at the same time offers a higher rate of convergence than that of RK in Eq. (19)

$$u^h(\mathbf{x}) = \sum_{I \in G_\mathbf{x}} \left\{ \Psi_I(\mathbf{x}) \left[a_I + \sum_{J=1}^{M} g_I^J(\mathbf{x}) d_I^J \right] \right\} \tag{78}$$

where $\Psi_I(\mathbf{x})$ is an RK function with compact support; and $g_I^J(\mathbf{x})$ is an RBF. Applying the approximation in Eq. (78) to the weighted strong form collocation as described in the section "Weighted Collocation Methods and Optimal Weights" is called the localized radial basis collocation method (L-RBCM).

This approximation utilizes the compactly supported partition of unity to patch the global RBFs together. Error analysis shows that if the error of the RK approximation is sufficiently small, the proposed method maintains the exponential convergence of RBFs, while significantly improving the condition of the discrete system, and yields a banded matrix (Chen et al. 2008) as discussed subsequently.

1. Using the partition of unity properties of the RK localizing function, there exists the following error bound (Chen et al. 2008):

$$\|u - u_I^h\|_{0,\Omega} \le \beta C \eta_0^{c/\delta} \|u\|_t \tag{79}$$

   where β is the maximum cover number for the RK localizing function. Other parameters are the same as defined earlier.
2. The enhanced stability in L-RBCM can be demonstrated by a perturbation analysis of the strong form collocation equations in Eq. (68) expressed in the following linear system:

$$\mathbf{Kd} = \mathbf{f} \tag{80}$$

The stability of the linear system can be measured by the condition number of $\mathbf{K}$. The following estimation of the condition number of L-RBCM has been provided (Chen et al. 2008):

$$\text{Cond}(\mathbf{K}) \approx O(a^{-3d/2}) \tag{81}$$

where d is the spatial dimension. In two-dimensional elasticity, the following comparison of condition numbers using RBCM with pure RBFs, RKCM with pure RK in Eq. (19), and L-RBCM with localized RBF in Eq. (78) can be obtained:

$$\begin{array}{ll} \text{RBCM:} & \text{Cond}(\mathbf{K}) \approx O(h^{-8}), \\ \text{RKPM:} & \text{Cond}(\mathbf{K}) \approx O(h^{-2}), \\ \text{L}-\text{RBCM:} & \text{Cond}(\mathbf{K}) \approx O(h^{-3}) \end{array} \tag{82}$$

The L-RBCM approach offers a significant improvement on stability over RBCM. Although the discrete system of L-RBCM is slightly less well-conditioned than that of RKPM, it offers higher convergence rates similar to that in RBCM.

Weighted Collocation Methods and Optimal Weights for Strong Form Collocation

When $N_C > N_S$, the collocation equations Eq. (68) recast in a matrix form as Eq. (80) leads to an overdetermined system, and a least-squares method can be applied for seeking the solution, equivalent to minimizing a weighted residual. The residual is defined as $e(\mathbf{d}) = 1/2(\mathbf{Kd} - \mathbf{f})^T \mathbf{W}(\mathbf{Kd} - \mathbf{f})$, where $\mathbf{W}$ is a symmetric weighting matrix, minimizing $e(\mathbf{d})$ yields

$$\mathbf{K}^T\mathbf{WKd} = \mathbf{K}^T\mathbf{Wf} \tag{83}$$

It has been shown that solving strong form collocation equations by a least-squares method is equivalent to minimizing a least-squares functional with quadrature (Hu et al. 2007) . It states to find $\mathbf{u}^h$ such that

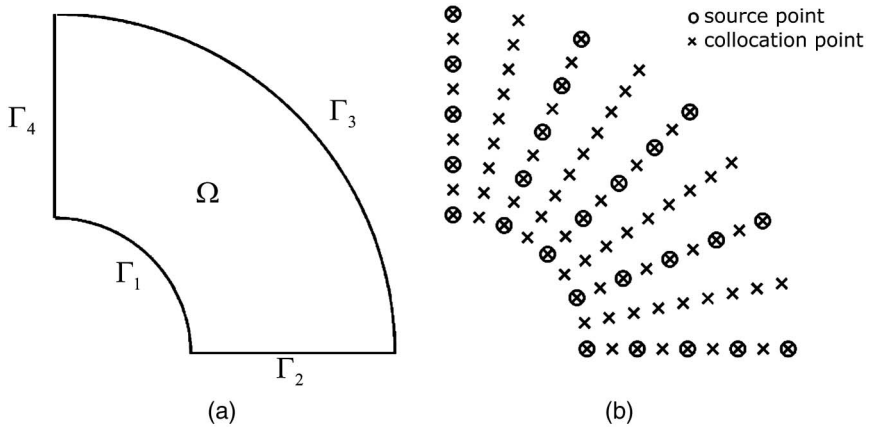

Fig. 17. Tube problem: (a) quarter model; (b) distribution of source points and collocation points

$$E(\mathbf{u}^h) = \inf_{\mathbf{v}\in V} E(\mathbf{v}) \tag{84}$$

where V is the admissible finite dimensional space spanned by meshfree shape functions; and

$$E(\mathbf{v}) = \frac{1}{2}\hat{\int}_{\Omega}(\mathbf{L}\mathbf{v}+\mathbf{b})^2 d\Omega + \frac{1}{2}\hat{\int}_{\partial\Omega_h}(\mathbf{B}_h\mathbf{v}-\mathbf{h})^2 d\Gamma + \frac{1}{2}\hat{\int}_{\partial\Omega_g}(\mathbf{B}_g\mathbf{v}-\mathbf{g})^2 d\Gamma \tag{85}$$

Recall that $\hat{\int}$ denotes integration with quadrature. It has been shown that the errors from the domain and boundary integrals in Eq. (85) are unbalanced (Hu et al. 2007). Therefore, a weighted least-squares functional can be introduced

$$E(\mathbf{v}) = \frac{1}{2}\int_{\Omega}(\mathbf{L}\mathbf{v}-\mathbf{f})^2 d\Omega + \frac{\alpha^h}{2}\int_{\partial\Omega_h}(\mathbf{B}_h\mathbf{v}-\mathbf{h})^2 d\Gamma + \frac{\alpha^g}{2}\int_{\partial\Omega_g}(\mathbf{B}_g\mathbf{v}-\mathbf{g})^2 d\Gamma \tag{86}$$

Here the weights α^h and α^g are determined by considering error balancing of the weighted least-squares functional associated with the domain and boundary equations (Hu et al. 2007)

$$\sqrt{\alpha_h} \approx O(1), \qquad \sqrt{\alpha_g} \approx O(\kappa N_S) \tag{87}$$

where $\kappa = \max(\lambda, \mu)$, or more generally, the maximum coefficient involved in the differential operator and boundary operator for the problem at hand. When dealing with nearly incompressible problems, $\kappa = \mu$ has been suggested (Chi et al. 2014) as λ grows unbounded in the incompressible limit.

Minimizing Eq. (86) is equivalent to solving the following weighted collocation equations by the least squares method:

$$\begin{aligned} &\sum_{I\in G_{\xi_J}} \mathbf{L} g_I(\boldsymbol{\xi}_J)\mathbf{u}_I = -\mathbf{b}(\boldsymbol{\xi}_J) && \forall\ \boldsymbol{\xi}_J \in \Omega, \\ &\sqrt{\alpha_h}\sum_{I\in G_{\xi_J}} \mathbf{B}_h g_I(\boldsymbol{\xi}_J)\mathbf{u}_I = \sqrt{\alpha_h}\mathbf{h}(\boldsymbol{\xi}_J) && \forall\ \boldsymbol{\xi}_J \in \partial\Omega_h, \\ &\sqrt{\alpha_g}\sum_{I\in G_{\xi_J}} \mathbf{B}_g g_I(\boldsymbol{\xi}_J)\mathbf{u}_I = \sqrt{\alpha_g}\mathbf{g}(\boldsymbol{\xi}_J) && \forall\ \boldsymbol{\xi}_J \in \partial\Omega_g \end{aligned} \tag{88}$$

For example, an infinitely long (plane-strain) elastic tube is subjected to an internal pressure. The tube is made of an elastic material with Young's modulus $E = 3\times10^7$ Pa, and Poisson ratio $\upsilon = 0.25$. The inner and outer radii of the tube are 4 and 10 m, respectively, and the inner surface of the tube is subjected to a pressure $P = 100\ \mathrm{N/m^2}$. Because of symmetry, only a quarter of the model, as shown in Fig. 17(a), is discretized by the RBF collocation method with proper symmetric boundary conditions specified. The corresponding boundary value problem can be expressed as

$$\nabla\cdot\boldsymbol{\sigma} = \mathbf{0} \quad \text{in } \Omega \tag{89}$$

with boundary conditions

$$\begin{aligned} &h_i = -Pn_i && \text{on } \Gamma_1 \\ &h_1 = 0, u_2 = 0 && \text{on } \Gamma_2 \\ &h_i = 0 && \text{on } \Gamma_3 \\ &h_2 = 0, u_1 = 0 && \text{on } \Gamma_4 \end{aligned} \tag{90}$$

where $h_i = \sigma_{ij}n_j$.

In this problem, both source points and collocation points are nonuniformly distributed as shown in Fig. 17(b). Three different discretizations, 7×7, 9×9, and 11×11 source points, are used, and the shape parameters c for the three discretizations are 10.0, 7.5, and 6.0, respectively. The number of corresponding collocation points is $(2N_1-1)(2N_2-1)$, where N_1 is the number of source points along the radial direction, and N_2 is the number of source points along the angular direction.

The direct collocation method (DCM) and weighted collocation method (WCM) with MQ RBFs are used in the numerical test. For WCM, weights for Dirichlet collocation equations $\sqrt{\alpha_g} = 10$ and Neumann collocation equations $\sqrt{\alpha_h} = 1$ are selected based on Eq. (87). The convergence in the L_2 norm and H^1 seminorm obtained by DCM and WCM are compared in Fig. 18. As is shown in the numerical results, the direct collocation method with proper weights for Dirichlet and Neumann boundaries offers a much improved solution over DCM.

Gradient Reproducing Kernel Collocation Method

While MLS/RK approximation functions can be arbitrarily smooth, taking derivatives of these functions is computationally costly. In particular, the high complexity in RKCM is caused by taking derivatives of the moment matrix inverse in the multidimensional MLS/RK shape functions (Hu et al. 2009). Further, for optimal convergence in RKCM, using a number of collocation points much larger than the number of source points is needed, and this adds additional computational effort (Hu et al. 2009, 2011). To enhance computational efficiency in RKCM, an implicit gradient approximation (see section "Derivative Approximations in

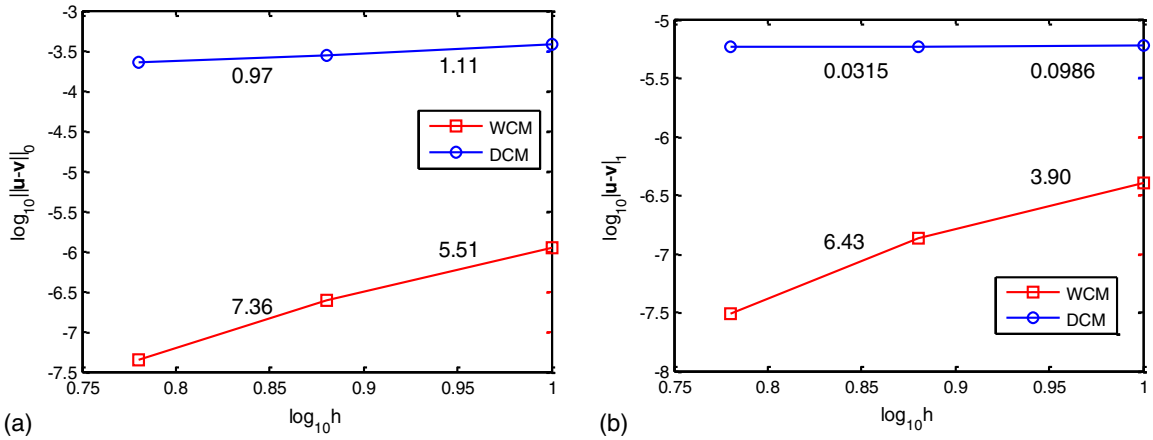

Fig. 18. Convergence in the tube problem in (a) the L_2 error norm; (b) the H^1 seminorm

Meshfree Methods") has been introduced for solving second order PDEs with strong form collocation, which has been termed the gradient reproducing kernel collocation method (G-RKCM) (Chi et al. 2013).

Consider the two-dimensional version of the elastic model problem in Eqs. (44)–(46). The approximations of the derivatives $\mathbf{u}_{,x}$ and $\mathbf{u}_{,y}$ are constructed by employing first order implicit gradients $\{\Psi_I^{\alpha}(\mathbf{x})\}_{|\alpha|=1}$ where $\Psi_I^{\alpha}(\mathbf{x})$ is given in Eq. (35)

$$\mathbf{u}_{,x} \approx \mathbf{u}_x^h = \sum_{I\in G_{\mathbf{x}}} \Psi_I^{(1,0)}(\mathbf{x})\mathbf{u}_I,$$
$$\mathbf{u}_{,y} \approx \mathbf{u}_y^h = \sum_{I\in G_{\mathbf{x}}} \Psi_I^{(0,1)}(\mathbf{x})\mathbf{u}_I \tag{91}$$

The approximation of second order derivatives of $\mathbf{u}$ is obtained by taking direct derivatives of $\mathbf{u}_x^h$ and $\mathbf{u}_y^h$, e.g.

$$\mathbf{u}_{,xx} \approx \mathbf{u}_{x,x}^h = \sum_{I\in G_{\mathbf{x}}} \Psi_{I,x}^{(1,0)}(\mathbf{x})\mathbf{u}_I,$$
$$\mathbf{u}_{,yy} \approx \mathbf{u}_{y,y}^h = \sum_{I\in G_{\mathbf{x}}} \Psi_{I,y}^{(0,1)}(\mathbf{x})\mathbf{u}_I \tag{92}$$

Introducing Eqs. (91) and (67) in the discretization in the strong form Eqs. (44)–(46) leads to

$$\begin{aligned} &\mathbf{L}_h^1\mathbf{u}_x^h + \mathbf{L}_h^2\mathbf{u}_y^h = -\mathbf{b} && \text{in } \Omega \\ &\mathbf{B}_h^1\mathbf{u}_x^h + \mathbf{B}_h^2\mathbf{u}_y^h = \mathbf{h} && \text{on } \partial\Omega_h \\ &\mathbf{B}_g\mathbf{u}^h = \mathbf{g} && \text{on } \partial\Omega_g \end{aligned} \tag{93}$$

where

$$\mathbf{L}_h^1 = \begin{bmatrix} (\lambda+2\mu)\dfrac{\partial}{\partial x} & \mu\dfrac{\partial}{\partial y} \\ \lambda\dfrac{\partial}{\partial y} & \mu\dfrac{\partial}{\partial x} \end{bmatrix}, \quad \mathbf{L}_h^2 = \begin{bmatrix} \mu\dfrac{\partial}{\partial y} & \lambda\dfrac{\partial}{\partial x} \\ \mu\dfrac{\partial}{\partial x} & (\lambda+2\mu)\dfrac{\partial}{\partial y} \end{bmatrix},$$
$$\mathbf{B}_h^1 = \begin{bmatrix} (\lambda+2\mu)n_x & \mu n_y \\ \lambda n_y & \mu n_x \end{bmatrix}, \quad \mathbf{B}_h^2 = \begin{bmatrix} \mu n_y & \lambda n_x \\ \mu n_x & (\lambda+2\mu)n_y \end{bmatrix} \tag{94}$$

When $N_C > N_S$, the overdetermined system can be obtained by a least-squares method with proper weights to achieve optimal solution accuracy

$$\begin{aligned} &\sum_{I\in G_{\xi_J}} [\mathbf{L}^1\Psi_I^{(1,0)}(\boldsymbol{\xi}_J) + \mathbf{L}^2\Psi_I^{(0,1)}(\boldsymbol{\xi}_J)]\mathbf{u}_I = -\mathbf{b}(\boldsymbol{\xi}_J) && \forall\, \boldsymbol{\xi}_J \in \Omega, \\ &\sqrt{\alpha_h}\sum_{I\in G_{\xi_J}} [\mathbf{B}_h^1\Psi_I^{(1,0)}(\boldsymbol{\xi}_J) + \mathbf{B}_h^2\Psi_I^{(0,1)}(\boldsymbol{\xi}_J)]\mathbf{u}_I = \sqrt{\alpha_h}\mathbf{h}(\boldsymbol{\xi}_J) && \forall\, \boldsymbol{\xi}_J \in \partial\Omega_h, \\ &\sqrt{\alpha_g}\sum_{I\in G_{\xi_J}} \mathbf{B}_g\Psi_I(\boldsymbol{\xi}_J)\mathbf{u}_I = \sqrt{\alpha_g}\mathbf{g}(\boldsymbol{\xi}_J) && \forall\, \boldsymbol{\xi}_J \in \partial\Omega_g \end{aligned} \tag{95}$$

For balance of the errors between the domain and boundary equations, the following weights should be selected:

$$\sqrt{\alpha_h} \approx O(1), \qquad \sqrt{\alpha_g} \approx O(\kappa a^{q-p-1}) \tag{96}$$

where $\kappa = \max(\lambda, \mu)$; a is the kernel support measure; p is the MLS/RK order in $\mathbf{u}^h$; and q is the order of $\mathbf{u}_x^h$ and $\mathbf{u}_y^h$. The convergence properties of G-RKCM have been shown to be as follows:

$$\|u - u^h\|_{1,\Omega} \approx O(a^{q-1}),$$
$$\|u_{,x} - u_x^h\|_{1,\Omega} + \|u_{,y} - u_y^h\|_{1,\Omega} \approx O(a^{q-1}) \tag{97}$$

$$\|u - u^h\|_{0,\Omega} \approx O(a^{q}),$$
$$\|u_{,x} - u_x^h\|_{0,\Omega} + \|u_{,y} - u_y^h\|_{0,\Omega} \approx O(a^{q}) \tag{98}$$

The following remarks should also be noted:

- The error estimate in Eqs. (97) and (98) indicates that the convergence of G-RKCM is only dependent on the polynomial degree q in the approximation of $\mathbf{u}_{,x}$ and $\mathbf{u}_{,y}$, and is independent of the polynomial degree p in the approximation of $\mathbf{u}$. Further, $q > 1$ is mandatory for convergence; and
- G-RKCM allows the use of $N_C = N_S$ for sufficient accuracy (Chi et al. 2013).

Subdomain Collocation for Heterogeneity and Discontinuities

Because of the overlapping supports of meshfree shape functions (particularly RBFs) and the high smoothness required in the strong form collocation methods, special treatments are required for problems with heterogeneity or discontinuities. The subdomain collocation method (Chen et al. 2009; Wang et al. 2010) has been introduced for this purpose.

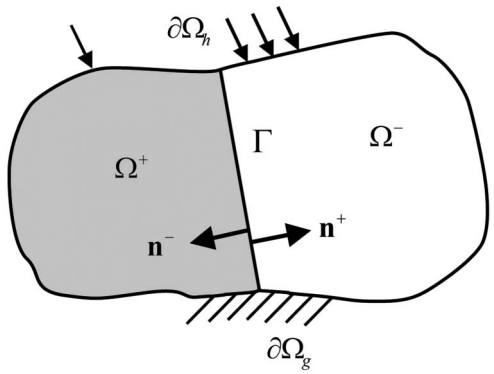

Fig. 19. Two subdomains of a problem with material heterogeneity

Take a heterogeneous elastic domain as an example, as shown in Fig. 19. The collocation of each subdomain is independently expressed as follows:

$$\begin{cases} \mathbf{L}^+\mathbf{u}^{h+} = -\mathbf{b}^+ & \text{in } \Omega^+ \\ \mathbf{B}_g^+\mathbf{u}^{h+} = \mathbf{g}^+ & \text{on } \partial\Omega^+ \cap \partial\Omega^g \\ \mathbf{B}_h^+\mathbf{u}^{h+} = \mathbf{h}^+ & \text{on } \partial\Omega^+ \cap \partial\Omega^h \end{cases} \tag{99}$$

$$\begin{cases} \mathbf{L}^-\mathbf{u}^{h-} = -\mathbf{b}^- & \text{in } \Omega^- \\ \mathbf{B}_g^-\mathbf{u}^{h-} = \mathbf{g}^- & \text{on } \partial\Omega^- \cap \partial\Omega^g \\ \mathbf{B}_h^-\mathbf{u}^{h-} = \mathbf{h}^- & \text{on } \partial\Omega^- \cap \partial\Omega^h \end{cases} \tag{100}$$

The approximation of $\mathbf{u}$ in each subdomain is performed by separate sets of basis functions

$$\mathbf{u}^h(\mathbf{x}) = \begin{cases} \mathbf{u}^{h+}(\mathbf{x}) = g_1^+(\mathbf{x})\mathbf{u}_1^+ + \cdots + g_{N_s^+}^+(\mathbf{x})\mathbf{u}_{N_s^+}^+, & \mathbf{x} \in \bar{\Omega}^+ \\ \mathbf{u}^{h-}(\mathbf{x}) = g_1^-(\mathbf{x})\mathbf{u}_1^- + \cdots + g_{N_s^-}^-(\mathbf{x})\mathbf{u}_{N_s^-}^-, & \mathbf{x} \in \bar{\Omega}^- \end{cases} \tag{101}$$

Here, Dirichlet and Neumann type interface conditions are introduced on the interface as follows for optimal convergence (Wang et al. 2010)

$$\begin{aligned} &\mathbf{u}^{h+} - \mathbf{u}^{h-} = \mathbf{0} && \text{on } \Gamma \\ &\mathbf{B}_h^+\mathbf{u}^{h+} + \mathbf{B}_h^-\mathbf{u}^{h-} = \mathbf{0} && \text{on } \Gamma \end{aligned} \tag{102}$$

As before, if $N_C > Ns$ a weighted least-squared method can be applied, and the weighted discretized collocation equations read

$$\mathbf{A}\mathbf{u} \equiv \begin{bmatrix} \mathbf{A}^+ \\ \mathbf{A}^- \\ \mathbf{\Lambda} \end{bmatrix} \mathbf{u} = \begin{bmatrix} \mathbf{b}^+ \\ \mathbf{b}^- \\ \mathbf{0} \end{bmatrix} \equiv \mathbf{b} \tag{103}$$

with submatrices defined as

$$\mathbf{A}^\pm = \begin{bmatrix} \mathbf{A}_L^\pm \\ \sqrt{\alpha_g^\pm}\mathbf{A}_g^\pm \\ \sqrt{\alpha_h^\pm}\mathbf{A}_h^\pm \end{bmatrix}; \qquad \mathbf{b}^\pm = \begin{bmatrix} \mathbf{b}_L^\pm \\ \sqrt{\alpha_g^\pm}\mathbf{b}_g^+ \\ \sqrt{\alpha_h^\pm}\mathbf{b}_h^+ \end{bmatrix}; \qquad \mathbf{\Lambda} = \begin{bmatrix} \sqrt{\bar{\alpha}_g}\mathbf{\Lambda}_g \\ \sqrt{\bar{\alpha}_h}\mathbf{\Lambda}_h \end{bmatrix} \tag{104}$$

where $\mathbf{A}_L^\pm$, $\mathbf{A}_g^\pm$, and $\mathbf{A}_h^\pm$ are matrices associated with the differential operators $\mathbf{L}^\pm$, $\mathbf{B}_g^\pm$ and $\mathbf{B}_h^\pm$, respectively; and $\mathbf{\Lambda}_g$ and $\mathbf{\Lambda}_h$ are associated with the Dirichlet and Neumann type interface conditions, respectively. For balanced errors from different terms associated with domains, boundaries, and the interface, the following weights have been derived (Chen et al. 2009):

$$\begin{aligned} &\sqrt{\alpha_g^+} = \sqrt{\alpha_g^-} = \sqrt{\bar{\alpha}_g} = O(\bar{k} \cdot \bar{N}_s), \\ &\sqrt{\alpha_h^+} = O(s^+), \\ &\sqrt{\alpha_h^-} = O(s^-), \\ &\sqrt{\bar{\alpha}_h} = O(1) \end{aligned} \tag{105}$$

where $k^\pm = \max(\lambda^\pm, \mu^\pm)$; $\bar{k} = \max(k^+, k^-)$; $\bar{N}_s = \max(N_s^+, N_s^-)$; $s^\pm = \bar{k}/k^\pm$; $\lambda^\pm$ and $\mu^\pm$ are Lamé constants in $\bar{\Omega}^\pm$; and $N_s^\pm$ is the number of source points in $\bar{\Omega}^\pm$.

The L-RBCM approach, combined with the subdomain collocation method, has been applied to problems with heterogeneities (weak discontinuities) (Chen et al. 2009) and cracks (strong discontinuities) (Wang et al. 2010).

Meshfree Method for Large Deformation Problems

Lagrangian Reproducing Kernel Approximation and Discretization

The RK approximation is constructed based on a set of points without a mesh and hence releases the strong dependence of the approximation accuracy on mesh quality. It is therefore well-suited for applications to extreme deformation problems. To illustrate, let $\mathbf{X}$ be the material coordinates for a body initially occupying the domain $\Omega_\mathbf{X}$ with the boundary $\Gamma_\mathbf{X}$, and $\mathbf{x}$ be the position of the material point $\mathbf{X}$ in the deformed configuration $\Omega_\mathbf{x}$ with the boundary $\Gamma_\mathbf{x}$ at time t. The position vector $\mathbf{x}$ is given by a one-to-one mapping function, $\mathbf{x} = \varphi(\mathbf{X}, t)$, and hence the Jacobian of the deformation gradient, $\det(\mathbf{F})$, where $F_{ij} = dx_i/dX_j$, is positive definite for problems without material damage and fragmentation.

The variational equation of motion with reference to the current configuration is

$$\int_{\Omega_x} \delta u_i \rho \ddot{u}_i d\Omega + \int_{\Omega_x} \delta u_{i,j}\sigma_{ij} d\Omega = \int_{\Omega_x} \delta u_i b_i d\Omega + \int_{\Gamma_x^h} \delta u_i h_i d\Gamma \tag{106}$$

where u_i is the displacement; ρ is the density of the material; σ_{ij} is the Cauchy stress; b_i is the body force; and h_i is the prescribed traction on the natural boundary $\Gamma_\mathbf{x}^h$. In the Lagrangian formulation, the Lagrangian RK shape functions $\Psi_I^\mathbf{X}(\mathbf{X})$ are constructed using the material coordinates in the reference configuration to yield

$$\Psi_I^\mathbf{X}(\mathbf{x}) = \mathbf{H}^T(\mathbf{0})\mathbf{M}^{-1}(\mathbf{X})\mathbf{H}(\mathbf{X} - \mathbf{X}_I)\phi_a(\mathbf{X} - \mathbf{X}_I) \tag{107}$$

where

$$\mathbf{M}(\mathbf{X}) = \sum_{I \in G_\mathbf{X}} \mathbf{H}(\mathbf{X} - \mathbf{X}_I)\mathbf{H}^T(\mathbf{X} - \mathbf{X}_I)\phi_a(\mathbf{X} - \mathbf{X}_I) \tag{108}$$

The discrete reproducing conditions are imposed in the reference configuration

$$\sum_{I \in G_\mathbf{X}} \Psi_I^\mathbf{X}(\mathbf{X})\mathbf{X}_I^\alpha = \mathbf{X}^\alpha, \quad |\alpha| \le n \tag{109}$$

The Lagrangian RK function has a deformation-dependent support size when mapped to the current configuration, as shown in Figs. 20(a and b).

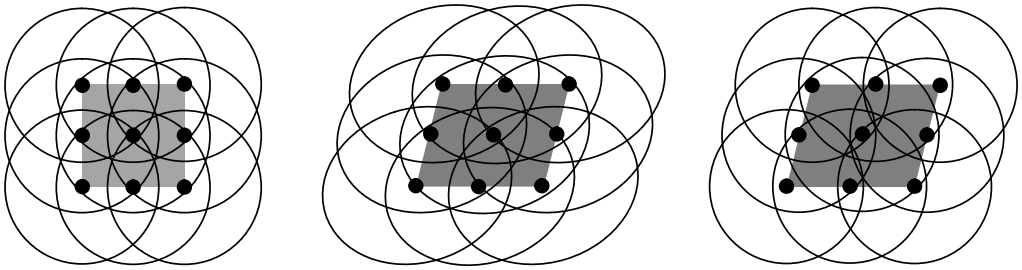

Fig. 20. Comparison of Lagrangian and semi-Lagrangian RK kernels: (a) undeformed configuration; (b) Lagrangian RK in the deformed configuration; (c) semi-Lagrangian RK in the deformed configuration

For path-dependent materials, the discretization of Eq. (106) by the Lagrangian RK approximation requires the spatial derivatives of $\Psi_I^{\mathbf{X}}(\mathbf{X})$ as follows:

$$\frac{\partial \Psi_I^{\mathbf{X}}(\mathbf{X})}{\partial x_i} = \frac{\partial \Psi_I^{\mathbf{X}}(\mathbf{X})}{\partial X_j} F_{ji}^{-1} \tag{110}$$

The deformation gradient $\mathbf{F}$ is first computed by taking the material spatial derivatives of $\Psi_I^{\mathbf{X}}(\mathbf{X})$, and $\mathbf{F}^{-1}$ is obtained directly by the inversion of $\mathbf{F}$. The Lagrangian formulation breaks down when the inverse of $\mathbf{F}$ is not well conditioned. For example, this may occur when extreme deformation leads to a nonpositive definite $\mathbf{F}$, or when material separation takes place in which $\mathbf{F}$ is singular. Thus, a semi-Lagrangian RK formulation is introduced in the following section to address this issue in modeling extreme deformation problems.

Semi-Lagrangian Reproducing Kernel Approximation and Discretization

In the semi-Lagrangian RK formulation, the nodal point $\mathbf{x}_I$ associated with the RK shape functions $\Psi_I(\mathbf{x})$ follows the motion of a material point, that is, $\mathbf{x}_I = \varphi(\mathbf{X}_I, t)$, whereas the support radius in the kernel function is defined independent of material deformation as shown in Figs. 20(a and c).

The semi-Lagrangian RK shape function is then formulated in the current configuration as

$$\Psi_I^{SL}(\mathbf{x}) = C(\mathbf{x}; \mathbf{x} - \mathbf{x}_I)\phi_a(\mathbf{x} - \mathbf{x}_I) \tag{111}$$

where $\mathbf{x}_I = \varphi(\mathbf{X}_I, t)$.

The correction function $C(\mathbf{x}; \mathbf{x} - \mathbf{x}_I)$ for ensuring the reproducing condition is defined in the Lagrangian description while the kernel function in defining the locality and continuity is not purely Lagrangian. Similar to the discussion in the section "Reproducing Kernel Approximation," the coefficient vector $\mathbf{b}(\mathbf{x})$ can be determined by imposing the following discrete reproducing condition:

$$\sum_{I \in G_{\mathbf{x}}} \Psi_I^{SL}(\mathbf{x}) \mathbf{x}_I^{\alpha} = \mathbf{x}^{\alpha}, \quad |\alpha| \le n \tag{112}$$

Substituting the coefficient vector $\mathbf{b}(\mathbf{x})$ into Eq. (111) yields the semi-Lagrangian reproducing kernel (semi-Lagrangian RK) shape function

$$\Psi_I^{SL}(\mathbf{x}) = \mathbf{H}^T(\mathbf{0})\mathbf{M}^{-1}(\mathbf{x})\mathbf{H}(\mathbf{x} - \mathbf{x}_I)\phi_a(\mathbf{x} - \mathbf{x}_I) \tag{113}$$

where

$$\mathbf{M}(\mathbf{x}) = \sum_{I \in G_{\mathbf{x}}} \mathbf{H}(\mathbf{x} - \mathbf{x}_I)\mathbf{H}^T(\mathbf{x} - \mathbf{x}_I)\phi_a(\mathbf{x} - \mathbf{x}_I) \tag{114}$$

The $\mathbf{x}$ coordinate in Ψ_I and $\mathbf{M}$ is also a function of time. Let the velocity v_i be the primary variable in Eq. (106), approximated by the semi-Lagrangian RK shape functions

$$v_i^h(\mathbf{x}, t) = \sum_{I \in G_{\mathbf{x}}} \Psi_I^{SL}(\mathbf{x}) v_{Ii}(t) \tag{115}$$

The corresponding semi-Lagrangian approximation of acceleration is given by

$$\ddot{u}_i^h(\mathbf{x}, t) = \dot{v}_i^h(\mathbf{x}, t) = \sum_{I \in G_{\mathbf{x}}} [\Psi_I^{SL}(\mathbf{x}) \dot{v}_{Ii}(t) + \check{\Psi}_I^{SL}(\mathbf{x}) v_{Ii}(t)] \tag{116}$$

where $\check{\Psi}_I^{SL}$ is the correction due to the time-dependent change of the semi-Lagrangian kernel $\dot{\phi}_a(\mathbf{x} - \mathbf{x}_I)$

$$\check{\Psi}_I^{SL}(\mathbf{x}) = C(\mathbf{x}; \mathbf{x} - \mathbf{x}_I)\dot{\phi}_a(\mathbf{x} - \mathbf{x}_I) \tag{117}$$

where $(\dot{\cdot})$ denotes the material time derivative and therefore

$$\dot{\phi}_a(\mathbf{x} - \mathbf{x}_I) = \dot{\phi}_a\left(\frac{\|\mathbf{x} - \mathbf{x}_I\|}{a}\right) = \phi'_a \frac{\mathbf{q} \cdot (\mathbf{v} - \mathbf{v}_I)}{a} \tag{118}$$

where

$$\mathbf{q} = (\mathbf{x} - \mathbf{x}_I)/\|\mathbf{x} - \mathbf{x}_I\| \tag{119}$$

and $\|\cdot\|$ designates the length of a vector. Note that the correction function C in Eq. (117) is used to ensure the reproducing condition of the time derivative of the semi-Lagrangian kernel $\dot{\phi}_a(\mathbf{x} - \mathbf{x}_I)$ and thus the time rate change of C is not considered.

Substituting Eq. (116) into Eq. (106) yields the following semi-discrete equation

$$\mathbf{M}\dot{\mathbf{v}} + \mathbf{N}\mathbf{v} = \mathbf{f}^{\text{ext}} - \mathbf{f}^{\text{int}} \tag{120}$$

where

$$\mathbf{M}_{IJ} = \int_{\Omega_x} \rho \Psi_I^{SL}(\mathbf{x}) \Psi_J^{SL}(\mathbf{x}) \mathbf{I} d\Omega \tag{121}$$

$$\mathbf{N}_{IJ} = \int_{\Omega_x} \rho \Psi_I^{SL}(\mathbf{x}) \check{\Psi}_J^{SL}(\mathbf{x}) \mathbf{I} d\Omega \tag{122}$$

$$\mathbf{f}_I^{\text{ext}} = \int_{\Omega_x} \Psi_I^{SL} \mathbf{b} d\Omega + \int_{\Gamma_x^h} \Psi_I^{SL} \mathbf{h} d\Gamma \tag{123}$$

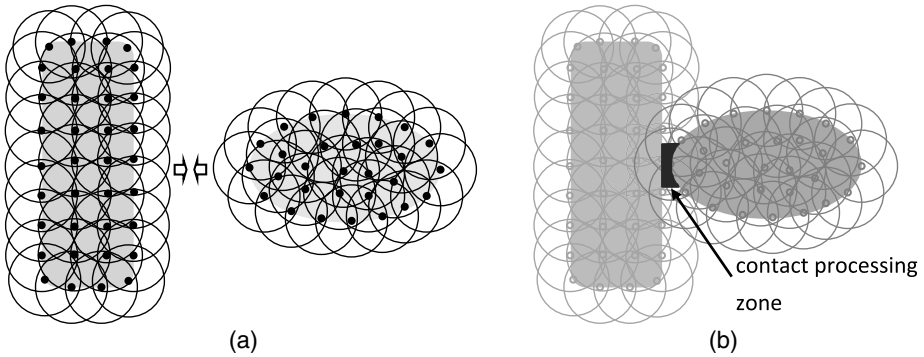

Fig. 21. Natural kernel contact algorithm by kernel interaction between contacting bodies: (a) two bodies without kernel interaction; (b) contact by kernel interaction due to proximity

$$\mathbf{f}_I^{\text{int}} = \int_{\Omega_x} \mathbf{B}_I^T \boldsymbol{\Sigma} d\Omega \tag{124}$$

Here, $\mathbf{I}$ denotes the identity matrix, $\mathbf{B}_I$ is the gradient matrix of $u_{(i,j)}$ associated with node I, $\boldsymbol{\Sigma}$ is the stress vector associated with σ_{ij}, and $\mathbf{b}$ and $\mathbf{h}$ are the body force and surface traction vectors, respectively. The temporal stability condition for the semi-Lagrangian RK formulation has been established (Guan et al. 2009).

The authors would like to provide the following remarks. If a nodal integration scheme, such as direct nodal integration, stabilized conforming nodal integration, and stabilized nonconforming nodal integration, is employed, the diagonal terms of $\mathbf{N}$ vanish and the off-diagonal terms of $\mathbf{N}$ have relatively negligible influence over Eq. (120). Therefore, the convective effect, $\mathbf{Nv}$ in Eq. (120), can be omitted in the semidiscrete equations of motion for the sake of computational efficiency.

Kernel Contact Algorithms

In extreme deformation problems with material separation, contact surfaces are unknown and are part of the solution. As a consequence the conventional contact algorithms, in which all possible contact surfaces are defined a priori, are ineffective in modeling such problems. Conversely, kernel contact (KC) algorithms (Chi et al. 2015; Guan et al. 2011) approximate the contact condition without relying on the predefined contact surfaces at the preprocessing stage. The overlap between the semi-Lagrangian RK shape functions induces internal forces between particles, ensuring the impenetrability between different bodies, as shown in Fig. 21, which leads to the so-called natural kernel contact algorithm. A layer of a friction-like elastoplastic material, as shown in Fig. 22, can be introduced in the contact processing zone to mimic the friction law, which leads to the contact algorithms in the sections "Friction-Like Plasticity Model" and "Semi-Lagrangian RK Discretization and Kernel Contact Algorithms."

Friction-Like Plasticity Model

In kernel contact, a friction-like material can be introduced between contacting bodies, Ω_c as shown in Fig. 22, to mimic the frictional contact conditions. Based on the analogy between Coulomb's friction law and the elastoplasticity flow rule, the variational contact equation leads to a constitutive equation governing the stress-strain relationship of a friction-like material such that Coulomb's friction is recovered (Chi et al. 2015; Guan et al. 2011)

$$\boldsymbol{\sigma}_c \cdot \mathbf{n} = t_N \mathbf{n} + \mathbf{t}_T \tag{125}$$

where $\boldsymbol{\sigma}_c$ is the Cauchy stress in Ω^c; $\mathbf{n}$ is the unit outward normal of the contact surface Γ^c; t_N is the normal component of the contact traction; and $\mathbf{t}_T$ is the tangential contact traction. Eq. (125) indicates that the stresses in the friction-like material are in balance with t_N and $\mathbf{t}_T$ on Γ^c. Therefore, an elastic-perfectly-plastic material, in which the stress $\boldsymbol{\sigma}_c$ in Ω^c obeys Eq. (125), can be introduced in the contact processing zone to mimic the Coulomb's friction law. To obtain $\boldsymbol{\sigma}_c$, consider the following yield function and the associated Karush-Kuhn-Tucker conditions based on local coordinates where the one-direction is aligned with the contact surface normal $\mathbf{n}$

$$f(\boldsymbol{\tau}) = \|\boldsymbol{\tau}\| + \mu \hat{\sigma}_{11} \le 0 \tag{126}$$

$$\dot{\mathbf{e}} = \gamma \frac{\partial f}{\partial \boldsymbol{\tau}} \tag{127}$$

$$\gamma \ge 0 \tag{128}$$

$$\gamma f = 0 \tag{129}$$

where $\boldsymbol{\tau} = [\,\hat{\sigma}_{12} \quad \hat{\sigma}_{13}\,]$; $\hat{\sigma}_{11} \le 0$ is the normal contact stress; $\dot{\mathbf{e}}$ is the tangential strain rate; $\hat{\boldsymbol{\sigma}} = \mathbf{L}\boldsymbol{\sigma}\mathbf{L}^T$ is the rotated Cauchy stress tensor onto the local coordinate system; the two-direction and three-direction are aligned with two mutually orthogonal unit vectors $\mathbf{p}$ and $\mathbf{q}$ in the tangent plane; and $\mathbf{L} = [\mathbf{n}, \mathbf{p}, \mathbf{q}]^T$. It is also assumed that the normal contact stress $\hat{\sigma}_{11}$ is known in Eq. (126). The yield stress $\mu|\hat{\sigma}_{11}|$ mimics the friction stress induced by the normal stress $\hat{\sigma}_{11}$, and the slip condition is represented by the yield condition in the plasticity model

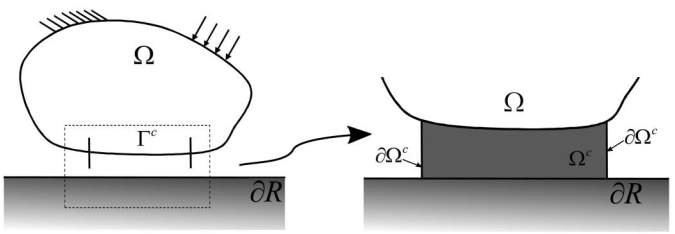

Fig. 22. Schematic of a deformable body contacting with a rigid surface, and an artificial material introduced between two bodies in contact, for enforcing the contact constraints

J. Eng. Mech., 2017, 143(4): 04017001

$$\begin{array}{lll} f<0, & & \text{stick condition (elastic)} \\ f=0, & \|\boldsymbol{\tau}\| = -\mu\hat{\sigma}_{11} & \text{slip condition (plastic)} \end{array} \tag{130}$$

This approach can be carried out by a predictor-corrector algorithm, in which the stresses calculated based on the overlapping supports of the contacting bodies are obtained in the predictor step, and in the corrector step the tangential stresses are corrected according to Eqs. (126)–(129) with $\hat{\sigma}_{11}$ fixed. To enhance the iteration convergence of the two-step approach, the radial return algorithm is introduced, where the trial is nonslip (an elastic trial), and the violation of the yield function (interpenetration) is corrected by the return mapping algorithm. Following the radial return mapping, the corrected contact stresses $\hat{\boldsymbol{\sigma}}_c$ in the local coordinate induced by the friction-like elastoplasticity model can be obtained as

$$\hat{\boldsymbol{\sigma}}_c = \hat{\boldsymbol{\sigma}}^{\text{trial}} + \lambda \begin{bmatrix} 0 & \hat{\sigma}_{12}^{\text{trial}} & \hat{\sigma}_{13}^{\text{trial}} \\ \hat{\sigma}_{12}^{\text{trial}} & 0 & 0 \\ \hat{\sigma}_{13}^{\text{trial}} & 0 & 0 \end{bmatrix} \equiv \hat{\boldsymbol{\sigma}}^{\text{trial}} + \lambda\hat{\boldsymbol{\xi}} \tag{131}$$

where $\hat{\boldsymbol{\sigma}}^{\text{trial}}$ is the Cauchy stress in the local coordinate system calculated by standard stress calculations through particle interaction without considering the artificial friction-like elastoplastic material and $\lambda = 0$ if $f(\boldsymbol{\tau}^{\text{trial}}) < 0$ and

$$\lambda = \frac{\mu|\hat{\sigma}_{11}^{\text{trial}}| - \|\boldsymbol{\tau}^{\text{trial}}\|}{\|\boldsymbol{\tau}^{\text{trial}}\|} \quad \text{if } f(\boldsymbol{\tau}^{\text{trial}}) \geq 0 \tag{132}$$

Finally, the corrected contact stress in the global coordinates is obtained by the inverse transformation

$$\boldsymbol{\sigma}_c = \mathbf{L}^T\hat{\boldsymbol{\sigma}}_c\mathbf{L} \equiv \boldsymbol{\sigma}^{\text{trial}} + \lambda\boldsymbol{\xi} \tag{133}$$

where

$$\boldsymbol{\xi} = (\mathbf{n} \otimes \boldsymbol{\sigma}^{\text{trial}} \cdot \mathbf{n} + \mathbf{n} \cdot \boldsymbol{\sigma}^{\text{trial}} \otimes \mathbf{n}) - 2t_N\mathbf{n} \otimes \mathbf{n} \tag{134}$$

Here, the orthogonality of $\mathbf{L}$ is applied to derive the previous relationship. Eq. (133) can then be directly used in the calculation of the contact forces described in the following section.

Semi-Lagrangian RK Discretization and Kernel Contact Algorithms

This section describes the semi-Lagrangian RK discretization and the contact force calculation in the KC algorithms. Consider continuum bodies Ω^A and Ω^B discretized by groups of points $G^A = \{\mathbf{x}_I | \mathbf{x}_I \in \Omega^A\}$ and $G^B = \{\mathbf{x}_I | \mathbf{x}_I \in \Omega^B\}$, respectively, with each point at $\mathbf{x}_I$ associated with a nodal volume V_I and a kernel function $\phi_a(\mathbf{x} - \mathbf{x}_I)$ with the support of radius a independent of material deformation. When the two bodies Ω^A and Ω^B approach each other and the semi-Lagrangian-RK shape functions form a partition of unity, the interaction between the RK points from the different bodies (Fig. 21) induces stresses

$$\boldsymbol{\sigma}(\mathbf{x}) = \sum_{I \in N^A \cup N^B} \mathbf{D}(\mathbf{x})\mathbf{B}_I(\mathbf{x})\mathbf{d}_I \tag{135}$$

where $N^A = \{I | \mathbf{x}_I \in G^A\}$; $N^B = \{I | \mathbf{x}_I \in G^B\}$; and $\mathbf{D}$ is the material response tensor of the contacting bodies. The contact stresses between contacting bodies are obtained by Eq. (135) when $\mathbf{n} \cdot \boldsymbol{\sigma} \cdot \mathbf{n} \leq 0$ in Ω_c. With the nodal integration schemes described in the section "Domain Integration in Galerkin Meshfree Methods," the internal force acting on a point I can then be obtained by

$$\mathbf{f}_I = \sum_{J \in N_I^C} \mathbf{B}_I^T(\mathbf{x}_J)\boldsymbol{\sigma}(\mathbf{x}_J)V_J \tag{136}$$

where $N_I^C = \{J | J \in N^A \cup N^B, \phi_{a_I}(\mathbf{x}_J - \mathbf{x}_I) \neq 0, \mathbf{r}_{IJ} \cdot \boldsymbol{\sigma}(\mathbf{x}_J) \cdot \mathbf{r}_{IJ} < 0, \mathbf{r}_{IJ} = (\mathbf{x}_J - \mathbf{x}_I)/\|\mathbf{x}_J - \mathbf{x}_I\|\}$ is the set that contains the neighbor points under the support of point I, while the contact stress between those points and point I is in compression. In this approach, the pairwise interactions due to overlapping kernel functions naturally prevent the interpenetration between different bodies. To model the frictional contact condition, an artificial layer of material with the friction-Like dissipating mechanism in the form of plasticity presented in the section "Friction-Like Plasticity Model" is introduced. With the consideration of the frictional contact effect, the summation of the interactive forces associated with point I is corrected as

$$\mathbf{f}_I = \sum_{J \in N_I^C} \bar{\mathbf{B}}_I^T(\mathbf{x}_J)\boldsymbol{\sigma}_c(\mathbf{x}_J)V_J = \sum_{J \in N_I^C} (\mathbf{f}_{IJ} + \mathbf{g}_{IJ}) \tag{137}$$

where $\mathbf{f}_{IJ} = \mathbf{B}_I^T(\mathbf{x}_J)\boldsymbol{\sigma}^{\text{trial}}(\mathbf{x}_J)V_J$; and $\mathbf{g}_{IJ} = \mathbf{B}_I^T(\mathbf{x}_J)\lambda\boldsymbol{\xi}(\mathbf{x}_J)V_J$.

One remaining issue to implement the KC algorithm in the semi-Lagrangian formulation is to determine the contact surface and surface normal from a purely point-based discretization. A level-set based method, where the level set function is chosen as the interpolant of material IDs using semi-Lagrangian RK shape functions has been proposed to obtain the contact surface and surface normal under the KC contact framework (Chi et al. 2015).

As an illustrative example, the Taylor bar impact problem (Taylor 1948) was first performed by Wilkins and Guinan (1973), and subsequently by others. An aluminum bar with initial height and radius of 2.346 and 0.391 cm, respectively, impacts a rigid wall with an initial velocity of 373.0 m/s. For the aluminum material, J_2 plasticity with isotropic hardening is considered with material properties Young's modulus $E = 78.2$ GPa, Poisson's ratio $\nu = 0.30$, and density $\rho = 2{,}700$ kg/m^3, and the yield function is taken as

$$K(\bar{e}_p) = \sigma_Y(1 + 125\bar{e}_p)^{0.1} \tag{138}$$

where $\sigma_Y = 0.29$ GPa.

The semi-Lagrangian formulation is considered with linear basis and quartic B-spline kernel functions with a normalized support of 2.8, and 29,637 nodes discretize the bar. The wall is also modeled and is considered frictionless, and the KC algorithms are employed for the bar-wall interaction. The four integration methods direct nodal integration (DNI), stabilized nonconforming nodal integration (SNNI), variationally consistent naturally stabilized nodal integration (VC-NSNI), and variationally consistent modified SNNI (VC-MSNNI) discussed in the section "Galerkin-Based Meshfree Method" are considered for comparison of the nodal integrations.

The deformed shape of the face of the bar is shown in Fig. 23, with material deformation plotted for visualization purposes, in order to observe any spurious oscillations in the solution, if present. The difference in solutions is apparent; DNI and SNNI both clearly show spurious oscillatory modes in the solution discussed in the section "Domain Integration in Galerkin Meshfree Methods" while the stabilized methods do not.

The deformed height and radius of the bar are shown in Table 2, where it is shown that DNI and SNNI predict a larger radius compared to the reference solutions, likely due to the very little resistance to the oscillatory mode of deformation. Another explanation is the numerical fractures in DNI and SNNI formed due

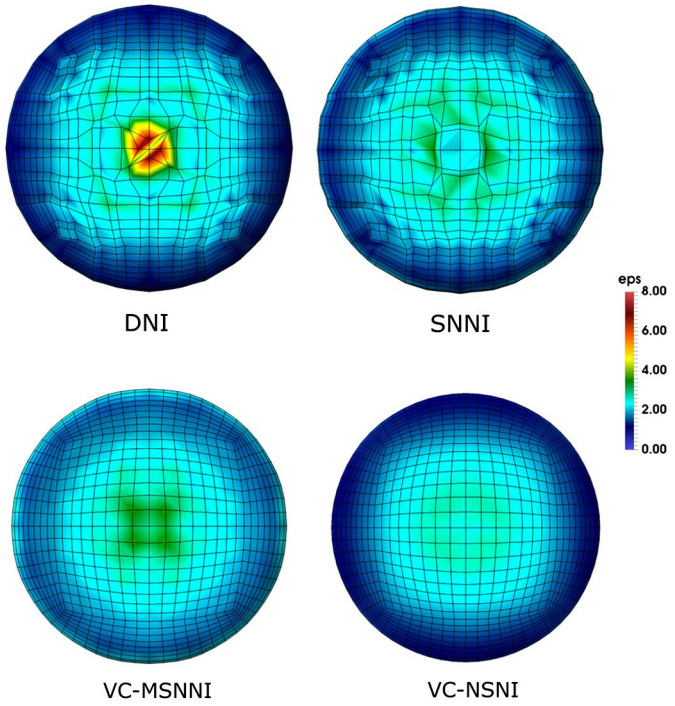

Fig. 23. Final deformation on the face of the Taylor bar for various nodal integration methods

Table 2. Deformed Height and Radius for Various Methods and the Experiment (Data from Hillman and Chen 2015)

Method	Radius (cm)	Height (cm)
SNNI	0.839	1.649
DNI	0.838	1.660
VC-MSNNI	0.801	1.649
VC-NSNI	0.775	1.651
RKPM (Gauss integration) (Chen et al. 1996)	0.827	1.645
Material point method (Sulsky et al. 1995)	0.78	1.65
Finite-element method (Taylor 1948)	0.742	1.652
Experimental (Wilkins and Guinan 1973)	—	1.651

to these spurious modes, as seen in Fig. 24, while VC-NSNI and VC-MSNNI give stable solutions. For the deformed height of the bar, all methods give reasonable heights compared to the reference solutions except for DNI. VC-NSNI and VC-MSNNI give the closest results to the experimental data and other methods compared.

Applications of Meshfree Methods

Application to Large Deformation Problems

Meshfree methods are particularly well-suited for large deformation problems where finite-element methods could fail due to mesh entanglement and other mesh related issues. The Lagrangian meshfree method in Eqs. (106)–(110) has been applied to many solid mechanics problems and applications, such as large deformation of hyperelastic materials and rubber (Chen and Wu 1997; Chen et al. 1997, 2000c, e), metal forming (Chen and Wang 2000a, b; Chen et al. 1998a, c; Wang et al. 2014; Yoon and Chen 2002; Yoon et al. 2001), and geomechanics problems (Wu et al. 2001), among others, showing robustness over FEM. For the presence of material separation where the Lagrangian description breaks down, the semi-Lagrangian formulation in Eqs. (111)–(137) was proposed (Guan et al. 2009, 2011; Kwok et al. 2015). Fig. 25 shows the application of semi-Lagrangian RKPM to the simulation of perforation of a concrete panel by a bullet (Yreux and Chen 2016), and Fig. 26 demonstrates a semi-Lagrangian RKPM simulation of a landslide due to the Loma Prieta earthquake. Several other researchers have developed and employed various meshfree methods discussed in the "Introduction" to reassociate connectivity for penetration and fragment-impact problems (Johnson et al. 1996; Li et al. 2012, 2013; Libersky et al. 1997; Ma et al. 2009; Parks et al. 2008; Rabczuk and Belytschko 2007; Rabczuk and Eibl 2003; Rabczuk et al. 2004; Randles and Libersky 1996; Ren and Li 2010; Silling and Askari 2005; Zhang et al. 2006). On a different path, discrete bonded particle methods have been developed and coupled with FEM for similar applications (Beissel et al. 2006; Johnson 1994; Johnson et al. 1986, 2000, 2002, 2013) [for a review, see (Johnson 2011)]. Recently, meshfree methods have gained traction in solving geomechanics problems with extremely large deformations such as slope stability with postfailure analysis (Andersen and Andersen 2010; Bui and Fukagawa 2013; Bui et al. 2008; Chen and Qiu 2014; Fukagawa et al. 2011; Kwok et al. 2015; Wang et al. 2011). More recently, several other meshfree formulations for nonlinear mechanics have been introduced (Yreux and Chen 2016; Chi et al. 2015; Hillman and Chen 2015; Hillman et al. 2014; Wu et al. 2016, 2016, 2014).

Adaptive Refinement

The naturally conforming properties of meshfree approximations, such as the MLS, RK, and PU approximations, allow adaptivity to be performed in a much more effective manner than the conventional finite element method (Duarte and Oden 1996b, a; Liu and Chen 1995; Liu et al. 1997a; Lu and Chen 2002; Rabczuk and Belytschko 2005; Rabczuk and Samaniego 2008;

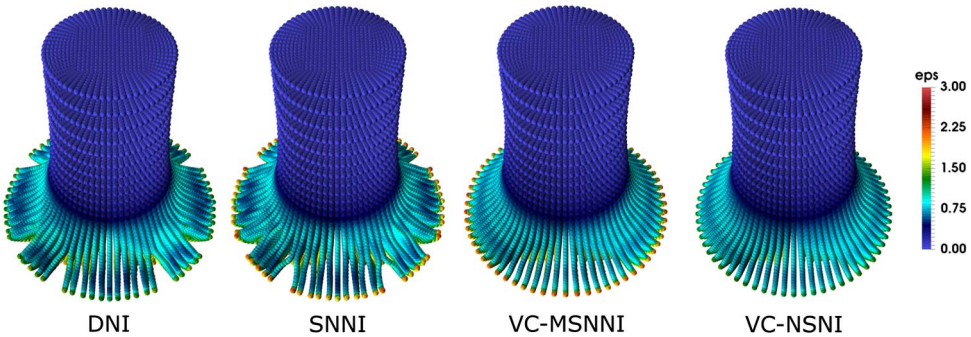

Fig. 24. Final deformation of the Taylor bar for various nodal integration methods

J. Eng. Mech., 2017, 143(4): 04017001

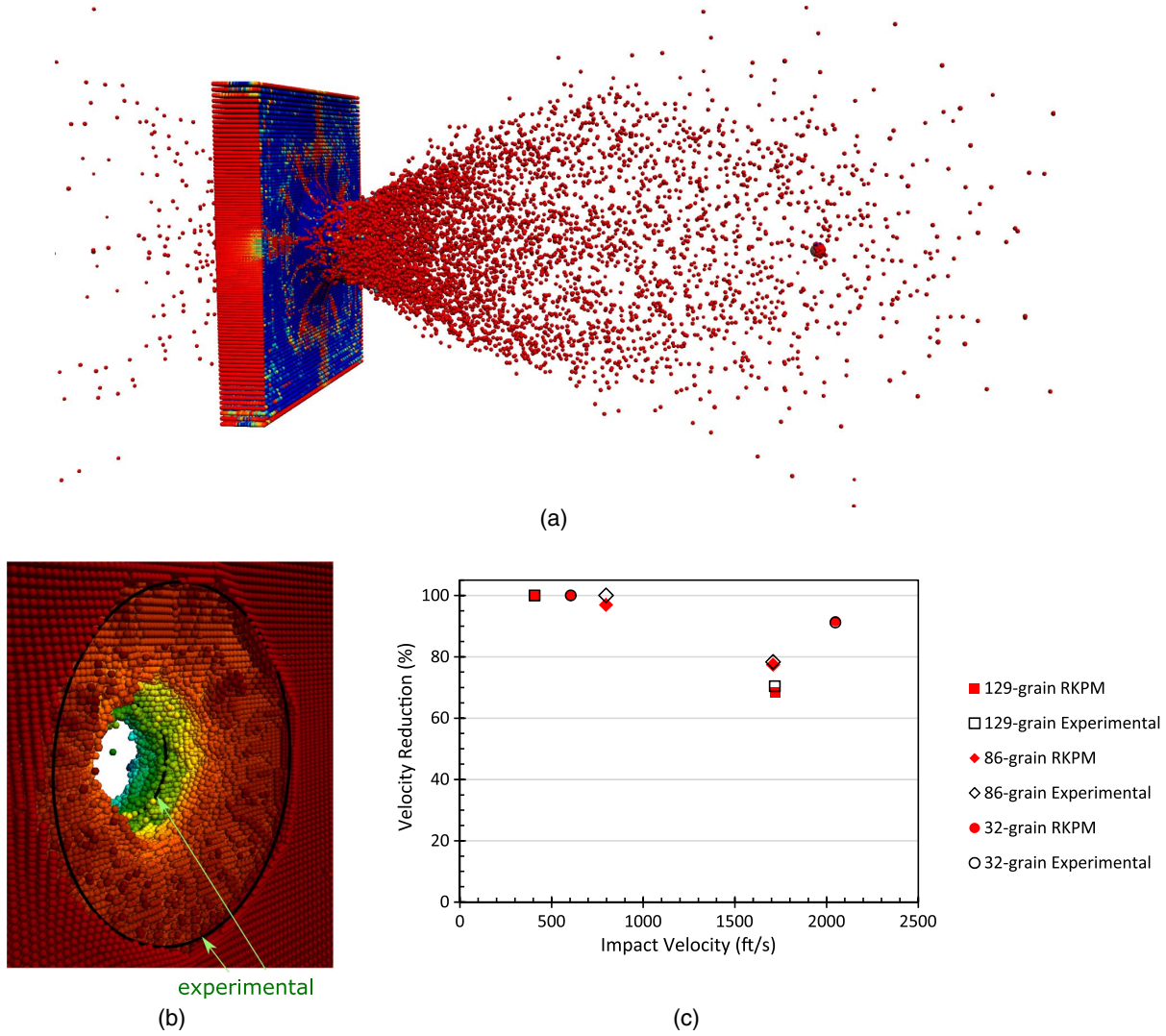

Fig. 25. Bullet penetrating a concrete panel: (a) deformed shape after impact; (b) crater shape; (c) velocity reduction for different sizes of projectiles

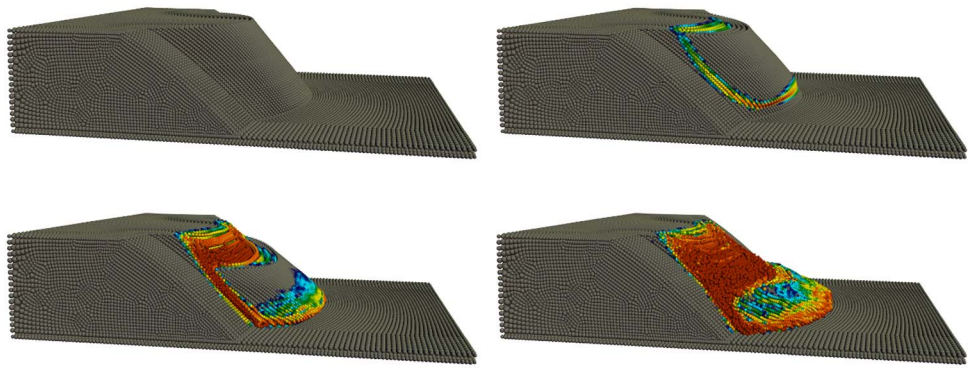

Fig. 26. Simulation of a landslide triggered by the 1989 Loma Prieta earthquake using semi-Lagrangian RKPM

You et al. 2003). Nodes can be inserted or removed with ease, and error indicators have been formulated to guide adaptive refinement. For example, the multiresolution RK-based method (Liu and Chen 1995; Liu et al. 1996a, c, 1997a) enables the scale decomposition of the RKPM solution by using the RK function as a low-pass filter, and the high-scale solution has been used as the error indicator for adaptive refinement (Liu and Jun 1998; Liu et al. 1995b, 1996a, 1997b; Uras et al. 1997). While p adaptivity is not so straightforward in RK-based and MLS-based methods, hp clouds allows the bases to vary throughout the domain such that

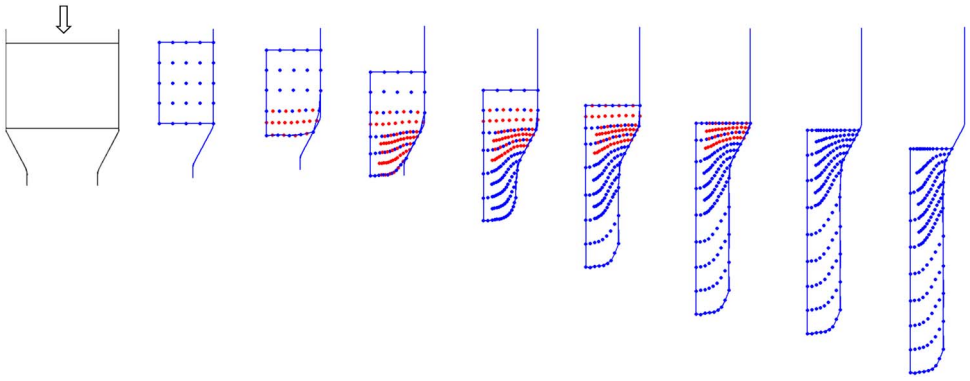

Fig. 27. RKPM modeling of metal extrusion with adaptive refinement

higher order accuracy can be obtained where needed (Duarte and Oden 1996a).

Application to Strain Localization

Researchers have employed the flexibility of meshfree methods for regularization in localization problems to circumvent ambiguous boundary conditions in gradient methods (Chen et al. 2000d, 2004, 2007b). Methods have also been developed and applied successfully to localization problems difficult for FEM (Li et al. 2000a, b, 2001, 2002; Liu and Jun 1998). More recently, the cracking particle method (Rabczuk and Belytschko 2004) has been developed for shear bands (Rabczuk and Samaniego 2008).

Application to Fracture Mechanics

Fracture mechanics is another area where meshfree methods offer a unique strength. Early on, it was recognized that meshfree formulations such as EFG could offer an effective alternative to FEM in modeling fracture by using the so-called visibility criterion (cutting the particle influence across a crack), and further provide easy adaptive refinement to attain accuracy near crack tips (Belytschko and Tabbara 1996; Belytschko et al. 1994a, 1995a, b). Alternatively, enrichment of the approximation functions for crack tip singularities can be considered intrinsically (Belytschko et al. 1996a; Fleming et al. 1997) or extrinsically (Fleming et al. 1997; Melenk and Babuška 1996; Ventura et al. 2002). The former approach involves some complications because MLS and basis RK functions in these methods cannot vary spatially. Approaches with extrinsic enrichments have been developed for meshfree methods (Rabczuk and Areias 2006; Rabczuk and Zi 2007; Rabczuk et al. 2007a, i), including techniques for accurate closure of crack fronts in meshfree methods, with the resulting method termed XEFG. Tracking the geometry of evolving cracks necessary for enrichment is a difficult task, particularly in three dimensions. To circumvent this issue, a cracking particle method has been proposed, where fracture is represented by a series of discontinuities located at the particles, with arbitrary orientation (Rabczuk and Belytschko 2004, 2007; Rabczuk et al. 2007a, 2010). The introduction of these discontinuities can be performed by detection of material instability. Alternatively, level-set methods for tracking of complicated crack geometry have been proposed (Bordas et al. 2008; Ventura et al. 2002; Zhuang et al. 2011).

Application to Contact Mechanics

By employing the arbitrary smoothness in meshfree approximation functions, a smooth contact algorithm has been proposed where the contact surface is represented by smooth (C^2 or higher) RK approximations, which allows continuum-based contact formulations (Chen and Wang 2000a; Wang 2000; Wang et al. 2014). This in turn allows improved convergence in contact iterations versus finite-element based contact with C^0 continuity, and enables robust analysis in applications such as metal forming, as shown in Fig. 27, where Lagrangian RKPM is used to model a metal extrusion processes with adaptive refinement, where points were inserted in the highly deformed region and were removed in the region undergoing elastic unloading.

Other Applications

Meshfree methods have been developed for several other applications where they have advantages over traditional approaches. In modeling *biomaterials*, meshfree methods are well suited for *image-based modeling* by using pixels as discretization nodes without the tedious procedures in three-dimensional geometry reconstruction from the images and mesh generation. Meshfree methods can also represent the smooth transition of material properties across material interfaces in biomaterials (Chen et al. 2015; Chi 2009). Fig. 28 shows a skeletal muscle modeled by the meshfree method, where image pixel points were used directly as the discretization points, and the associated stress distribution is computed using material properties and fiber orientations defined at the pixel points.

Another good application of meshfree methods is for problems that involve higher order differentiation in the PDE, such as thin *plate and shell problems* (Chen and Wang 2006; Krysl and Belytschko 1995, 1996; Liu and Chen 2001; Long and Atluri 2001; Wang and Chen 2008; Wang and Peng 2013) where meshfree approximation functions with higher order continuity can be employed with virtually no additional effort. The application of the meshfree method to *quantum mechanics* has been proposed by utilizing the orbital functions as the enrichment of polynomial bases for *p*-like adaptive refinement (Chen et al. 2007a). For *shape optimization*, meshfree methods can avoid mesh distortion in the iterative process (Kim et al. 2000a, g, 2001). Meshfree methods for *fluid mechanics* (Fries and Matthias 2006a, b; Günther et al. 2000; Hillman and Chen 2016; Huerta and Fernández-Méndez 2003; Li and Liu 1999a; Liu et al. 1995b, 1997b) have been proposed using multiresolution analysis in conjunction with adaptive refinement (Günther et al. 2000; Liu et al. 1995b, 1997b). The smooth meshfree approximation functions are well suited for Petrov-Galerkin stabilization (Huerta and Fernández-Méndez 2003), and meshfree methods are more effective in handling moving domains and obstacles (Fries and Matthias 2006a, b).

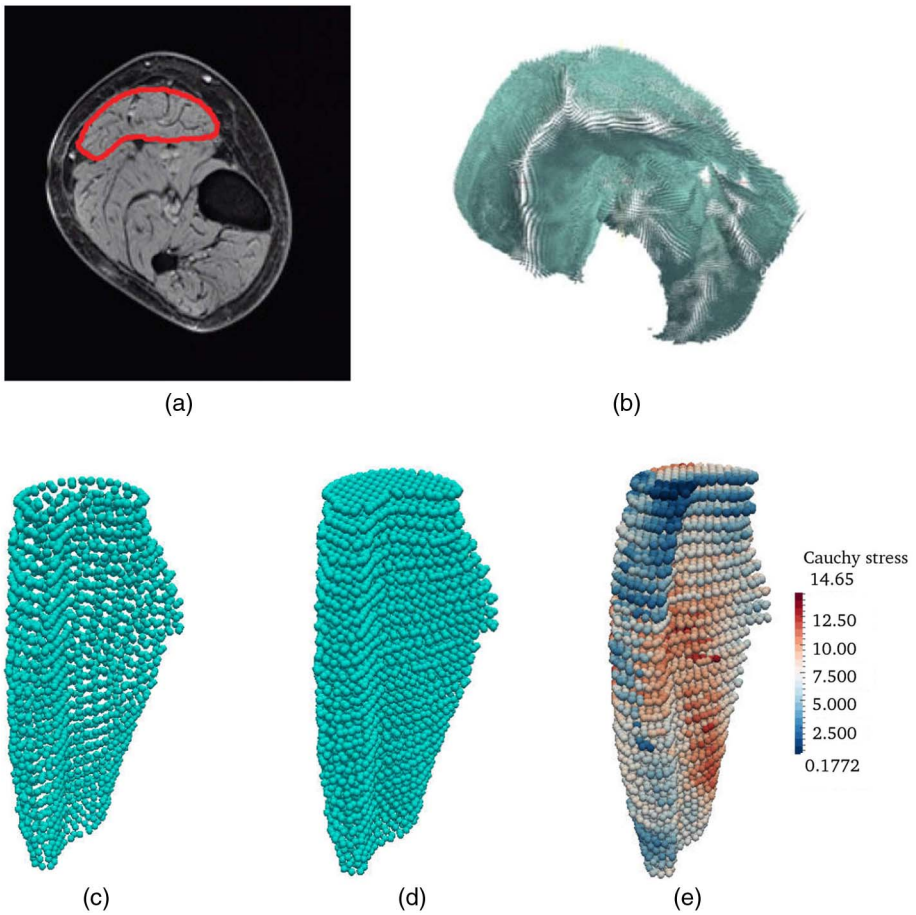

Fig. 28. Image based RKCM modeling of skeletal muscle (a) MRI image; (b) DTI vector plot; (c) RK source points; (d) RK collocation points; (e) maximum principal Cauchy stress resulting from muscle contraction

Conclusions and Outlook

Meshfree methods offer an alternative to traditional mesh-based methods, where the conforming condition is relaxed to simply PU subordinate to an open cover. Meshfree approximations can offer arbitrarily smooth or rough approximations at no cost. In meshfree approximations such as MLS and RK, the order of completeness and order of continuity in the approximations are entirely uncoupled in contrast to many other numerical methods. Because of these two properties h-refinement and p-refinement are simplified considerably. In addition, the strong tie between the quality of the discretization and the quality of the numerical solution to PDEs is reduced, which makes these methods well-suited for large deformation problems without cumbersome procedures such as remeshing, moving meshes, and erosion. The burden of producing an analysis suitable discretization via meshing is also greatly relieved. These features have made the application of meshfree methods widespread in the past two decades.

For the practical application of meshfree methods, efforts have been devoted to ensure solution accuracy, stability, and efficiency. To date, essential boundary condition enforcement is almost trivial in meshfree methods. The formidable computational cost of high-order quadrature has been greatly alleviated (or eliminated) through novel techniques such as SCNI and VCI, which have since been showing robustness in many applications. Significant advances have also been made in spatial stability, where several accurate and efficient stabilized nodal integration methods have been developed. With the progress in nodal integration, truly meshless methods are now available, and they are particularly effective for problems with extreme loadings, such as fragment-impact processes.

Several issues remain, some of which are common to both mesh-based and meshfree methods. A prime example is the simulation of high-density, three-dimensional cracking, which remains challenging, even for meshfree methods. To the authors' knowledge, the potential to alleviate time-consuming model generation in the meshfree method has not been fully realized. The ability to collocate partial differential equations directly (strong form collocation) offers a promising avenue for meshfree methods; however, the effort devoted to advancing the strong form collocation method has not been on par with the development of Galerkin meshfree methods, especially in the area of strong form collocation for large deformation, fracture mechanics, and contact-impact problems. These challenges call for future research in meshfree methods.

Acknowledgments

The support of this work by the U.S. Army Engineer Research and Development Center under contract W15QKN-12-9-1006 to University of California, San Diego, and the U.S. Army Corps of Engineers SERDP Program under contract W912HQ-16-P-0002 to the University of Illinois at Chicago is greatly acknowledged.

References

Aluru, N. R. (2000). "A point collocation method based on reproducing kernel approximations." *Int. J. Numer. Methods Eng.*, 47(6), 1083–1121.

Andersen, S., and Andersen, L. (2010). "Modelling of landslides with the material-point method." *Comput. Geosci.*, 14(1), 137–147.

Arroyo, M., and Ortiz, M. (2006). "Local maximum-entropy approximation schemes: A seamless bridge between finite elements and meshfree methods." *Int. J. Numer. Methods Eng.*, 65(13), 2167–2202.

Ataie-Ashtiani, B., and Farhadi, L. (2006). "A stable moving-particle semi-implicit method for free surface flows." *Fluid Dyn. Res.*, 38(4), 241–256.

Atluri, S. N., Kim, H. G., and Cho, J. Y. (1999). "Critical assessment of the truly meshless local Petrov-Galerkin (MLPG), and local boundary integral equation (LBIE) methods." *Comput. Mech.*, 24(5), 348–372.

Atluri, S. N., and Shen, S. (2002). *The meshless local Petrov-Galerkin (MLPG) method*, Tech Science Press, Duluth, GA.

Atluri, S. N., and Zhu, T. L. (1998). "A new meshless local Petrov-Galerkin (MLPG) approach in computational mechanics." *Comput. Mech.*, 22(2), 117–127.

Auricchio, F., Da Veiga, L. B., Hughes, T. J. R., Reali, A., and Sangalli, G. (2010). "Isogeometric collocation methods." *Math. Models Methods Appl. Sci.*, 20(11), 2075–2107.

Babuška, I., Banerjee, U., and Osborn, J. E. (2003). "Meshless and generalized finite element methods: A survey of some major results." *Meshfree methods for partial differential equations*, Springer, Berlin, 1–20.

Babuška, I., Banerjee, U., Osborn, J. E., and Li, Q. (2008). "Quadrature for meshless methods." *Int. J. Numer. Methods Eng.*, 76(9), 1434–1470.

Babuška, I., Banerjee, U., Osborn, J. E., and Zhang, Q. (2009). "Effect of numerical integration on meshless methods." *Comput. Methods Appl. Mech. Eng.*, 198(37–40), 2886–2897.

Babuška, I., and Melenk, J. M. (1997). "The partition of unity method." *Int. J. Numer. Methods Eng.*, 40(4), 727–758.

Bardenhagen, S. G., and Kober, E. M. (2004). "The generalized interpolation material point method." *Comput. Model. Eng. Sci.*, 5(6), 477–495.

Barta, J. (1937). "Über die Näherungsweise Lösung einiger Zweidimensionaler Elastizität Aufgaben." *ZAMM – J. Appl. Math. Mech.*, 17(3), 184–185.

Beissel, S. R., and Belytschko, T. (1996). "Nodal integration of the element-free Galerkin method." *Comput. Methods Appl. Mech. Eng.*, 139(1–4), 49–74.

Beissel, S. R., Gerlach, C. A., and Johnson, G. R. (2006). "Hypervelocity impact computations with finite elements and meshfree particles." *Int. J. Impact Eng.*, 33(1–12), 80–90.

Belikov, V. V, Ivanov, V. D., Kontorovich, V. K., Korytnik, S. A., and Semenov, A. Y. (1997). "The non-Sibsonian interpolation: A new method of interpolation of the values of a function on an arbitrary set of points." *Comput. Math. Math. Phys.*, 37(1), 9–15.

Belytschko, T., and Black, T. (1999). "Elastic crack growth in finite elements with minimal remeshing." *Int. J. Numer. Methods Eng.*, 45(5), 601–620.

Belytschko, T., Gu, L., and Lu, Y. Y. (1994a). "Fracture and crack growth by element free Galerkin methods." *Model. Simul. Mater. Sci. Eng.*, 2(3A), 519–534.

Belytschko, T., Guo, Y., Liu, W. K., and Xiao, S. P. (2000). "A unifieded stability analysis of meshless particle methods." *Int. J. Numer. Methods Eng.*, 48(9), 1359–1400.

Belytschko, T., Krongauz, Y., Fleming, M., Organ, D., and Liu, W. K. (1996a). "Smoothing and accelerated computations in the element free Galerkin method." *J. Comput. Appl. Math.*, 74(1–2), 111–126.

Belytschko, T., Krongauz, Y., Organ, D., Fleming, M., and Krysl, P. (1996b). "Meshless methods: An overview and recent developments." *Comput. Methods Appl. Mech. Eng.*, 139(1–4), 3–47.

Belytschko, T., Lu, Y. Y., and Gu, L. (1994b). "Element-free Galerkin methods." *Int. J. Numer. Methods Eng.*, 37(2), 229–256.

Belytschko, T., Lu, Y. Y., and Gu, L. (1995a). "Crack propagation by element-free Galerkin methods." *Eng. Fract. Mech.*, 51(2), 295–315.

Belytschko, T., Lu, Y. Y., Gu, L., and Tabbara, M. (1995b). "Element-free galerkin methods for static and dynamic fracture." *Int. J. Solids Struct.*, 32(17–18), 2547–2570.

Belytschko, T., and Tabbara, M. (1996). "Dynamic fracture using element-free Galerkin methods." *Int. J. Numer. Methods Eng.*, 39(6), 923–938.

Benamou, J. D., and Brenier, Y. (1999). "A numerical method for the optimal time-continuous mass transport problem and related problems." *Contemporary mathematics*, American Mathematical Society, Providence, RI, 1–12.

Benson, D. J., et al, . (2010). "A generalized finite element formulation for arbitrary basis functions: From isogeometric analysis to XFEM." *Int. J. Numer. Methods Eng.*, 83(6), 765–785.

Benz, W., and Asphaug, E. (1995). "Simulations of brittle solids using smooth particle hydrodynamics." *Comput. Phys. Commun.*, 87(1), 253–265.

Bessa, M. A., Foster, J. T., Belytschko, T., and Liu, W. K. (2014). "A meshfree unification: Reproducing kernel peridynamics." *Comput. Mech.*, 53(6), 1251–1264.

Bonet, J., and Kulasegaram, S. (2000). "Correction and stabilization of smooth particle hydrodynamics methods with applications in metal forming simulations." *Int. J. Numer. Methods Eng.*, 47(6), 1189–1214.

Bordas, S. P. A., Rabczuk, T., and Zi, G. (2008). "Three-dimensional crack initiation, propagation, branching and junction in non-linear materials by an extended meshfree method without asymptotic enrichment." *Eng. Fract. Mech.*, 75(5), 943–960.

Brackbill, J. U., Kothe, D. B., and Ruppel, H. M. (1988). "FLIP: A low-dissipation, particle-in-cell method for fluid flow." *Comput. Phys. Commun.*, 48(1), 25–38.

Brackbill, J. U., and Ruppel, H. M. (1986). "FLIP: A method for adaptively zoned, particle-in-cell calculations of fluid flows in two dimensions." *J. Comput. Phys.*, 65(2), 314–343.

Braun, J., and Sambridge, M. (1995). "A numerical method for solving partial differential equations on highly irregular evolving grids." *Nature*, 376(6542), 655–660.

Buhmann, M. D., and Micchelli, C. A. (1992). "Multiquadric interpolation improved." *Comput. Math. Appl.*, 24(12), 21–25.

Bui, H. H., and Fukagawa, R. (2013). "An improved SPH method for saturated soils and its application to investigate the mechanisms of embankment failure: Case of hydrostatic pore-water pressure." *Int. J. Numer. Anal. Methods Geomech.*, 37(1), 31–50.

Bui, H. H., Fukagawa, R., Sako, K., and Ohno, S. (2008). "Lagrangian meshfree particles method (SPH) for large deformation and failure flows of geomaterial using elastic—Plastic soil constitutive model." *Int. J. Numer. Anal. Methods Geomech.*, 32(12), 1537–1570.

Cecil, T., Qian, J., and Osher, S. (2004). "Numerical methods for high dimensional Hamilton-Jacobi equations using radial basis functions." *J. Comput. Phys.*, 196(1), 327–347.

Chen, J. S., et al. (2011). "A multiscale meshfree approach for modeling fragment penetration into ultra high-strength concrete." *ERDC/GSL TR-11-35*, U.S. Army Engineer Research and Development Center, Vicksburg, MS.

Chen, J. S., et al. (2015). "Pixel-based meshfree modelling of skeletal muscles." *Comput. Methods Biomech. Biomed. Eng.: Imag. Visualization*, 4(2), 73–85.

Chen, J. S., and Belytschko, T. (2011). "Meshless and mesh free methods." *Encyclopedia of applied and computational mathematics*, B. Engquist, ed., Springer, Berlin, 886–894.

Chen, J. S., Han, W., You, Y., and Meng, X. (2003). "A reproducing kernel method with nodal interpolation property." *Int. J. Numer. Methods Eng.*, 56(7), 935–960.

Chen, J. S., Hillman, M., and Rüter, M. (2013). "An arbitrary order variationally consistent integration for Galerkin meshfree methods." *Int. J. Numer. Methods Eng.*, 95(5), 387–418.

Chen, J. S., Hu, W., and Hu, H. Y. (2008). "Reproducing kernel enhanced local radial basis collocation method." *Int. J. Numer. Methods Eng.*, 75(5), 600–627.

Chen, J. S., Hu, W., and Puso, M. A. (2007a). "Orbital HP-clouds for solving Schrödinger equation in quantum mechanics." *Comput. Methods Appl. Mech. Eng.*, 196(37), 3693–3705.

Chen, J. S., Hu, W., Puso, M. A., Wu, Y., and Zhang, X. (2007b). "Strain smoothing for stabilization and regularization of galerkin meshfree methods." *Lecture Notes in Computational Science and Engineering*, 57, Springer, Berlin, 57–75.

Chen, J. S., Pan, C., Roque, C. M. O. L., and Wang, H. P. (1998a). "A Lagrangian reproducing kernel particle method for metal forming analysis." *Comput. Mech.*, 22(3), 289–307.

Chen, J. S., Pan, C., and Wu, C. T. (1997). "Large deformation analysis of rubber based on a reproducing kernel particle method." *Comput. Mech.*, 19(3), 211–227.

Chen, J. S., Pan, C., Wu, C. T., and Liu, W. K. (1996). "Reproducing kernel particle methods for large deformation analysis of non-linear structures." *Comput. Methods Appl. Mech. Eng.*, 139(1-4), 195–227.

Chen, J. S., Roque, C. M. O. L., Pan, C., and Button, S. T. (1998c). "Analysis of metal forming process based on meshless method." *J. Mater. Process. Technol.*, 80–81, 642–646.

Chen, J. S., and Wang, D. (2006). "A constrained reproducing kernel particle formulation for shear deformable shell in Cartesian coordinates." *Int. J. Numer. Methods Eng.*, 68(2), 151–172.

Chen, J. S., and Wang, H. P. (2000a). "Meshfree smooth surface contact algorithm for sheet metal forming." *SAE Technical Paper No. 1103-01-2000*.

Chen, J. S., and Wang, H. P. (2000b). "New boundary condition treatments in meshfree computation of contact problems." *Comput. Methods Appl. Mech. Eng.*, 187(3–4), 441–468.

Chen, J. S., Wang, H. P., Yoon, S., and You, Y. (2000c). "Some recent improvements in meshfree methods for incompressible finite elasticity boundary value problems with contact." *Comput. Mech.*, 25(2–3), 137–156.

Chen, J. S., Wang, L., Hu, H. Y., and Chi, S. W. (2009). "Subdomain radial basis collocation method for heterogeneous media." *Int. J. Numer. Methods Eng.*, 80(2), 163–190.

Chen, J. S., and Wu, C. T. (1997). "On computational issues in large deformation analysis of rubber bushings." *J. Struct. Mech.*, 25(3), 287–309.

Chen, J. S., Wu, C. T., and Belytschko, T. (2000d). "Regularization of material instabilities by meshfree approximations with intrinsic length scales." *Int. J. Numer. Methods Eng.*, 47(7), 1303–1322.

Chen, J. S., Wu, C. T., and Yoon, S. (2001). "A stabilized conforming nodal integration for Galerkin mesh-free methods." *Int. J. Numer. Meth. Eng.*, 50(2), 435–466.

Chen, J. S., Yoon, S., Wang, H. P., and Liu, W. K. (2000e). "An improved reproducing kernel particle method for nearly incompressible finite elasticity." *Comput. Methods Appl. Mech. Eng.*, 181(1–3), 117–145.

Chen, J. S., Yoon, S., and Wu, C. T. (2002). "Non-linear version of stabilized conforming nodal integration for Galerkin mesh-free methods." *Int. J. Numer. Methods Eng.*, 53(12), 2587–2615.

Chen, J. S., Zhang, X., and Belytschko, T. (2004). "An implicit gradient model by a reproducing kernel strain regularization in strain localization problems." *Comput. Methods Appl. Mech. Eng.*, 193(27–29), 2827–2844.

Chen, W., and Qiu, T. (2014). "Simulation of earthquake-induced slope deformation using SPH method." *Int. J. Numer. Anal. Methods Geomech.*, 38(3), 297–330.

Chi, S. W. (2009). "Image-based computational mechanics frameworks for skeletal muscles." Ph.D. dissertation, Univ. of California, Los Angeles.

Chi, S. W., Chen, J. S., and Hu, H. Y. (2014). "A weighted collocation on the strong form with mixed radial basis approximations for incompressible linear elasticity." *Comput. Mech.*, 53(2), 309–324.

Chi, S. W., Chen, J. S., Hu, H. Y., and Yang, J. P. (2013). "A gradient reproducing kernel collocation method for boundary value problems." *Int. J. Numer. Methods Eng.*, 93(13), 1381–1402.

Chi, S. W., Lee, C. H., Chen, J. S., and Guan, P. C. (2015). "A level set enhanced natural kernel contact algorithm for impact and penetration modeling." *Int. J. Numer. Methods Eng.*, 102(3–4), 839–866.

Chui, C. K., Stöckler, J., and Ward, J. D. (1996). "Analytic wavelets generated by radial functions." *Adv. Comput. Math.*, 5(1), 95–123.

Cottrell, J. A., Hughes, T. J. R., and Bazilevs, Y. (2009). *Isogeometric analysis: Toward integration of CAD and FEA*, Wiley, Chichester, U.K.

Cyron, C. J., Arroyo, M., and Ortiz, M. (2009). "Smooth, second order, non-negative meshfree approximants selected by maximum entropy." *Int. J. Numer. Methods Eng.*, 79(13), 1605–1632.

De, S., and Bathe, K. J. (2000). "The method of finite spheres." *Comput. Mech.*, 25(4), 329–345.

De, S., and Bathe, K. J. (2001). "The method of finite spheres with improved numerical integration." *Comput. Struct.*, 79(22), 2183–2196.

Dilts, G. A. (1999). "Moving-least-squares hydrodynamics—I. Consistency and stability." *Int. J. Numer. Methods Eng.*, 44(8), 1115–1155.

Dolbow, J., and Belytschko, T. (1999). "Numerical integration of the Galerkin weak form in meshfree methods." *Comput. Mech.*, 23(3), 219–230.

Duan, Q., and Belytschko, T. (2009). "Gradient and dilatational stabilizations for stress-point integration in the element-free Galerkin method." *Int. J. Numer. Methods Eng.*, 77(6), 776–798.

Duan, Q., Li, X., Zhang, H., and Belytschko, T. (2012). "Second-order accurate derivatives and integration schemes for meshfree methods." *Int. J. Numer. Methods Eng.*, 92(4), 399–424.

Duarte, C. A. M., Babuška, I., and Oden, J. T. (2000). "Generalized finite element methods for three-dimensional structural mechanics problems." *Comput. Struct.*, 77(2), 215–232.

Duarte, C. A. M., and Kim, D. J. (2008). "Analysis and applications of a generalized finite element method with global-local enrichment functions." *Comput. Methods Appl. Mech. Eng.*, 197(6–8), 487–504.

Duarte, C. A. M., and Oden, J. T. (1996a). "An h-p adaptive method using clouds." *Comput. Methods Appl. Mech. Eng.*, 139(1–4), 237–262.

Duarte, C. A. M., and Oden, J. T. (1996b). "H-p clouds—An h-p meshless method." *Numer. Methods Partial Differ. Equ.*, 12(6), 673–705.

Duflot, M., and Nguyen-Dang, H. (2002). "A truly meshless Galerkin method based on a moving least squares quadrature." *Commun. Numer. Methods Eng.*, 18(6), 441–449.

Dyka, C. T., and Ingel, R. P. (1995). "An approach for tension instability in smoothed particle hydrodynamics (SPH)." *Comput. Struct.*, 57(4), 573–580.

Dyka, C. T., Randles, P. W., and Ingel, R. P. (1997). "Stress points for tension instability in SPH." *Int. J. Numer. Methods Eng.*, 40(13), 2325–2341.

Fasshauer, G. E. (1999). "Solving differential equations with radial basis functions: Multilevel methods and smoothing." *Adv. Comput. Math.*, 11(2–3), 139–159.

Fernández-Méndez, S., and Huerta, A. (2004). "Imposing essential boundary conditions in mesh-free methods." *Comput. Methods Appl. Mech. Eng.*, 193(12), 1257–1275.

Fleming, M., Chu, Y. A., Moran, B., and Belytschko, T. (1997). "Enriched element-free Galerkin methods for crack tip fields." *Int. J. Numer. Methods Eng.*, 40(8), 1483–1504.

Foster, J. T., Silling, S. A., and Chen, W. W. (2010). "Viscoplasticity using peridynamics." *Int. J. Numer. Methods Eng.*, 81(10), 1242–1258.

Franke, C., and Schaback, R. (1998). "Solving partial differential equations by collocation using radial basis functions." *Appl. Math. Comput.*, 93(1), 73–82.

Franke, R. (1982). "Scattered data interpolation: Tests of some methods." *Math. Comput.*, 38(157), 181–200.

Frazer, R. A., Jones, W. N. P., and Skan, S. W. (1937). "Approximations to functions and to the solutions of differential equations." HSMO, London.

Fries, T. P., and Belytschko, T. (2008). "Convergence and stabilization of stress-point integration in mesh-free and particle methods." *Int. J. Numer. Methods Eng.*, 74(7), 1067–1087.

Fries, T. P., and Matthias, H. (2006a). "A stabilized and coupled meshfree/meshbased method for the incompressible Navier-Stokes equations—Part I: Stabilization." *Comput. Methods Appl. Mech. Eng.*, 195(44), 6205–6224.

Fries, T. P., and Matthias, H. (2006b). "A stabilized and coupled meshfree/meshbased method for the incompressible Navier-Stokes equations—Part II: Coupling." *Comput. Methods Appl. Mech. Eng.*, 195(44–47), 6191–6204.

Fukagawa, R., Sako, K., Bui, H. H., and Wells, J. C. (2011). "Slope stability analysis and discontinuous slope failure simulation by

elasto-plastic smoothed particle hydrodynamics (SPH)." *Géotechnique*, 61(7), 565–574.
Ghorashi, S. S., Valizadeh, N., and Mohammadi, S. (2012). "Extended isogeometric analysis for simulation of stationary and propagating cracks." *Int. J. Numer. Methods Eng.*, 89(9), 1069–1101.
Gingold, R. A., and Monaghan, J. J. (1977). "Smoothed particle hydrodynamics: Theory and application to non-spherical stars." Oxford University Press, Oxford, U.K., 375–389.
González, D., Cueto, E., and Doblaré, M. (2010). "A higher order method based on local maximum entropy approximation." *Int. J. Numer. Methods Eng.*, 83(6), 741–764.
Gosz, J., and Liu, W. K. (1996). "Admissible approximations for essential boundary conditions in the reproducing kernel particle method." *Comput. Mech.*, 19(1), 120–135.
Griebel, M., and Schweitzer, M. A. (2000). "A particle-partition of unity method for the solution of elliptic, parabolic, and hyperbolic PDEs." *SIAM J. Sci. Comput.*, 22(3), 853–890.
Griebel, M., and Schweitzer, M. A. (2002a). "A particle-partition of unity method—Part II: Efficient cover construction and reliable integration." *SIAM J. Sci. Comput.*, 23(5), 1655–1682.
Griebel, M., and Schweitzer, M. A. (2002b). "A particle-partition of unity method—Part III: A multilevel solver." *SIAM J. Sci. Comput.*, 24(2), 377–409.
Griebel, M., and Schweitzer, M. A. (2003b). "A particle-partition of unity method. Part V: Boundary conditions." *Geometric analysis and nonlinear partial differential equations*, Springer, Berlin, 1–25.
Griebel, M., and Schweitzer, M. A. (2003a). "A particle-partition of unity method. Part IV: Parallelization." *Meshfree methods for partial differential equations*, Springer, New York, 161–192.
Guan, P. C. (2009). "Adaptive coupling of FEM and RKPM formulations for contact and impact problems." Ph.D. dissertation, Univ. of California, Los Angeles.
Guan, P. C., et al. (2009). "Semi-Lagrangian reproducing kernel formulation and application to modeling earth moving operations." *Mech. Mater.*, 41(6), 670–683.
Guan, P. C., Chi, S. W., Chen, J. S., Slawson, T. R., and Roth, M. J. (2011). "Semi-Lagrangian reproducing kernel particle method for fragment-impact problems." *Int. J. Impact Eng.*, 38(12), 1033–1047.
Günther, F. C., and Liu, W. K. (1998). "Implementation of boundary conditions for meshless methods." *Comput. Methods Appl. Mech. Eng.*, 163(1–4), 205–230.
Günther, F. C., Liu, W. K., Diachin, D., and Christon, M. A. (2000). "Multi-scale meshfree parallel computations for viscous, compressible flows." *Comput. Methods Appl. Mech. Eng.*, 190(3–4), 279–303.
Gupta, V., Duarte, C. A. M., Babuška, I., and Banerjee, U. (2013). "A stable and optimally convergent generalized FEM (SGFEM) for linear elastic fracture mechanics." *Comput. Methods Appl. Mech. Eng.*, 266, 23–39.
Gupta, V., Duarte, C. A. M., Babuška, I., and Banerjee, U. (2015). "Stable GFEM (SGFEM): Improved conditioning and accuracy of GFEM/XFEM for three-dimensional fracture mechanics." *Comput. Methods Appl. Mech. Eng.*, 289, 355–386.
Gupta, V., Kim, D. J., and Duarte, C. A. M. (2012). "Analysis and improvements of global-local enrichments for the generalized finite element method." *Comput. Methods Appl. Mech. Eng.*, 245–246, 47–62.
Han, W., and Meng, X. (2001). "Error analysis of the reproducing kernel particle method." *Comput. Methods Appl. Mech. Eng.*, 190(46–47), 6157–6181.
Han, W., Wagner, G. J., and Liu, W. K. (2002). "Convergence analysis of a hierarchical enrichment of Dirichlet boundary conditions in a mesh-free method." *Int. J. Numer. Methods Eng.*, 53(6), 1323–1336.
Hardy, R. L. (1971). "Multiquadric equations of topography and other irregular surfaces." *J. Geophys. Res.*, 76(8), 1905–1915.
Hardy, R. L. (1990). "Theory and applications of the multiquadric-biharmonic method 20 years of discovery 1968–1988." *Comput. Math. Appl.*, 19(8), 163–208.
Harlow, F. H. (1964). "The particle-in-cell computing method for fluid dynamics." *Methods in computational physics*, Academic Press, New York, 319–343.
Hillman, M., and Chen, J. S. (2015). "An accelerated, convergent, and stable nodal integration in Galerkin meshfree methods for linear and nonlinear mechanics." *Int. J. Numer. Methods Eng.*, 107(7), 603–630.
Hillman, M., and Chen, J. S. (2016). "Nodally integrated implicit gradient reproducing kernel particle method for convection dominated problems." *Comput. Methods Appl. Mech. Eng.*, 299, 381–400.
Hillman, M., Chen, J. S., and Bazilevs, Y. (2015). "Variationally consistent domain integration for isogeometric analysis." *Comput. Methods Appl. Mech. Eng.*, 284, 521–540.
Hillman, M., Chen, J. S., and Chi, S. W. (2014). "Stabilized and variationally consistent nodal integration for meshfree modeling of impact problems." *Comp. Part. Mech*, 1(3), 245–256.
Hon, Y. C., and Schaback, R. (2001). "On unsymmetric collocation by radial basis functions." *Appl. Math. Comput.*, 119(2–3), 177–186.
Hu, H. Y., Chen, J. S., and Hu, W. (2007). "Weighted radial basis collocation method for boundary value problems." *Int. J. Numer. Methods Eng.*, 69(13), 2736–2757.
Hu, H. Y., Chen, J. S., and Hu, W. (2011). "Error analysis of collocation method based on reproducing kernel approximation." *Numer. Methods Partial Differ. Equ.*, 27(3), 554–580.
Hu, H. Y., Lai, C. K., and Chen, J. S. (2009). "A study on convergence and complexity of reproducing kernel collocation method." *Interact. Multiscale Mech.*, 2(3), 295–319.
Hu, H. Y., Li, Z. C., and Cheng, A. H. D. (2005). "Radial basis collocation methods for elliptic boundary value problems." *Comput. Math. Appl.*, 50(1), 289–320.
Huerta, A., and Fernández-Méndez, S. (2003). "Time accurate consistently stabilized mesh-free methods for convection dominated problems." *Int. J. Numer. Methods Eng.*, 56(9), 1225–1242.
Hughes, T. J. R., Cottrell, J. A., and Bazilevs, Y. (2005). "Isogeometric analysis: CAD, finite elements, NURBS, exact geometry and mesh refinement." *Comput. Methods Appl. Mech. Eng.*, 194(39–41), 4135–4195.
Idelsohn, S. R., Calvo, N., and Oñate, E. (2003a). "Polyhedrization of an arbitrary 3D point set." *Comput. Methods Appl. Mech. Eng.*, 192(22), 2649–2667.
Idelsohn, S. R., Marti, J., Becker, P., and Oñate, E. (2014). "Analysis of multifluid flows with large time steps using the particle finite element method." *Int. J. Numer. Methods Fluids*, 75(9), 621–644.
Idelsohn, S. R., Nigro, N., Limache, A., and Oñate, E. (2012). "Large time-step explicit integration method for solving problems with dominant convection." *Comput. Methods Appl. Mech. Eng.*, 217–220, 168–185.
Idelsohn, S. R., Oñate, E., Calvo, N., and Del Pin, F. (2003f). "The meshless finite element method." *Int. J. Numer. Methods Eng.*, 58(6), 893–912.
Idelsohn, S. R., Oñate, E., and Del Pin, F. (2003b). "A Lagrangian meshless finite element method applied to fluid-structure interaction problems." *Comput. Struct.*, 81(8-11), 655–671.
Idelsohn, S. R., Oñate, E., and Del Pin, F. (2004). "The particle finite element method: A powerful tool to solve incompressible flows with free-surfaces and breaking waves." *Int. J. Numer. Methods Eng.*, 61(7), 964–989.
Jaynes, E. T. (1957). "Information theory and statistical mechanics." *Phys. Rev.*, 106(4), 620–630.
Jensen, P. S. (1972). "Finite difference techniques for variable grids." *Comput. Struct.*, 2(1–2), 17–29.
Johnson, G. R. (1994). "Linking of Lagrangian particle methods to standard finite element methods for high velocity impact computations." *Nucl. Eng. Des.*, 150(2–3), 265–274.
Johnson, G. R. (2011). "Numerical algorithms and material models for high-velocity impact computations." *Int. J. Impact Eng.*, 38(6), 456–472.
Johnson, G. R., Beissel, S. R., and Gerlach, C. A. (2013). "A combined particle-element method for high-velocity impact computations." *Proc. Eng.*, 58, 269–278.
Johnson, G. R., Beissel, S. R., and Stryk, R. A. (2000). "A generalized particle algorithm for high velocity impact computations." *Comput. Mech.*, 25(2–3), 245–256.
Johnson, G. R., Beissel, S. R., and Stryk, R. A. (2002). "An improved generalized particle algorithm that includes boundaries and interfaces." *Int. J. Numer. Methods Eng.*, 53(4), 875–904.

Johnson, G. R., Stryk, R. A., and Beissel, S. R. (1996). "SPH for high velocity impact computations." *Comput. Methods Appl. Mech. Eng.*, 139(1–4), 347–373.
Johnson, G. R., Stryk, R. A., and Dodd, J. G. (1986). "Dynamic Lagrangian computations for solids, with variable nodal connectivity for severe distortions." *Int. J. Numer. Methods Eng.*, 23(3), 509–522.
Kaljevic, I., and Saigal, S. (1997). "An improved element free Galerkin formulation." *Int. J. Numer. Methods Eng.*, 40(16), 2953–2974.
Kansa, E. J. (1990a). "Multiquadrics—A scattered data approximation scheme with applications to computational fluid-dynamics—I. Surface approximations and partial derivative estimates." *Comput. Math. Appl.*, 19(8), 127–145.
Kansa, E. J. (1990b). "Multiquadrics—A scattered data approximation scheme with applications to computational fluid-dynamics—II. Solutions to parabolic, hyperbolic and elliptic partial differential equations." *Comput. Math. Appl.*, 19(8), 147–161.
Kansa, E. J., and Hon, Y. C. (2000). "Circumventing the ill-conditioning problem with multiquadric radial basis functions: Applications to elliptic partial differential equations." *Comput. Math. Appl.*, 39(7–8), 123–137.
Khayyer, A., and Gotoh, H. (2010). "A higher order Laplacian model for enhancement and stabilization of pressure calculation by the MPS method." *Appl. Ocean Res.*, 32(1), 124–131.
Khayyer, A., and Gotoh, H. (2011). "Enhancement of stability and accuracy of the moving particle semi-implicit method." *J. Comput. Phys.*, 230(8), 3093–3118.
Kim, D. J., Pereira, J. P. A., and Duarte, C. A. M. (2010). "Analysis of three-dimensional fracture mechanics problems: A two-scale approach using coarse-generalized FEM meshes." *Int. J. Numer. Methods Eng.*, 81(3), 335–365.
Kim, J., and Duarte, C. A. M. (2015). "A new generalized finite element method for two-scale simulations of propagating cohesive fractures in 3-D." *Int. J. Numer. Methods Eng.*, 104(13), 1139–1172.
Kim, N. H., Choi, K. K., and Chen, J. S. (2000a). "Shape design sensitivity analysis and optimization of elasto-plasticity with frictional contact." *AIAA J.*, 38(9), 1742–1753.
Kim, N. H., Choi, K. K., and Chen, J. S. (2001). "Die shape design optimization of sheet metal stamping process using meshfree method." *Int. J. Numer. Methods Eng.*, 51(12), 1385–1405.
Kim, N. H., Choi, K. K., Chen, J. S., and Park, Y. H. (2000g). "Meshless shape design sensitivity analysis and optimization for contact problem with friction." *Comput. Mech.*, 25(2-3), 157–168.
Kondo, M., and Koshizuka, S. (2011). "Improvement of stability in moving particle semi-implicit method." *Int. J. Numer. Methods Fluids*, 65(6), 638–654.
Koshizuka, S., Ikeda, H., and Oka, Y. (1999). "Numerical analysis of fragmentation mechanisms in vapor explosions." *Nucl. Eng. Des.*, 189(1), 423–433.
Koshizuka, S., Nobe, A., and Oka, Y. (1998). "Numerical analysis of breaking waves using the moving particle semi-implicit method." *Int. J. Numer. Methods Fluids*, 26(7), 751–769.
Koshizuka, S., and Oka, Y. (1996). "Moving-particle semi-implicit method for fragmentation of incompressible fluid." *Nucl. Sci. Eng.*, 123(3), 421–434.
Krongauz, Y., and Belytschko, T. (1996). "Enforcement of essential boundary conditions in meshless approximations using finite elements." *Comput. Methods Appl. Mech. Eng.*, 131(1–2), 133–145.
Krongauz, Y., and Belytschko, T. (1997). "Consistent pseudo-derivatives in meshless methods." *Comput. Methods Appl. Mech. Eng.*, 146(3–4), 371–386.
Krysl, P., and Belytschko, T. (1995). "Analysis of thin plates by the element-free Galerkin method." *Comput. Mech.*, 17(1–2), 26–35.
Krysl, P., and Belytschko, T. (1996). "Analysis of thin shells by the element-free Galerkin method." *Int. J. Solids Struct.*, 33(20-22), 3057–3080.
Kwok, O. L. A., Guan, P. C., Cheng, W. P., and Sun, C. T. (2015). "Semi-Lagrangian reproducing kernel particle method for slope stability analysis and post-failure simulation." *KSCE J. Civ. Eng.*, 19(1), 107–115.
Lancaster, P., and Salkauskas, K. (1981). "Surfaces generated by moving least squares methods." *Math. Comput.*, 37(155), 141–158.
Lanczos, C. (1938). "Trigonometric interpolation of empirical and analytical functions." *J. Math. Phys.*, 17(1), 123–199.
Li, B., Habbal, F., and Ortiz, M. (2010). "Optimal transportation meshfree approximation schemes for fluid and plastic flows." *Int. J. Numer. Methods Eng.*, 83(12), 1541–1579.
Li, B., Kidane, A., Ravichandran, G., and Ortiz, M. (2012). "Verification and validation of the optimal transportation meshfree (OTM) simulation of terminal ballistics." *Int. J. Impact Eng.*, 42, 25–36.
Li, B., Perotti, L., Adams, M., Mihaly, J., Rosakis, A. J., Stalzer, M., and Ortiz, M. (2013). "Large scale optimal transportation meshfree (OTM) simulations of hypervelocity impact." *Proc. Eng.*, 58, 320–327.
Li, J. (2005). "Mixed methods for fourth-order elliptic and parabolic problems using radial basis functions." *Adv. Comput. Math.*, 23(1–2), 21–30.
Li, S., Hao, W., and Liu, W. K. (2000a). "Mesh-free simulations of shear banding in large deformation." *Int. J. Solids Struct.*, 37(48–50), 7185–7206.
Li, S., Hao, W., and Liu, W. K. (2000b). "Numerical simulations of large deformation of thin shell structures using meshfree methods." *Comput. Mech.*, 25(2-3), 102–116.
Li, S., and Liu, W. K. (1996). "Moving least-square reproducing kernel method. Part II: Fourier analysis." *Comput. Methods Appl. Mech. Eng.*, 139(1–4), 159–193.
Li, S., and Liu, W. K. (1998). "Synchronized reproducing kernel interpolant via multiple wavelet expansion." *Comput. Mech.*, 21(1), 28–47.
Li, S., and Liu, W. K. (1999a). "Reproducing kernel hierarchical partition of unity. Part II—Applications." *Int. J. Numer. Methods Eng.*, 45(3), 289–317.
Li, S., and Liu, W. K. (1999b). "Reproducing kernel hierarchical partition of unity. Part I—Formulation and theory." *Int. J. Numer. Methods Eng.*, 45(3), 251–288.
Li, S., and Liu, W. K. (2007). *Meshfree particle methods*, Springer, Berlin.
Li, S., Liu, W. K., Qian, D., and Guduru, P. R. (2001). "Dynamic shear band propagation and micro-structure of adiabatic shear band." *Comput. Methods Appl. Mech. Eng.*, 191(1-2), 73–92.
Li, S., Liu, W. K., Rosakis, A. J., Belytschko, T., and Hao, W. (2002). "Mesh-free Galerkin simulations of dynamic shear band propagation and failure mode transition." *Int. J. Solids Struct.*, 39(5), 1213–1240.
Libersky, L. D., and Petschek, A. G. (1991). "Smooth particle hydrodynamics with strength of materials." *Advances in the free-Lagrange method including contributions on adaptive gridding and the smooth particle hydrodynamics method*, Springer, Berlin, 248–257.
Libersky, L. D., Randles, P. W., Carney, T. C., and Dickinson, D. L. (1997). "Recent improvements in SPH modeling of hypervelocity impact." *Int. J. Impact Eng.*, 20(6–10), 525–532.
Liszka, T. J. (1984). "An interpolation method for an irregular net of nodes." *Int. J. Numer. Methods Eng.*, 20(9), 1599–1612.
Liszka, T. J., and Orkisz, J. (1980). "The finite difference method at arbitrary irregular grids and its application in applied mechanics." *Comput. Struct.*, 11(1–2), 83–95.
Liu, G. R. (2008). "A generalized gradient smoothing technique and the smoothed bilinear form for galerkin formulation of a wide class of computational methods." *Int. J. Comput. Methods*, 05(02), 199–236.
Liu, G. R. (2009). *Meshfree methods: Moving beyond the finite element method*, CRC Press, Boca Raton, FL.
Liu, G. R., and Chen, X. L. (2001). "A mesh-free method for static and free vibration analyses of thin plates of complicated shape." *J. Sound Vibr.*, 241(5), 839–855.
Liu, G. R., Dai, K. Y., and Nguyen, T. T. (2007a). "A smoothed finite element method for mechanics problems." *Comput. Mech.*, 39(6), 859–877.
Liu, G. R., and Gu, Y. T. (2001). "A local radial point interpolation method (LRPIM) for free vibration analyses of 2-D solids." *J. Sound Vibr.*, 246(1), 29–46.
Liu, G. R., and Nguyen-Thoi, T. (2010). *Smoothed finite element methods*, CRC Press, NJ.
Liu, G. R., Zhang, G. Y., Wang, Y. Y., Zhong, Z. H., Li, G. Y., and Han, X. (2007b). "A nodal integration technique for meshfree radial point interpolation method (NI-RPIM)." *Int. J. Solids Struct.*, 44(11–12), 3840–3860.

Liu, W. K., and Chen, Y. (1995). "Wavelet and multiple scale reproducing kernel methods." *Int. J. Numer. Methods Fluids*, 21(10), 901–931.
Liu, W. K., Chen, Y., Chang, C. T., and Belytschko, T. (1996a). "Advances in multiple scale kernel particle methods." *Comput. Mech.*, 18(2), 73–111.
Liu, W. K., Chen, Y., Jun, S., Chen, J. S., Belytschko, T., Pan, C., Uras, R. A., and Chang, C. T. (1996b). "Overview and applications of the reproducing kernel particle methods." *Archiv. Comput. Methods Eng.*, 3(1), 3–80.
Liu, W. K., Chen, Y., Uras, R. A., and Chang, C. T. (1996c). "Generalized multiple scale reproducing kernel particle methods." *Comput. Methods Appl. Mech. Eng.*, 139(1–4), 91–157.
Liu, W. K., Han, W., Lu, H., Li, S., and Cao, J. (2004). "Reproducing kernel element method. Part I: Theoretical formulation." *Comput. Methods Appl. Mech. Eng.*, 193(12–14), 933–951.
Liu, W. K., Hao, W., Chen, Y., Jun, S., and Gosz, J. (1997a). "Multiresolution reproducing kernel particle methods." *Comput. Mech.*, 20(4), 295–309.
Liu, W. K., and Jun, S. (1998). "Multiple-scale reproducing kernel particle methods for large deformation problems." *Int. J. Numer. Methods Eng.*, 41(7), 1339–1362.
Liu, W. K., Jun, S., Li, S., Adee, J., and Belytschko, T. (1995a). "Reproducing kernel particle methods for structural dynamics." *Int. J. Numer. Methods Eng.*, 38(10), 1655–1679.
Liu, W. K., Jun, S., Sihling, D. T., Chen, Y. J., and Hao, W. (1997b). "Multiresolution reproducing kernel particle method for computational fluid dynamics." *Int. J. Numer. Methods Fluids*, 24(12), 1391–1415.
Liu, W. K., Jun, S., and Zhang, Y. F. (1995b). "Reproducing kernel particle methods." *Int. J. Numer. Methods Fluids*, 20(8–9), 1081-1106.
Liu, W. K., Li, S., and Belytschko, T. (1997c). "Moving least-square reproducing kernel methods. I: Methodology and convergence." *Comput. Methods Appl. Mech. Eng.*, 143(1–2), 113–154.
Liu, W. K., Ong, J. S. J., and Uras, R. A. (1985). "Finite element stabilization matrices-a unification approach." *Comput. Methods Appl. Mech. Eng.*, 53(1), 13–46.
Liu, Y., and Belytschko, T. (2010). "A new support integration scheme for the weakform in mesh-free methods." *Int. J. Numer. Methods Eng.*, 82(6), 699–715.
Long, S., and Atluri, S. N. (2001). "A meshless local petrov-galerkin method for solving the bending problem of a thin plate." *Comput. Model. Eng. Sci.*, 3(1), 53–63.
Lu, H., and Chen, J. S. (2002). "Adaptive Galerkin particle method." *Lect. Notes Comput. Sci. Eng.*, 26, 251–267.
Lu, Y. Y., Belytschko, T., and Gu, L. (1994). "A new implementation of the element free Galerkin method." *Comput. Methods Appl. Mech. Eng.*, 113(3–4), 397–414.
Lucy, L. B. (1977). "A numerical approach to the testing of the fission hypothesis." *Astron. J.*, 82, 1013–1024.
Ma, S., Zhang, X., and Qiu, X. M. (2009). "Comparison study of MPM and SPH in modeling hypervelocity impact problems." *Int. J. Impact Eng.*, 36(2), 272–282.
Madych, W. R. (1992). "Miscellaneous error bounds for multiquadric and related interpolators." *Comput. Math. Appl.*, 24(12), 121–138.
Madych, W. R., and Nelson, S. A. (1990). "Multivariate interpolation and conditionally positive definite functions II." *Math. Comput.*, 54(189), 211–230.
Melenk, J. M. (1995). "On generalized finite element methods." Ph.D. dissertation, Univ. of Maryland, College Park, MD.
Melenk, J. M., and Babuška, I. (1996). "The partition of unity finite element method: Basic theory and applications." *Comput. Methods Appl. Mech. Eng.*, 139(1–4), 289–314.
Moës, N., Dolbow, J., and Belytschko, T. (1999). "A finite element method for crack growth without remeshing." *Int. J. Numer. Meth. Eng.*, 46(1), 131–150.
Monaghan, J. J. (1982). "Why particle methods work." *SIAM J. Sci. Stat. Comput.*, 3(4), 422–433.
Monaghan, J. J. (1988). "An introduction to SPH." *Comput. Phys. Commun.*, 48(1), 89–96.
Monaghan, J. J. (2000). "SPH without a tensile instability." *J. Comput. Phys.*, 159(2), 290–311.
Nagashima, T. (1999). "Node-by-node meshless approach and its applications to structural analyses." *Int. J. Numer. Methods Eng.*, 46(3), 341–385.
Nayroles, B., Touzot, G., and Villon, P. (1992). "Generalizing the finite element method: Diffuse approximation and diffuse elements." *Comput. Mech.*, 10(5), 307–318.
Nitsche, J. (1971). "Über ein Variationsprinzip zur Lösung von Dirichlet-Problemen bei Verwendung von Teilräumen, die keinen Randbedingungen unterworfen sind." *Abhandlungen aus dem mathematischen Seminar der Universität Hamburg*, Springer, Berlin, 9–15.
Oden, J. T., Duarte, C. A. M., and Zienkiewicz, O. C. (1998). "A new cloud-based hp finite element method." *Comput. Methods Appl. Mech. Eng.*, 153(1–2), 117–126.
Oñate, E., and Idelsohn, S. R. (1998). "A mesh-free finite point method for advective-diffusive transport and fluid flow problems." *Comput. Mech.*, 21(4–5), 283–292.
Oñate, E., Idelsohn, S. R., Zienkiewicz, O. C., and Taylor, R. L. (1996a). "A finite point method in computational mechanics: Applications to convective transport and fluid flow." *Int. J. Numer. Methods Eng.*, 39(22), 3839–3866.
Oñate, E., Idelsohn, S. R., Zienkiewicz, O. C., Taylor, R. L., Sacco, C., and Idelsohnl, S. (1996b). "A stabilized finite point method for analysis of fluid mechanics problems." *Comput. Methods Appl. Mech. Eng.*, 139(96), 315–346.
Parks, M. L., Lehoucq, R. B., Plimpton, S. J., and Silling, S. A. (2008). "Implementing peridynamics within a molecular dynamics code." *Comput. Phys. Commun.*, 179(11), 777–783.
Pereira, J. P. A., Kim, D. J., and Duarte, C. A. M. (2012). "A two-scale approach for the analysis of propagating three-dimensional fractures." *Comput. Mech.*, 49(1), 99–121.
Perrones, N., and Kao, R. (1974). "A general-finite difference method for arbitrary meshes." *Comput. Struct.*, 5(I), 45–57.
Puso, M. A., Chen, J. S., Zywicz, E., and Elmer, W. (2008). "Meshfree and finite element nodal integration methods." *Int. J. Numer. Methods Eng.*, 74(3), 416–446.
Puso, M. A., Zywicz, E., and Chen, J. S. (2007). "A new stabilized nodal integration approach." *Lect. Notes Comput. Sci. Eng.*, 57, 207–217.
Rabczuk, T., and Areias, P. M. A. (2006). "A meshfree thin shell for arbitrary evolving cracks based on an extrinsic basis." *Comput. Model. Eng. Sci.*, 16(2), 115–130.
Rabczuk, T., Areias, P. M. A., and Belytschko, T. (2007a). "A meshfree thin shell method for non-linear dynamic fracture." *Int. J. Numer. Methods Eng.*, 72(5), 524–548.
Rabczuk, T., and Belytschko, T. (2004). "Cracking particles: A simplified meshfree method for arbitrary evolving cracks." *Int. J. Numer. Methods Eng.*, 61(13), 2316–2343.
Rabczuk, T., and Belytschko, T. (2005). "Adaptivity for structured meshfree particle methods in 2D and 3D." *Int. J. Numer. Methods Eng.*, 63(11), 1559–1582.
Rabczuk, T., and Belytschko, T. (2007). "A three-dimensional large deformation meshfree method for arbitrary evolving cracks." *Comput. Methods Appl. Mech. Eng.*, 196(29–30), 2777–2799.
Rabczuk, T., Bordas, S. P. A., and Zi, G. (2007i). "A three-dimensional meshfree method for continuous multiple-crack initiation, propagation and junction in statics and dynamics." *Comput. Mech.*, 40(3), 473–495.
Rabczuk, T., and Eibl, J. (2003). "Simulation of high velocity concrete fragmentation using SPH/MLSPH." *Int. J. Numer. Methods Eng.*, 56(10), 1421–1444.
Rabczuk, T., Eibl, J., and Stempniewski, L. (2004). "Numerical analysis of high speed concrete fragmentation using a meshfree Lagrangian method." *Eng. Fract. Mech.*, 71(4-6), 547–556.
Rabczuk, T., and Samaniego, E. (2008). "Discontinuous modelling of shear bands using adaptive meshfree methods." *Comput. Methods Appl. Mech. Eng.*, 197(6-8), 641–658.
Rabczuk, T., and Zi, G. (2007). "A meshfree method based on the local partition of unity for cohesive cracks." *Comput. Mech.*, 39(6), 743–760.
Rabczuk, T., Zi, G., Bordas, S. P. A., and Nguyen-Xuan, H. (2010). "A simple and robust three-dimensional cracking-particle method without enrichment." *Comput. Methods Appl. Mech. Eng.*, 199(37–40), 2437–2455.

Randles, P. W., and Libersky, L. D. (1996). "Smoothed particle hydrodynamics: Some recent improvements and applications." *Comput. Methods Appl. Mech. Eng. Comput. Methods Appl. Mech. Eng.*, 139(1–4), 375–408.

Randles, P. W., and Libersky, L. D. (2000). "Normalized SPH with stress points." *Int. J. Numer. Meth. Eng.*, 48(10), 1445–1462.

Ren, B., and Li, S. (2010). "Meshfree simulations of plugging failures in high-speed impacts." *Comput. Struct.*, 88(15–16), 909–923.

Romero, I., and Armero, F. (2002). "The partition of unity quadrature in meshless methods." *Int. J. Numer. Methods Eng.*, 54(7), 987–1006.

Rosolen, A., Millán, D., and Arroyo, M. (2013). "Second-order convex maximum entropy approximants with applications to high-order PDE." *Int. J. Numer. Methods Eng.*, 94(2), 150–182.

Rüter, M., Hillman, M., and Chen, J. S. (2013). "Corrected stabilized non-conforming nodal integration in meshfree methods." *Lect. Notes Comput. Sci. Eng.*, 75–92.

Sadeghirad, A., Brannon, R. M., and Burghardt, J. (2011). "A convected particle domain interpolation technique to extend applicability of the material point method for problems involving massive deformations." *Int. J. Numer. Methods Eng.*, 86(12), 1435–1456.

Savitzky, A., and Golay, M. J. E. (1964). "Smoothing and differentiation of data by simplified least squares procedures." *Anal. Chem.*, 36(8), 1627–1639.

Shepard, D. (1968). "A two-dimensional interpolation function for irregularly-spaced data." *23rd ACM National Conf.*, ACM, New York, 517–524.

Sherburn, J. A., Roth, M. J., Chen, J. S., and Hillman, M. (2015). "Meshfree modeling of concrete slab perforation using a reproducing kernel particle impact and penetration formulation." *Int. J. Impact Eng.*, 86, 96–110.

Sibson, R. (1980). "A vector identity for the Dirichlet tessellation." *Math. Proc. Cambridge Philos. Soc.*, 87(01), 151.

Silling, S. A. (2000). "Reformulation of elasticity theory for discontinuities and long-range forces." *J. Mech. Phys. Solids*, 48(1), 175–209.

Silling, S. A., and Askari, E. (2005). "A meshfree method based on the peridynamic model of solid mechanics." *Comput. Struct.*, 83(17–18), 1526–1535.

Silling, S. A., Epton, M. A., Weckner, O., Xu, J., and Askari, E. (2007). "Peridynamic states and constitutive modeling." *J. Elast.*, 88(2), 151–184.

Silling, S. A., and Lehoucq, R. B. (2008). "Convergence of peridynamics to classical elasticity theory." *J. Elast.*, 93(1), 13–37.

Slater, J. (1934). "Electronic energy bands in metal." *Phys. Rev.*, 45(11), 794–801.

Strouboulis, T., Babuška, I., and Copps, K. (2000a). "The design and analysis of the generalized finite element method." *Comput. Methods Appl. Mech. Eng.*, 181(1–3), 43–69.

Strouboulis, T., Copps, K., and Babuška, I. (2000b). "The generalized finite element method: An example of its implementation and illustration of its performance." *Int. J. Numer. Methods Eng.*, 47(8), 1401–1417.

Strouboulis, T., Copps, K., and Babuška, I. (2001). "The generalized finite element method." *Comput. Methods Appl. Mech. Eng.*, 190(32), 4081–4193.

Sukumar, N. (2004). "Construction of polygonal interpolants: A maximum entropy approach." *Int. J. Numer. Methods Eng.*, 61(12), 2159–2181.

Sukumar, N. (2013). "Quadratic maximum-entropy serendipity shape functions for arbitrary planar polygons." *Comput. Methods Appl. Mech. Eng.*, 263, 27–41.

Sukumar, N., and Belytschko, T. (1998). "The natural element method in solid mechanics." *Int. J. Numer. Methods Eng.*, 43(5), 839–887.

Sulsky, D. L., Chen, Z., and Schreyer, H. L. (1994). "A particle method for history-dependent materials." *Comput. Methods Appl. Mech. Eng.*, 118(1–2), 179–196.

Sulsky, D. L., and Schreyer, H. L. (1996). "Axisymmetric form of the material point method with applications to upsetting and Taylor impact problems." *Comput. Methods Appl. Mech. Eng.*, 139(1–4), 409–429.

Sulsky, D. L., Zhou, S. J., and Schreyer, H. L. (1995). "Application of a particle-in-cell method to solid mechanics." *Comput. Phys. Commun.*, 87(1–2), 236–252.

Swegle, J. W., Attaway, S. W., Heinstein, M. W., Mello, F. J., and Hicks, D. L. (1994). "An analysis of smoothed particle hydrodynamics." Sandia National Labs, Albuquerque, NM.

Swegle, J. W., Hicks, D. L., and Attaway, S. W. (1995). "Smoothed particle hydrodynamics stability analysis." *J. Comput. Phys.*, 116(1), 123–134.

Sze, K. Y., Chen, J. S., Sheng, N., and Liu, X. H. (2004). "Stabilized conforming nodal integration: Exactness and variational justification." *Finite Elem. Anal. Des.*, 41(2), 147–171.

Taylor, G. (1948). "The use of flat-ended projectiles for determining dynamic yield stress. I: Theoretical considerations." *Proc. R. Soc. London A: Math. Phys. Eng. Sci.*, 194(1038), 289–299.

Tupek, M. R., Rimoli, J. J., and Radovitzky, R. (2013). "An approach for incorporating classical continuum damage models in state-based peridynamics." *Comput. Methods Appl. Mech. Eng.*, 263, 20–26.

Uras, R. A., Chang, C. T., Chen, Y., and Liu, W. K. (1997). "Multiresolution reproducing kernel particle methods in acoustics." *J. Comput. Acoust.*, 5(01), 71–94.

Ventura, G., Xu, J. X., and Belytschko, T. (2002). "A vector level set method and new discontinuity approximations for crack growth by EFG." *Int. J. Numer. Methods Eng.*, 54(6), 923–944.

Wagner, G. J., and Liu, W. K. (2000). "Application of essential boundary conditions in mesh-free methods: A corrected collocation method." *Int. J. Numer. Methods Eng.*, 47(8), 1367–1379.

Wang, D., and Chen, J. S. (2004). "Locking-free stabilized conforming nodal integration for meshfree Mindlin-Reissner plate formulation." *Comput. Methods Appl. Mech. Eng.*, 193(12–14), 1065–1083.

Wang, D., and Chen, J. S. (2008). "A Hermite reproducing kernel approximation for thin-plate analysis with sub-domain stabilized conforming integration." *Int. J. Numer. Methods Eng.*, 74(3), 368–390.

Wang, D., and Chen, P. (2014). "Quasi-convex reproducing kernel meshfree method." *Comput. Mech.*, 54(3), 689–709.

Wang, D., Li, Z., Li, L., and Wu, Y. (2011). "Three dimensional efficient meshfree simulation of large deformation failure evolution in soil medium." *Sci. China Technol. Sci.*, 54(3), 573–580.

Wang, D., and Peng, H. (2013). "A hermite reproducing kernel Galerkin meshfree approach for buckling analysis of thin plates." *Comput. Mech.*, 51(6), 1013–1029.

Wang, D., and Wu, J. (2016). "An efficient nesting sub-domain gradient smoothing integration algorithm with quadratic exactness for Galerkin meshfree methods." *Comput. Methods Appl. Mech. Eng.*, 298, 485–519.

Wang, H. P. (2000). "Meshfree smooth contact formulation and boundary condition treatments in multi-body contact." Ph.D. dissertation, Univ. of Iowa, Iowa City, IA.

Wang, H. P., Wu, C. T., and Chen, J. S. (2014). "A reproducing kernel smooth contact formulation for metal forming simulations." *Comput. Mech.*, 54(1), 151–169.

Wang, J. G., and Liu, G. R. (2002). "A point interpolation meshless method based on radial basis functions." *Int. J. Numer. Methods Eng.*, 54(11), 1623–1648.

Wang, L., Chen, J. S., and Hu, H. Y. (2010). "Subdomain radial basis collocation method for fracture mechanics." *Int. J. Numer. Methods Eng.*, 83(7), 851–876.

Warren, T. L., Silling, S. A., Askari, A., Weckner, O., Epton, M. A., and Xu, J. (2009). "A non-ordinary state-based peridynamic method to model solid material deformation and fracture." *Int. J. Solids Struct.*, 46(5), 1186–1195.

Wei, H., Chen, J. S., and Hillman, M. (2016). "A stabilized nodally integrated meshfree formulation for fully coupled hydro-mechanical analysis of fluid-saturated porous media." *Comput. Fluids*, 141, 105–115.

Wendland, H. (1995). "Piecewise polynomial, positive definite and compactly supported radial functions of minimal degree." *Adv. Comput. Math.*, 4(1), 389–396.

Wendland, H. (1999). "Meshless Galerkin methods using radial basis functions." *Math. Comput. Am. Math. Soc.*, 68(228), 1521–1531.

Wilkins, M. L., and Guinan, M. W. (1973). "Impact of cylinders on a rigid boundary." *J. Appl. Phys.*, 44(3), 1200–1206.

Wong, A. S. M., Hon, Y. C., Li, T. S., Chung, S. L., and Kansa, E. J. (1999). "Multizone decomposition for simulation of time-dependent problems using the multiquadric scheme." *Comput. Math. Appl.*, 37(8), 23–43.

Wu, C. T., Chen, J. S., Chi, L., and Huck, F. (2001). "Lagrangian meshfree formulation for analysis of geotechnical materials." *J. Eng. Mech.*, 10.1061/(ASCE)0733-9399(2001)127:5(440), 440–449.
Wu, C. T., Chi, S. W., Koishi, M., and Wu, Y. (2016). "Strain gradient stabilization with dual stress points for the meshfree nodal integration method in inelastic analyses." *Int. J. Numer. Methods Eng.*, 107, 3–30.
Wu, C. T., Koishi, M., and Hu, W. (2015). "A displacement smoothing induced strain gradient stabilization for the meshfree Galerkin nodal integration method." *Comput. Mech.*, 56(1), 19–37.
Wu, C. T., Park, C. K., and Chen, J. S. (2011). "A generalized approximation for the meshfree analysis of solids." *Int. J. Numer. Methods Eng.*, 85(6), 693–722.
Wu, Y., Wang, D., and Wu, C. T. (2014). "Three dimensional fragmentation simulation of concrete structures with a nodally regularized meshfree method." *Theor. Appl. Fract. Mech.*, 72(1), 89–99.
Wu, Y., Wang, D., Wu, C. T., and Zhang, H. (2016). "A direct displacement smoothing meshfree particle formulation for impact failure modeling." *Int. J. Impact Eng.*, 87, 169–185.
Wu, Z., and Schaback, R. (1993). "Local error estimates for radial basis function interpolation of scattered data." *IMA J. Numer. Anal.*, 13(1), 13–27.
Yagawa, G., and Yamada, T. (1996). "Free mesh method: A new meshless finite element method." *Comput. Mech.*, V18(5), 383–386.
Yoo, J. W., Moran, B., and Chen, J. S. (2004). "Stabilized conforming nodal integration in the natural-element method." *Int. J. Numer. Methods Eng.*, 60(5), 861–890.
Yoon, J. (2001). "Spectral approximation orders of radial basis function interpolation on the Sobolev space." *SIAM J. Math. Anal.*, 33(4), 946–958.
Yoon, S., and Chen, J. S. (2002). "Accelerated meshfree method for metal forming simulation." *Finite Elem. Anal. Des.*, 38(10), 937–948.
Yoon, S., Wu, C. T., Wang, H. P., and Chen, J. S. (2001). "Efficient meshfree formulation for metal forming simulations." *J. Eng. Mater. Technol.*, 123(4), 462.
You, Y., Chen, J. S., and Lu, H. (2003). "Filters, reproducing kernel, and adaptive meshfree method." *Comput. Mech.*, 31(3), 316–326.
Yreux, E., and Chen, J. S. (2016). "A quasi-linear reproducing kernel particle method." *Int. J. Numer. Methods Eng.*, 109(7), 1045–1064.
Zhang, L. T., Wagner, G. J., and Liu, W. K. (2002). "A parallelized meshfree method with boundary enrichment for large-scale CFD." *J. Comput. Phys.*, 176(2), 483–506.
Zhang, X., Sze, K. Y., and Ma, S. (2006). "An explicit material point finite element method for hyper-velocity impact." *Int. J. Numer. Methods Eng.*, 66(4), 689–706.
Zhu, T. L., and Atluri, S. N. (1998). "A modified collocation method and a penalty formulation for enforcing the essential boundary conditions in the element free Galerkin method." *Comput. Mech.*, 21(3), 211–222.
Zhu, T. L., Zhang, J. D., and Atluri, S. N. (1998). "A local boundary integral equation (LBIE) method in computational mechanics a meshless discretization approach." *Comput. Mech.*, 21(3), 223–235.
Zhuang, X., Augarde, C., and Bordas, S. P. A. (2011). "Accurate fracture modelling using meshless methods, the visibility criterion and level sets: Formulation and 2D modelling." *Int. J. Numer. Methods Eng.*, 86(2), 249–268.
Zhuang, X., Zhu, H., and Augarde, C. (2014). "An improved meshless Shepard and least squares method possessing the delta property and requiring no singular weight function." *Comput. Mech.*, 53(2), 343–357.
Zienkiewicz, O. C., and Taylor, R. L. (1977). *The finite element method*, McGraw-Hill, London.